Plasma Physics Reports, Vol. 26, No. 6, 2000, pp. 465–476. Translated from Fizika Plazmy, Vol. 26, No. 6, 2000, pp. 499–510.

TOKAMAKS

Description of Turbulent Convection in a Plasma with the Help of Interacting Lorentz Oscillators

M. V. Ossipenko and S. V. Tsaun

Russian Research Centre Kurchatov Institute, pl. Kurchatova 1, Moscow, 123182 Russia

Received August 12, 1999; in final form, November 25, 1999

Abstract—A four-field model is proposed that describes turbulent plasma convection inside the separatrix during the L–H transition. It is shown that the Braginskii four-field hydrodynamic equations, which describe fluctuations of the electron and ion temperatures, plasma density, and electrostatic potential in tokamak edge plasmas, can be reduced to three Lorentz-like systems of equations coupled through the equation for the kinetic energy of the fluctuations, i.e., to a four-field edge turbulent layer model describing the nonlinear dynamics of convective cells in the presence of a sheared flow. For three coupled oscillators, the critical pressure gradient corresponding to transitions to both L- and H-modes is found to be much lower than that for an individual oscillator, which describes turbulent convection driven by fluctuations of one type. The edge turbulent layer model makes it possible to describe the formation of a transport barrier inside the separatrix during the L–H transition; calculate heat and particle fluxes via ion and electron channels; and, in combination with the transport code for a core plasma, compute the auxiliary heating power required for a transition to the H-mode. © *2000 MAIK "Nauka/Interperiodica".*

1. INTRODUCTION

The DIII-D experiments [1] aimed at studying the conditions for triggering the transition to an improved confinement regime (the H-mode) showed that the threshold power for the L–H transition is very sensitive to the local values of the plasma parameters in the separatrix region, specifically, the electron and ion temperatures, T_e and T_i, and the plasma density n at the inner boundary of the transport barrier. That is why the threshold power should be calculated using a physically realistic model of turbulent convection near the separatrix surface. The two-field model developed in [2] turned out to be inadequate for describing the experiments quantitatively, because it was constructed without allowance for fluctuations of the electron density and temperature. In the two-field model, the transport barrier forms as a result of the suppression of convective cells by a sheared flow when the ion temperature gradient in a turbulent layer (TL) is above a critical level. Here, we extend the edge turbulent layer (ETL) model to describe turbulent convection excited in the separatrix region of a tokamak plasma taking into account four types of interacting fluctuations, specifically, fluctuations of the electron and ion temperatures, plasma density, and electric potential at the plasma edge. We show that the critical parameter for the onset of turbulent convection is the total plasma pressure gradient in the TL. By TL we mean a narrow edge region of a tokamak plasma inside the separatrix, where large-scale convective cells are excited as a result of the onset of a resistive interchange instability. In moving inward from the separatrix in the direction of the minor radius, the electron temperature increases so that the plasma conductivity becomes higher, thereby stabilizing the instability. In computations, the pressure gradient at the inner boundary of the transport barrier was set to be proportional to $(T_e + T_i)n$, because our model implies that, in simulating the scenarios of discharges, the barrier width and the parameter values at the separatrix should be fixed in each run of the code. The numerical results and analytic estimates allow us to conclude that, in the four-field ETL model, the first critical pressure gradient for the onset of turbulence in the L-mode and the second critical pressure gradient for the generation of the sheared flow that suppresses turbulence in the H-mode are both much lower than those in the case with fluctuations of only one type.

In contrast to the two-field combined ASTRA–ETL model [2], the four-field ETL model combined with the ASTRA transport code [3] makes it possible to compute the power threshold for the L–H transition more exactly and to determine the threshold power as a function of T_e, T_i, and n at the inner boundary of the transport barrier.

Our paper is organized as follows. In Section 2, we describe the four-field ETL model (a detailed derivation of the ETL model equations is presented in the Appendix) and analyze the stability of two and three coupled Lorentz oscillators. In Section 3, we describe the calibration of the four-field ETL model. In Section 4, we present the results of calculating turbulent fluctuations with the four-field ETL model and compare them with analytic predictions and experimental data. Conclusions are drawn in Section 5.

1063-780X/00/2606-0465$20.00

2. FOUR-FIELD ETL MODEL

The four-field ETL model results from the reduced Braginskii equations in the electrostatic approximation [4]. Since the model is aimed at describing edge turbulent convection across the magnetic field, we omit, for simplicity, the equation for longitudinal ion motion. We use two different equations to describe the electron and ion temperatures, because the difference between them seems to be an important parameter determining the threshold power for the L–H transition. The dimensionless nonlinear equations describing turbulence driven by the drift-resistive-ballooning instability have the form (see the Appendix)

$$\frac{\partial \Delta\varphi}{\partial t} + [\mathbf{e}_\varsigma \times \nabla\varphi]\nabla\Delta\varphi + g_B\frac{\partial n(T_i + T_e)}{\partial y} = \sigma(\tilde{\varphi} - \alpha\tilde{T}_e - \tilde{n}) + \mu\Delta^2\varphi, \quad (1)$$

$$\frac{\partial T_i}{\partial t} + [\mathbf{e}_\varsigma \times \nabla\varphi]\nabla T_i + (g_{T_i} - g_B)\frac{\partial\varphi}{\partial y} = \chi_i\Delta T_i + Q_{ei}, \quad (2)$$

$$\frac{\partial T_e}{\partial t} + [\mathbf{e}_\varsigma \times \nabla\varphi]\nabla T_e + (g_{T_e} - g_B)\frac{\partial\varphi}{\partial y} = \frac{2}{3}\alpha\sigma(\tilde{\varphi} - \alpha_1\tilde{T}_e - \tilde{n}) + \chi_e\Delta T_e - Q_{ei}, \quad (3)$$

$$\frac{\partial n}{\partial t} + [\mathbf{e}_\varsigma \times \nabla\varphi]\nabla n + (g_n - g_B)\frac{\partial\varphi}{\partial y} = \sigma(\tilde{\varphi} - \alpha\tilde{T}_e - \tilde{n}) + D\Delta n, \quad (4)$$

where $\alpha = 1.71$ and $\alpha_1 = \alpha + 3.16$ are constants, φ is the electrostatic potential ϕ normalized to T_{Se}/e, n is the electron density normalized to its value n_S at the separatrix, and T_e and T_i are the electron and ion temperatures expressed in units of the electron temperature T_{Se} at the separatrix. The fluctuating quantities are represented as

$$f = f_0(x, t) + \tilde{f}(x, y, t), \quad (5)$$

where f stands for φ, T_i, T_e, and n. The averaged quantities are assumed to have the form

$$\langle T_i\rangle = 1 + (1 - x\rho/L)(T_{Bi}(t) - T_{Si})/T_{Se},$$

$$\langle T_e\rangle = 1 + (1 - x\rho/L)(T_{Be}(t) - T_{Se})/T_{Se},$$

$$\langle n\rangle = 1 + (1 - x\rho/L)(n_B(t) - n_S)/n_S.$$

Here, the subscripts B and S refer to the quantities taken at the inner surface of a transport barrier of width L and at the separatrix, respectively; x and y are the coordinates in the radial and poloidal directions (Fig. 1), normalized to the ion Larmor radius $\rho = C_s/\omega_c$, where C_s is the speed of sound in terms of the electron temperature; the time t is in units of the inverse ion gyrofrequency ω_c^{-1}; $\langle T\rangle$ and $\langle n\rangle$ describe the averaged (across the TL) drops in the dimensionless temperatures and density; $g_{Te} \equiv -d\langle T_e\rangle/dx = \rho(T_{Be} - T_{Se})/(LT_{Se})$, $g_{Ti} \equiv -d\langle T_i\rangle/dx = \rho(T_{Bi} - T_{Si})/(LT_{Se})$, $g_n \equiv -d\langle n\rangle/dx = \rho(n_B - n_S)/(Ln_S)$; $g_B = \rho/R$ is the normalized magnetic field line curvature on the outer side of the tokamak; R is the major radius of the plasma column; $\sigma = \sqrt{M_i/m_e}k_\parallel^2\rho\lambda_e$ is the coefficient proportional to the Spitzer plasma conductivity; $k_\parallel = 1/qR$ (we assume that the correlation length in the convective cells in the magnetic field direction is on the order of qR); λ_e is the electron mean free path; and the coefficients of viscosity (μ), thermal diffusivity (χ_i and χ_e), and diffusion (D) are normalized to ρC_s. The term $Q_{ei} = P_{ei}/(T_{Se}\omega_c)$ accounts for the energy transfer from electrons to ions due to Coulomb collisions.

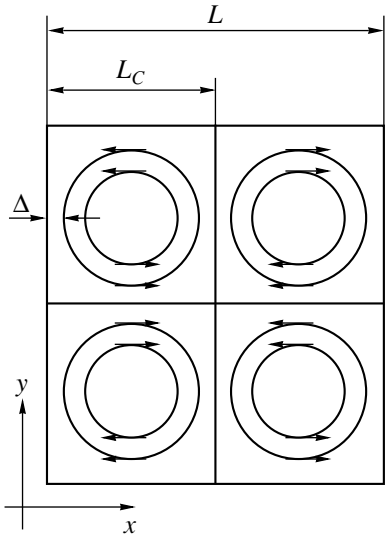

Fig. 1. Convective cells in the TL.

Note that equations (1) and (2) taken with $\sigma = 0$, $T_e = 0$, and $n = \text{const}$ coincide with the Boussinesq equations describing thermal convection in a horizontal layer of a liquid heated from below [5]. The Lorentz system of equations can be derived from the Boussinesq equations in the case of two-dimensional convection by taking into account the interaction between three spatial modes: two unstable modes with amplitudes X and Y, which describe the convective cells, and a stable mode with amplitude Z, which represents the deformation of the averaged temperature profile. The Lorentz system of equations is traditionally written as [5]

$$\dot{X} = -\mathrm{Pr}\,X + \mathrm{Pr}\,Y,$$

$$\dot{Y} = -Y + rX - XZ, \quad (6)$$

$$\dot{Z} = -bZ + XY,$$

where Pr is the Prandtl number, r is the normalized Rayleigh number, and b is a numerical factor.

In order to reduce equations (1)–(4) to the Lorentz-like system, we follow the procedure that was used in [6] to construct the two-field ETL model. To do this, we must take into account the first three harmonics in the Fourier expansion of the fluctuating quantities,

$$\begin{aligned}\varphi &= (V/k_x)\sin k_x x \\ &+ [X_c\cos k_y y + X_s\sin k_y y](1/k)\sin k_x x \\ &+ [\varphi_{2c}\cos k_y y + \varphi_{2s}\sin k_y y]\sin 2k_x x, \\ f &= Z\sin 2k_x x + [Y_c\cos k_y y + Y_s\sin k_y y]\sin k_x x \\ &+ [f_{2s}\sin k_y y + f_{2c}\cos k_y y]\sin 2k_x x.\end{aligned}$$

Here, $k_x = k_y = \rho\pi/L_C$, where L_C is the size of a convective cell (Fig. 1), and f again stands for n, T_e, and T_i. Then, for simplicity, we assume that the phase shift between the fluctuations of the temperatures, density, and potential is $\alpha_k = \pi/2$ (note that $f_k = A\varphi_k\exp(i\alpha_k)$), which corresponds to the most intense flux, because $Q_k = k_y A\varphi_k\varphi_{-k}\sin\alpha_k$. This assumption allows us to reduce the number of harmonics by one-half:

$$\begin{aligned}\varphi &= (V/k_x)\sin k_x x + (X_c/k)\cos k_y y\sin k_x x \\ &+ \varphi_{2s}\sin k_y y\sin 2k_x x, \\ f &= Z\sin 2k_x x + Y_s\sin k_y y\sin k_x x \\ &+ f_{2c}\cos k_y y\sin 2k_x x.\end{aligned} \tag{7}$$

Since the Fourier expansion (7) does not differ between T_e, T_i, and n, we introduce the subscripts e, i, and n for the corresponding perturbation amplitudes Z of the averaged profiles and the amplitudes Y of the turbulent fluctuations. The equations of the four-field ETL model are written for the global variables, which are normalized as follows:

$$\begin{aligned}V &= \frac{cE_r}{C_s B}, \quad X = \frac{e\phi_{rms}}{T_{Se}}\frac{\pi\rho}{L}, \quad Y_i = \frac{T_{i\,rms}}{2T_{Se}}, \\ Y_e &= \frac{T_{e\,rms}}{2T_{Se}}, \quad Y_n = \frac{n_{rms}}{2n_S},\end{aligned} \tag{8}$$

where the subscript *rms* indicates the root mean square value of the fluctuation amplitude,

$$\phi_{rms} = \left(\sum_k |\phi_k|^2\right)^{1/2}. \tag{9}$$

In order to elucidate the asymptotic relation to the Lorentz equations, we keep the notation adopted in working with the Lorentz system. The amplitudes X, Y, and Z in system (6) coincide with the amplitudes X_c, Y_s, and Z in expansions (7).

The four-field ETL model includes the following the equations:

$$V\colon \dot V = V_1 X^2 V - V_2 V + V_3, \tag{10}$$

$$\tilde V\colon \dot X = -V_1 X V^2 + I_2[Y_i + Y_e + I_{2n}Y_n] - I_3 X, \tag{11}$$

$$\tilde T_i\colon \dot Y_i = -J_1 X Z_i + J_{2i}X - J_{3i}Y_i, \tag{12}$$

$$T_{i0}\colon \dot Z_i = Z_1 X Y_i - Z_{2i}Z_i + \hat Q(Z_e - Z_i), \tag{13}$$

$$\tilde T_e\colon \dot Y_e = -J_1 X Z_e + J_{2e}X - J_{3e}Y_e - J_{4e}Y_n, \tag{14}$$

$$T_{e0}\colon \dot Z_e = Z_1 X Y_e - Z_{2e}Z_e - \hat Q(Z_e - Z_i), \tag{15}$$

$$\tilde n\colon \dot Y_n = -J_1 X Z_n + J_{2n}X - J_{3n}Y_n - J_{4n}Y_e, \tag{16}$$

$$n_0\colon \dot Z_n = Z_1 X Y_n - Z_{2n}Z_n, \tag{17}$$

where V is the amplitude of the sheared flow associated with $\mathbf{E}\times\mathbf{B}$ drift, $X^2/2$ is the kinetic energy of the fluctuations, $Y^2/2$ is the thermal energy of the fluctuations, and Z is the y-averaged deviation of the temperature and density profiles from the linear profiles. The constant V_1 depends on the time during which the energy is exchanged between the first (X) and second (φ_2) modes of fluctuations. This time cannot be determined correctly in the ETL model, in which the equations are written for the global variables (in order to guarantee the conservation laws) and the harmonics are used merely to estimate the nonlinear terms [6]. Consequently, the factor V_1 should be found from the test calculations aimed at the calibration of the ETL model by comparing the computed and experimental kinetic energies of the fluctuations, $V_2 = (\nu + \nu_{cx})/\omega_c$, where

$$\nu = \frac{\omega_T \nu_*}{(1+\nu_*)(1+\nu_*\varepsilon^{3/2})} \tag{18}$$

is the neoclassical viscosity coefficient [7] and

$$\nu_{cx} = \langle \nu\sigma\rangle_{cx} n_n \tag{19}$$

is the simplest representation of a friction coefficient incorporating the charge exchange of the ions with neutrals with a zero mean poloidal velocity. In (18), the ion collisionality parameter has the form $\nu_* = \nu_i/(\omega_T\varepsilon^{3/2})$, where ν_i is the ion collision frequency, $\omega_T = V_{Ti}/qR$ is the bounce frequency, V_{Ti} is the ion thermal velocity, R is the major radius of the plasma, q is the safety factor, $\varepsilon = a/R$ is the inverse aspect ratio, and n_n is the neutral density in the TL. The small source term V_3 in (10) describes a seed flow with a low velocity (10^{-5} m/s) that gives rise to the "peeling" instability, when the convective cells become unstable against the generation of a sheared flow. The rest of the notation in (11)–(17) is as follows:

$$\begin{aligned}&I_2 = g_B/\sqrt{2}, \quad I_{2n} = 1 + \frac{T_{Si}}{T_{Se}}, \quad I_3 = \sigma k^{-2} + \mu k^2, \\ &J_1 = k_x/\sqrt{2}, \quad J_{2i} = (g_{Ti} - g_B)/\sqrt{2}, \quad J_{3i} = \chi_i k^2, \\ &Z_1 = k_x/\sqrt{2}, \quad Z_{2e} = 4\delta\chi_e k_x^2, \quad Z_{2i} = 4\delta\chi_i k_x^2, \\ &Z_{2n} = 4\delta D k_x^2, \quad J_{2e} = (g_{Te} - g_B)/\sqrt{2},\end{aligned} \tag{20}$$

$$J_{3e} = \frac{2}{3}\alpha\alpha_1\sigma + \chi_e k^2, \quad J_{4e} = \frac{2}{3}\alpha\sigma,$$

$$J_{2n} = (g_n - g_B)/\sqrt{2}, \quad J_{3n} = \sigma + Dk^2, \quad J_{4n} = \alpha\sigma.$$

For the parameter values close to the experimental ones, we have $J_{4e}/J_{3e} \approx J_{4n}/J_{3n} \approx 0.1 \ll 1$, so that, for simplicity, we can set $J_{4e} = J_{4n} = 0$.

We assume that the viscosity and thermal diffusivity are due to self-similar small-scale turbulence that ensures an energy sink on small scales,

$$\mu = \chi_i = \chi_e = D = CD_B/\rho C_s, \tag{21}$$

where the numerical coefficient C should be found from the calibration of the model and $D_B = \rho C_s/16$ is the Bohm diffusion coefficient. The wavenumber has the form $k = (k_x^2 + k_y^2)^{1/2} = \sqrt{2}\,\rho\pi/L_C$, where the convective-cell size L_C is determined from the balance between the growth rate of the interchange instability and the rate of dissipation along the magnetic field lines due to the longitudinal electron conduction, $\frac{\partial\Delta\varphi}{\partial t} \approx \sigma\varphi$ or $\frac{\pi^2\rho^2\gamma_g\varphi}{L_C^2\omega_c} \approx \sigma\varphi$ with $\gamma_g = C_s/(RL_C)^{1/2}$:

$$L_C \approx \left(\frac{\pi^2\rho^3}{\sigma R^{1/2}}\right)^{0.4}. \tag{22}$$

For an Ohmic L-mode discharge in DIII-D (shot no. 82830 [8]) with the parameters

$$\begin{gathered} R = 1.67\ \text{m},\ a = 0.63\ \text{m},\ B = 2.17\ \text{T}, \\ I_{pl} = 1.37\ \text{MA},\ q = 4.55,\ b/a = 1.8, \\ n_S = 1.5\times10^{19}\ \text{m}^{-3},\ T_{Se} = 30\ \text{eV},\ T_{Si} = 30\ \text{eV}, \\ n_B = 2.3\times10^{19}\ \text{m}^{-3},\ T_{Be} = 75\ \text{eV},\ T_{Bi} = 75\ \text{eV}, \end{gathered} \tag{23}$$

we obtain $L_C \approx 1$ cm. In simulations, the TL width is assumed to be fixed ($L = 2L_C$), because the TL is composed of convective cells rotating in pairs in opposite directions (Fig. 1). The factor $\delta = (L_C/\Delta)^2$ in Z_2 accounts for the formation of a diffusive boundary layer of width Δ inside each convective cell [2].

The terms $\hat{Q}(Z_e - Z_i)$ in equations (12) and (14) describe the energy exchange between electrons and ions through Coulomb collisions. The total power transferred from electrons to ions is

$$\hat{Q} = \frac{2}{L}\int_0^L Q_{ei}\sin\frac{2\pi x}{L}dx = 4\times10^{-15}\frac{Z}{AT_{Se}}\left[\frac{n_{Be}}{T_{Be}^{3/2}} + \frac{n_{Se}}{T_{Se}^{3/2}}\right] \times\left[\frac{1}{\pi}(T_{Si} - T_{Bi} - T_{Se} + T_{Be}) + (Z_e - Z_i)T_{Se}\right].$$

The first term should be substituted into the evolutionary equations for the electron and ion temperatures at the separatrix. However, in calculations, this term was disregarded, because the electron and ion temperatures at the separatrix were assumed to be fixed. In equations (13) and (15), we took into account only the heat transfer term that depends on $Z_e - Z_i$,

$$\hat{Q} = 4\times10^{-15}\frac{Z}{A}\left[\frac{n_{Be}}{T_{Be}^{3/2}} + \frac{n_{Se}}{T_{Se}^{3/2}}\right](Z_e - Z_i)T_{Se}.$$

In comparison with the two-field ETL model [2], which includes only V, X, Y_i, and Z_i, the four-field ETL model (10)–(17) is less stable: it can be shown that three (or two) coupled Lorentz oscillators may be unstable even if each of them has only a trivial solution. To prove this assertion, we consider the following simplified subsystem, which describes the interaction between the fluctuations of the ion temperature and density in the case of a shearless flow velocity:

$$\tilde{V}\colon \dot{X} = I_2[Y_i + I_{2n}Y_n] - I_3X, \tag{24}$$

$$\tilde{T}_i\colon \dot{Y}_i = -J_1XZ_i + J_{2i}X - J_{3i}Y_i, \tag{25}$$

$$T_i^0\colon \dot{Z}_i = Z_1XY_i - Z_{2i}Z_i, \tag{26}$$

$$\tilde{n}\colon \dot{Y}_n = -J_1XZ_n + J_{2n}X - J_{3n}Y_n, \tag{27}$$

$$n^0\colon \dot{Z}_n = Z_1XY_n - Z_{2n}Z_n. \tag{28}$$

This subsystem consists of two Lorentz oscillators, which are described by equations (24)–(26) and by equations (24), (27), and (28) and are coupled through equation (24). The equilibrium solution describing steady-state convection has the form

$$\begin{gathered} Z_i = Z_1XY_i/Z_{2i},\ Y_i = J_{2i}X/(J_{3i} + J_1Z_1X^2/Z_{2i}), \\ Z_n = Z_1XY_n/Z_{2n},\ Y_n = J_{2n}X/(J_{3n} + J_1Z_1X^2/Z_{2n}), \\ X^2 = \kappa/(J_1Z_1), \end{gathered} \tag{29}$$

where κ is a nonnegative root of the equation

$$\begin{gathered} I_3\kappa^2 - [Z_{2i}(I_2J_{2i} - I_3J_{3i}) + Z_{2n}(I_2I_{2n}J_{2n} - I_3J_{3n})]\kappa \\ + Z_{2i}Z_{2n}(J_{3n}J_{3i}I_3 - J_{3i}J_{2n}I_2I_{2n} - J_{3n}J_{2i}I_2) = 0. \end{gathered} \tag{30}$$

We analyze three limiting cases in which the condition for steady-state convection to exist can be evaluated analytically.

(i) In the case $J_{2n} = 0$, we again deal with the two-field ETL model [2], which is described by one Lorentz oscillator (24)–(26) with the following standard parameters of system (6):

$$\text{Pr} = I_3/J_{3i} = (\sigma k^{-2} + \mu k^2)/\chi_i k^2,$$

$$r = I_2J_{2i}/I_3J_{3i} = (g_{Ti} - g_B)g_B/[2\chi_i k^2(\sigma k^{-2} + \mu k^2)],$$

$$b = Z_{2i}/J_{3i} = 2\delta.$$

The critical ion temperature gradient for the onset of convective cells is determined by the condition

$$X^2 = Z_{2i}[I_2J_{2i} - I_3J_{3i}]/(J_1Z_1I_3) > 0 \quad (31a)$$

(i.e., $r = I_2J_{2i}/I_3J_{3i} > 1$), so that the critical ion temperature gradient is

$$g_{Ti} = 2(\sigma k^{-2} + \mu k^2)\chi_i k^2/g_B + g_B. \quad (31b)$$

(ii) In the case $J_{3i}Z_{2i} = J_{3n}Z_{2n}$, we can simplify equation (30) so that it becomes possible to write out the instability criterion for two coupled Lorentz oscillators,

$$X^2 = [I_2(Z_{2i}J_{2i} + I_{2n}Z_{2n}J_{2n}) - I_3Z_{2i}J_{3i}]/(J_1Z_1I_3) > 0. \quad (32a)$$

Comparing (32a) with (31a), we can see that the instability threshold for two coupled oscillators is lower than that for each of them, $J_{2i} + I_{2n}J_{2n}Z_{2n}/Z_{2i} > I_3J_{3i}/I_2$. For $g_{Ti} \approx g_n$, the threshold is lower by a factor of two:

$$g_{Ti} + (1 + T_{Si}/T_{Se})g_n = 2(\sigma k^{-2} + \mu k^2)\chi_i k^2/g_B + (2 + T_{Si}/T_{Se})g_B. \quad (32b)$$

(iii) In the case $J_{3n}I_3 - J_{2n}I_2I_{2n}$ and $J_{3i}I_3 - J_{2i}I_2 > 0$, each of the two oscillators is characterized by the solution that describes completely damped fluctuations. Consequently, in equation (30) for X^2, the factor in front of κ is negative and a positive solution exists only if the free term is negative:

$$J_{2i} + I_{2n}J_{2n}J_{3i}/J_{3n} > I_3J_{3i}/I_2,$$

i.e., only under the condition

$$I_3J_{3i}/I_2 < J_{2i} + I_{2n}J_{2n}J_{3i}/J_{3n} < 2I_3J_{3i}/I_2. \quad (33)$$

While each of the two oscillators is linearly stable in the vicinity of zero, a system of two coupled oscillators is subjected to a linear instability that gives rise to convective cells. Below, we will show that the experimental parameter values (23) correspond just to this case.

3. CALIBRATION OF THE ETL MODEL

The coefficients in the ETL model equations (10)–(17) contain three constants that should be found from the calibration calculations. These are V_1 in equation (10); C in formula (21) for the seed transport coefficients; and δ, which accounts for the amplitudes Z_{2i}, Z_{2e}, and Z_{2n} of the small-scale harmonics of the perturbed averaged profiles in (20). The constants V_1 and C can be found by comparing the computed and measured values of the amplitude of the potential fluctuations, $e\phi_{rms}/T_{Se} = X(L/\pi\rho)$, and the particle flux $\Gamma^{turb} = C_s n\Gamma$ (where $\Gamma = (k_y/k)XY_n$) in the H-mode. For an H-mode discharge, in which $V \neq 0$, equation (10) has the time-independent solution $X_H^2 = V_2/V_1$, so that we obtain $V_1 = V_2/X_H^2$. According to the data presented in [8], this estimate gives

$$V_1 = 0.08. \quad (34)$$

By virtue of (29), the turbulent particle flux and the amplitude of the potential fluctuations are related by

$$\Gamma = (k_y/k)J_{2n}X^2/(J_{3n} + J_1Z_1X^2/Z_{2n}). \quad (35)$$

In the approximation $J_{3i}Z_{2i} = J_{3e}Z_{2e} = J_{3n}Z_{2n}$, equation (11) taken with Y_i and Y_n from (29) (note that Y_e has a form analogous to Y_i) yields the following relationship, which is valid in the steady state:

$$-V_1V^2 + I_2[J_{2i} + J_{2e} + I_{2n}J_{2n}]/(J_{3n} + J_1Z_1X^2/Z_{2n}) - I_3 = 0.$$

Substituting the experimental values of the turbulent particle flux Γ_H and the amplitudes of the potential and velocity fluctuations X_H and V (all obtained for H-mode discharges) into formulas (20) and (35), we arrive at

$$C = 16\{g_B[(g_{Ti} + g_{Te} - 2g_B)/(g_n - g_B) + 1 + T_{Si}/T_{Se}]\Gamma_H X_H^2 - V_1V^2 - \sigma k^{-2}\}/k^2. \quad (36a)$$

For H-mode discharges, the term $J_1Z_1X^2/Z_{2n}$ with the constant δ in (35) is much smaller than J_{3n}. For L-mode discharges, this difference is less marked. Consequently, the constant δ can be determined more precisely by inserting the values of Γ_L and X_L obtained experimentally for L-mode discharges into (35):

$$\delta = 2X_L^2/[((g_n - g_B)X_L^2/2\Gamma_L - \sigma - Ck^2/16)C]. \quad (36b)$$

With the parameters values (23), which were presented in [8] for DIII-D shot no. 82830, we find

$$C = 0.6, \delta = 8.$$

Figure 2 shows the particle flux Γ^{turb} versus δ for fluctuation amplitudes corresponding to the L- and H-modes. We can see that the problem of determining δ from the experimental values of the flux and fluctuation amplitudes is well posed only for low-intensity fluxes in L-mode discharges. The experimentally measured flux $\Gamma^{turb} = (15 \pm 4) \times 10^{20}$ m^{-2} s^{-1} presented in [8] lies just in the range that is convenient for calculations. Since, in the range $\delta > 8$, the flux becomes independent of δ, the errors in determining this constant weakly affect the results of computations with the full ASTRA–ETL model, in which the fluxes are the output parameters of the ETL model.

The calibration of the ETL model was performed at fixed temperature and density gradients in the TL. In the combined ASTRA–ETL model, the gradients are calculated self-consistently: the coincidence of the computed and experimental fluctuation amplitudes serves as a criterion for the correctness of the full

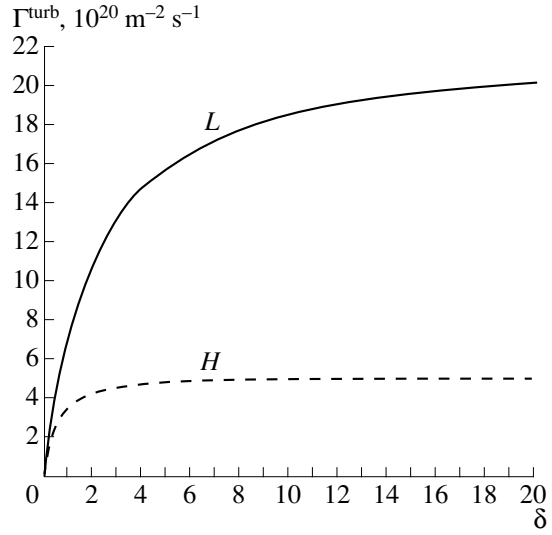

Fig. 2. Turbulent particle flux vs. δ in the L- and H-modes.

model. Calculations based on the ETL model were carried out with the profiles of n and T taken at the time at which the fluctuation amplitude starts to decrease, i.e., just before the L–H transition (at t = 1520 ms). Consequently, the profiles with the corresponding edge gradients of n and T can yield a bifurcated solution describing either L-mode (when $V = 0$) or H-mode (when $V \neq 0$) discharges. The combined ASTRA–ETL code utilized the values of n and T at the separatrix only. The results of calibration computations for the ETL model and simulations of the L–H transition scenario for shot no. 82830 [8] by running the ASTRA–ETL code are summarized in the table.

In simulating the scenario of the discharge, we found that the neutral density at the separatrix for which the mean plasma density coincided with the experimental one was equal to $n_n = 3 \times 10^{16}$ m^{-3}. In the full ASTRA–ETL model, the turbulent particle flux and the fluctuation amplitudes of the density and potential coincided with the experimental ones only in the H-mode. The calculations carried out for the L-mode showed that, for a given power, the plasma pressure gradient and, accordingly, the particle flux intensity in the TL are lower than those measured in the experiment.

Figure 3 shows the time evolutions of the sheared flow velocity V, the fluctuation amplitude $e\phi_{rms}/T$, and the particle flux Γ^{turb} during the L–H transition. In the ETL model, the transition time is determined by the growth rate of the sheared flow and is approximately equal to 500 μs. In the full ASTRA–ETL model, the transition time is longer (about 10 ms), because a pedestal on the ion and electron temperature profiles forms on the diffusive time scale (corresponding to the diffusive rebuilding of the ion and electron temperature profiles) with a rate governed by the rate of power supply from the core plasma to the TL. In shot no. 82830, the L–H transition is very slow: it occurs over a time of about 10 ms. This indicates that the input power is close to the threshold power. Consequently, the difference between the L- and H-modes appears to be more qualitative than quantitative: although, in the H-mode, the turbulence-driven $\mathbf{E} \times \mathbf{B}$ velocity is about 4000 m/s and the level to which the turbulent fluxes are suppressed is lower than that in the L-mode by one-half, the temperature and density profiles near the separatrix in these modes differ only slightly.

4. DYNAMICS OF THREE COUPLED LORENTZ OSCILLATORS

The calibrated four-field ETL model makes it possible to determine the threshold pressure gradients in the TL that are required to trigger transitions from the Ohmic regime to the L- and H-modes. It turns out that, under the experimental conditions (23), each individual oscillator [specifically, the one described by equations (11)–(13) for fluctuations $\tilde{T}_i$ at $\tilde{T}_e = 0$ and $\tilde{n} = 0$; the one described by equations (11), (14), and (15) for fluctuations $\tilde{T}_e$ at $\tilde{T}_i = 0$ and $\tilde{n} = 0$; and the one described by equations (11), (16), and (17) for fluctuations $\tilde{n}$ at $\tilde{T}_i = 0$ and $\tilde{T}_e = 0$], as well as each pair of oscillators [e.g., the pair described by (24)–(28) for $\tilde{T}_i$ and $\tilde{n}$], is characterized exclusively by the solutions that describe fluctuations damped to zero. However, for three coupled Lorentz oscillators, there exists a solution that describes the L–H transition (see Fig. 3 and the table).

Table

	Mode	L_n, mm	L_{Te}, mm	n_{rms}/n	$e\phi_{rms}/T$	Γ^{turb}, 10^{20} m^{-2} s^{-1}	V, m/s
Experiment	L	17	18	0.3–0.4	0.15–0.3	15 ± 4	0
ETL	L	48	23	0.26	0.44	18	0
ASTRA-ETL	L	60	26	0.14	0.28	6	0
Experiment	H	2.5	6	0.1–0.2	0.15–0.3	4 ± 1.5	5000
ETL	H	48	23	0.15	0.22	5.3	3790
ASTRA-ETL	H	40	25	0.13	0.23	5.6	4100

In this case, the instability condition is satisfied, because all three gradients ($\nabla T_e \propto g_{Te}$, $\nabla T_i \propto g_{Ti}$, and $\nabla n \propto g_n$) contribute to the pressure gradient $\nabla p \propto g$, which drives the instability in the TL. Here,

$$g \equiv \frac{n_B + n_S}{2n_S}(g_{Ti} + g_{Te}) + \frac{T_{Be} + T_{Se} + T_{Bi} + T_{Si}}{2T_{S_e}} g_n = \frac{\rho}{L}\frac{n_B(T_{Bi} + T_{Be}) - n_S(T_{Si} + T_{Se})}{n_S T_{Se}} \quad (37)$$

is the effective pressure gradient.

For the system of three oscillators, we can represent the condition for the onset of steady-state convection in the L-mode ($X^2 > 0$) in a form analogous to (31b) and (32b),

$$g > 2(\sigma k^{-2} + \mu k^2)\chi_i k^2 / g_B + (3 + T_{Si}/T_{Se}) g_B \equiv g^*, \quad (38)$$

under the simplifying assumption $J_{3i}Z_{2i} = J_{3e}Z_{2e} = J_{3n}Z_{2n}$, which, by virtue of (20), is satisfied with an accuracy of 10% in the parameter range under consideration.

In the case of three oscillators, the criterion for a transition to the H-mode can be obtained from condition (32a):

$$X_L^2 = [I_2(Z_{2i}J_{2i} + Z_{2e}J_{2e} + I_{2n}Z_{2n}J_{2n}) - I_3 Z_{2i} J_{3i}]/(J_1 Z_1 I_3) > V_2/V_1. \quad (39)$$

This criterion differs from (38) in that it contains an additional term on the right-hand side:

$$g > 2(\sigma k^{-2} + \mu k^2)\chi_i k^2 / g_B + (3 + T_{Si}/T_{Se}) g_B + (V_2/V_1)(\sigma k^{-2} + \mu k^2)/(4\delta\chi_i g_B) \equiv g^{**}. \quad (40)$$

Under this condition, solution (39) for the L-mode becomes unstable, which corresponds to a transition to the H-mode characterized by the solution

$$X_H^2 = V_2/V_1. \quad (41)$$

The critical values of g^* and g^{**} depend on which particular gradient (∇T_e, ∇T_i, or ∇n) is responsible for triggering transitions to the L- and H-modes. This is due to the fact that the coefficients $\sigma(T_e, n)$ and $V_2(T_i, n)$ on the right-hand side of equations (38) and (39) are functions of the turbulent layer–averaged parameters T_e, T_i, and n.

Figure 4 shows the fluctuation amplitude $e\phi_{rms}/T_{Se}$ and the sheared flow velocity V versus g in the cases of one and three oscillators. The plots in this figure were computed under the assumption that g changes only due to the increase in the ion temperature T_{Bi} at the inner boundary of the TL, i.e., the growth of g_{Ti} at fixed g_n and g_{Te}. We can distinguish the following three ranges of the parameter g.

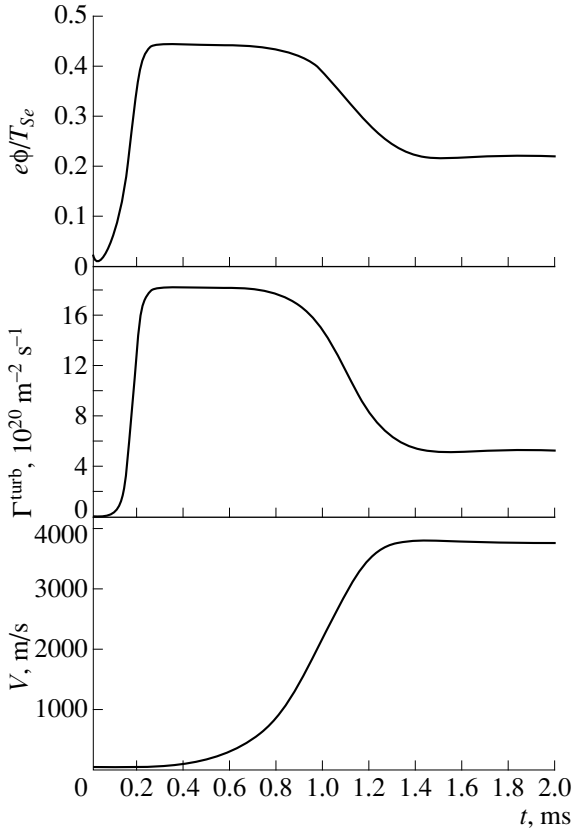

Fig. 3. Time history of the L–H transition.

(i) For $g < g^*$, no fluctuations are excited, which corresponds to the Ohmic mode.

(ii) The range $g^* < g < g^{**}$ is characterized by the onset of steady-state convection such that

$$\frac{e\phi_{rms}}{T_{Se}} \propto \sqrt{g - g^*}, \quad V \equiv 0, \quad (42)$$

which corresponds to the L-mode (38).

(iii) For $g > g^{**}$, convective cells are unstable against the generation of a sheared flow with the velocity

$$V \propto \sqrt{g - g^{**}}, \quad \frac{e\phi_{rms}}{T_{Se}} = \frac{L}{\pi\rho}\sqrt{\frac{V_2}{V_1}} = \text{const}, \quad (43)$$

which corresponds to the H-mode (40). If the sheared flow is suppressed by one or another means, then the solution X_L corresponding to the L-mode (39) can also exist in this range (it is indicated by the dashed curve in Fig. 4a).

According to Fig. 4b, the threshold pressure gradient g^{**} for the L–H transition simulated using the four-field ETL model with three Lorentz oscillators is $g^{**} = 0.087$ at $T_{Bi} = 0.057$ keV, while the threshold obtained from the two-field ETL model [2] with one oscillator is equal to $g^{**} = 0.15$ at $T_{Bi} = 0.13$ keV. Consequently, in

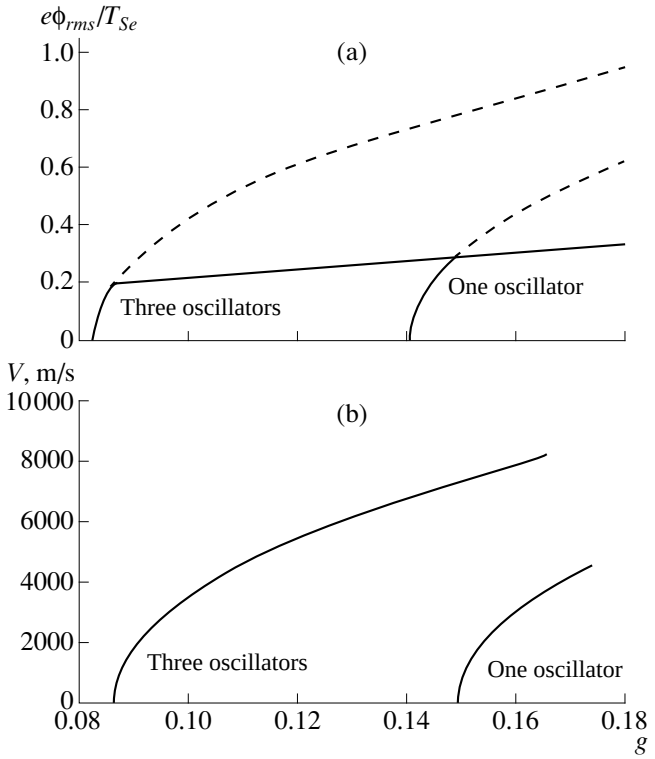

Fig. 4. (a) Fluctuation amplitude $e\phi_{rms}/T_{Se}$ and (b) sheared flow velocity V versus g for one-oscillator and three-oscillator models. The parameter g changes because of the growth of T_{Bi}. The dashed curve is the unstable solution corresponding to the L-mode.

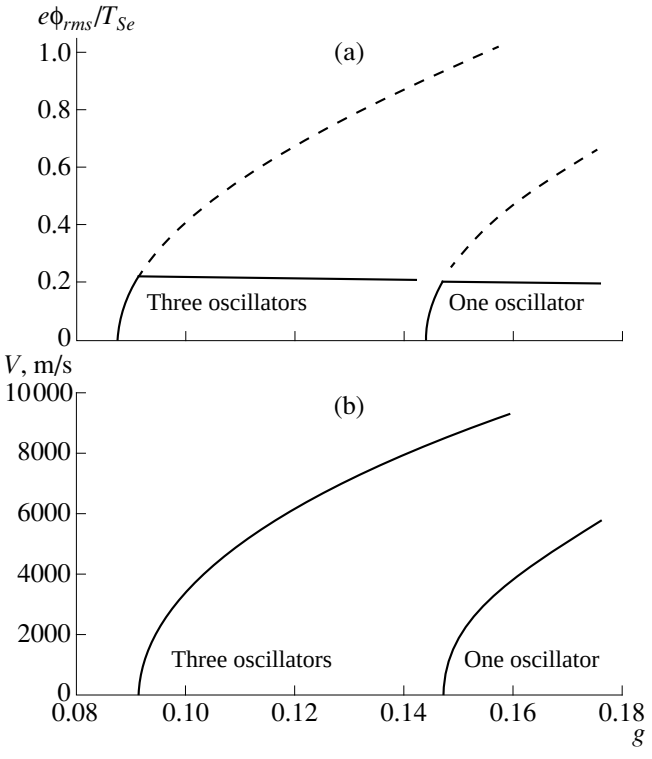

Fig. 5. (a) Fluctuation amplitude $e\phi_{rms}/T_{Se}$ and (b) sheared flow velocity V versus g for one-oscillator and three-oscillator models. The parameter g changes because of the growth of n_B.

the four-field ETL model, the threshold ion temperature gradient (and, accordingly, the threshold power) for the L–H transition is lower by a factor of about two than the threshold in the two-field ETL model. We thus conclude that the threshold power can be accurately estimated only if the interaction between the fluctuations of the potential, density, and electron and ion temperatures is taken into account. In the four-field ETL models, the instant at which a sheared flow begins to be generated is regarded as the start of the L–H transition. If the pressure gradient is slightly above the threshold, then the sheared flow velocity is low and the fluctuations are suppressed only slightly. The degree to which the fluctuations are suppressed can be estimated from Fig. 4a by comparing $e\phi_{rms}/T_{Se}$ in the L-mode (dashed curve) and in the H-mode (solid curve). To achieve a twofold reduction in the fluctuation amplitude and, accordingly, a fourfold reduction in the flux intensity $\Gamma \propto \phi^2$, it is necessary that $g = 0.1$–0.11. The results of simulations with the ETL model presented in the table correspond precisely to the minimum threshold gradient $g = 0.102$ for the transition to the H-mode with a substantially improved plasma confinement.

Figure 5 differs from Fig. 4 in that the parameter g changes because of the growth of the density n_B at the inner boundary of the TL, i.e., the growth of g_n at fixed g_{Ti} and g_{Te}. According to Fig. 5b, the threshold pressure gradient g^{**} for the L–H transition simulated using the four-field ETL model is $g^{**} = 0.092$ at $n_B = 1.99 \times 10^{19}$ m^{-3}, while the threshold obtained from the two-field ETL model is equal to $g^{**} = 0.147$ at $n_B = 3.65 \times 10^{19}$ m^{-3}. For an L–H transition triggered by the increase in the density gradient, the threshold g^{**} is slightly higher and $e\phi_{rms}/T_{Se}$ falls off gradually as g increases, which differs from the situation illustrated in Fig. 4a, where $e\phi_{rms}/T_{Se}$ gradually rises. This difference results from the fact that the neoclassical viscosity ν in the coefficient V_2 in (41) grows as T_{Bi} increases and falls off as n_B rises.

When g changes due to the increase in g_{Te}, it is impossible to determine the threshold for the L–H transition under the experimental conditions (23). For any value of T_{Be} and the remaining parameters in (23) being fixed, an individual oscillator has only a trivial solution, because, in criterion (38) for the interchange instability, the right-hand side, containing $\sigma \propto (T_{Be} + T_{Se})^2$, increases faster as T_{Be} grows in comparison with the left-hand side, containing $g_{Te} \propto T_{Be} - T_{Se}$. In the case of three oscillators, a decrease in T_{Se} (the remaining parameters in (23) being fixed) does not lead to the suppression of fluctuations, because σ falls off faster than g_{Te}.

5. CONCLUSION

We have proposed the four-field ETL model of turbulent plasma convection near the separatrix surface. The model is aimed at describing the interaction between four types of fluctuations (fluctuations of the ion and electron temperatures, plasma density, and electrostatic potential) by three systems of Lorentz-like equations (for $\tilde{T}_e$, $\tilde{T}_i$, and $\tilde{n}$) coupled through the equation for potential fluctuations. When T_{Be}, T_{Bi}, and n_B are specified at the inner boundary of the TL and T_{Se}, T_{Si}, and n_S are fixed at the separatrix, the ETL model makes it possible to calculate the fluctuation amplitudes, sheared flow velocity, and also heat and particle fluxes via ion and electron channels. We have shown that, in the four-field ETL model, the first critical pressure gradient for the onset of turbulence in the L-mode and the second critical pressure gradient for the generation of the sheared flow that suppresses turbulence in the H-mode are both much lower than those in the two-field ETL model. Under the experimental conditions (23), each of the oscillators for fluctuations $\tilde{T}_i$, $\tilde{T}_e$, or $\tilde{n}$, as well as each pair of oscillators (e.g., $\tilde{T}_i$ and $\tilde{n}$), has only a solution that describes fluctuations damped to zero, whereas, for the three coupled oscillators, there exists a solution corresponding to the L–H transition.

We have shown that, in the four-field ETL model, the effective pressure gradient in the TL, $\nabla p = \frac{n_B(T_{Bi} + T_{Be}) - n_S(T_{Si} + T_{Se})}{L} = \frac{g n_S T_{Se}}{\rho}$, is the main control parameter; moreover, the threshold values of g^* and g^{**} depend on which particular gradient (∇T_e, ∇T_i, or ∇n) is responsible for triggering transitions to the L- and H-modes. The threshold for the L–H transition is lowest when the electron temperature in the TL is minimum and the critical pressure gradient is achieved owing to the increase in the ion temperature gradient and the density gradient. This is due to the fact that the increase in the electron temperature raises the coefficient proportional to the plasma conductivity $\sigma(T_e, n)$ on the right-hand side of conditions (38) and (40) for transitions to L- and H-modes. In other words, if the input power is deposited exclusively in the electrons, then the transition to an improved confinement mode can be achieved via the suppression of turbulence due to the high plasma conductivity rather than by the sheared flow.

In combination with the transport code for a core plasma, the four-field ETL model can be used to compute the auxiliary heating power required for a transition to the H-mode and to determine the threshold power for the L–H transition as a function of the averaged quantities n and B and the values of T_{Se}, T_{Si}, and n_S at the separatrix.

ACKNOWLEDGMENTS

This work was supported in part by the Russian Foundation for Basic Research, project no. 96-15-96815 (under the program "Leading Scientific Schools").

APPENDIX

The set of equations (1)–(4) was derived from the Braginskii two-fluid MHD equations [4]. We sum up the equations of electron and ion motion and neglect both the oblique viscosity tensor and electron inertia to obtain the equation of motion of a plasma as a whole:

$$M_i n \frac{d\mathbf{V}}{dt} = -\nabla p + \frac{1}{c}[\mathbf{j} \times \mathbf{B}] + M_i n \mu \Delta \mathbf{V}, \qquad (A.1)$$

where $p = n(T_i + T_e)$. Neglecting the Hall effect and electron inertia converts the equation of electron motion to Ohm's law for the plasma:

$$\frac{1}{\sigma_{Sp}}\mathbf{j} = \mathbf{E} + \frac{1}{c}[\mathbf{V} \times \mathbf{B}] + \frac{\nabla p_e}{en} - R_T, \qquad (A.2)$$

where $p_e = nT_e$, $\mathbf{E} = -\nabla\phi$, $\sigma_{Sp} = e^2 n \lambda_e/(m_e V_{Te})$, V_{Te} is the electron thermal velocity, and $R_T = -0.7 \ln \nabla_\parallel T_e$ is the thermal force. We apply the operation $\mathrm{curl}\frac{1}{B}$ … to equation (A.1) and consider the projection of the resulting equation onto the direction of the magnetic field, $\mathbf{b} = \mathbf{B}/B$. We also take into account the following relationships:

(i) $\mathbf{B} = B\mathbf{e}_\zeta + B_\theta \mathbf{e}_\theta$, where θ and ζ are the poloidal and toroidal angles; moreover, for $B_\theta/B \ll 1$, we can set $\mathbf{b} \approx \mathbf{e}_\zeta$ and $B \propto 1/(1 + \varepsilon\cos\theta)$, where $\varepsilon = r/R$ and r is the minor plasma radius.

(ii) Neglecting classical diffusion and drift-induced corrections in equation (A.2) yields

$$\mathbf{V}_\perp = \frac{c}{B}[\mathbf{b} \times \nabla\phi], \quad \mathbf{b}\,\mathrm{curl}\frac{1}{B}\mathbf{V}_\perp = \frac{c}{B^2}\Delta_\perp \phi. \qquad (A.3)$$

(iii) $\mathbf{b}\,\mathrm{curl}\frac{1}{B}\nabla p = \mathbf{b} \cdot \left[\nabla\frac{1}{B} \times \nabla p\right] \approx \frac{1}{BR}\left(\frac{\cos\theta}{r}\frac{\partial p}{\partial \theta} + \sin\theta\frac{\partial p}{\partial r}\right) \approx \frac{1}{BR}\frac{\partial p}{\partial y}$, where $y = r\theta$. This relationship is valid at the outer circumference of the torus for small θ such that $\cos\theta \approx 1$ and $\sin\theta \approx 0$. Consequently, in the ETL model, the turbulence is assumed to be driven by an interchange instability at the outer circumference of the torus.

(iv) $\mathbf{b}\,\mathrm{curl}\frac{1}{B}[\mathbf{j} \times \mathbf{B}] = (\mathbf{b}\nabla) j_\parallel$ for $\mathrm{div}\,\mathbf{j} = 0$.

Then, we obtain the equation

$$\frac{M_i n_S c}{B^2}\frac{d\Delta_\perp \phi}{dt} = -\frac{1}{BR}\frac{\partial p}{\partial y} + \frac{1}{c}(\mathbf{b}\nabla) j_\parallel + M_i n_S \mu \frac{c}{B^2}\Delta_\perp^2 \phi, \quad \text{(A.4)}$$

where $j_\parallel = \mathbf{b}\cdot\mathbf{j}$ is the magnetic field–aligned current.

We substitute the projection of equation (A.2) onto the magnetic field direction into equation (A.4),

$$j_\parallel = \sigma_{Sp}\left(-(\mathbf{b}\nabla)\phi + \frac{1}{en}(\mathbf{b}\nabla)p_e + \frac{1}{e}0.71(\mathbf{b}\nabla)T_e\right). \quad \text{(A.5)}$$

We also replace the operator $(\mathbf{b}\nabla)$ by $k_\parallel$ and switch to the dimensionless variables $\varphi = e\phi/T_{Se}$, $\hat{t} = t\omega_c$, $\hat{x} = x/\rho$, $\hat{y} = y/\rho$, and $x = r - r_B$, where r_B is the radial coordinate of the inner boundary of the transport barrier. As a result, we arrive at equation (1). In equations (1)–(4) and in what follows, we omit the caret sign over the dimensionless variables. For simplicity, we also ignore ion motion along the magnetic field lines.

Equations (2)–(4) follow from equations (2.3e,i) and (2.1) in [4]:

$$\frac{\partial T_i}{\partial t} + \frac{c}{B}[\mathbf{b}\times\nabla\varphi]\nabla T_i - \frac{c}{B}\left(\frac{d\langle T_i\rangle}{dx} + \frac{n_S}{R}\right)\frac{\partial\varphi}{\partial y} = \chi_i \Delta T_i + P_{ei}, \quad \text{(A.6)}$$

$$\frac{\partial T_e}{\partial t} + \frac{c}{B}[\mathbf{b}\times\nabla\varphi]\nabla T_e + \frac{c}{B}\left(-\frac{d\langle T_e\rangle}{dx} + \frac{n_S}{R}\right)\frac{\partial\varphi}{\partial y} = -1.14T_e(\mathbf{b}\nabla)V_{e\parallel} + \chi_{e\parallel}(\mathbf{b}\nabla)^2 T_e + \chi_e\Delta_\perp T_e - P_{ei}, \quad \text{(A.7)}$$

$$\frac{\partial n}{\partial t} + \frac{c}{B}[\mathbf{b}\times\nabla\varphi]\nabla n - \frac{c}{B}\left(\frac{d\langle n\rangle}{dx} + \frac{n_S}{R}\right)\frac{\partial\varphi}{\partial y} = -(\mathbf{b}\nabla)nV_{e\parallel} + D\Delta_\perp n, \quad \text{(A.8)}$$

where the first term on the right-hand side of (A.7) is evaluated with allowance for the relationships $\mathbf{V}_e = \mathbf{V}_\perp + \mathbf{V}_{e\parallel}$ and $\operatorname{div}\mathbf{V}_\perp = 0$ and without allowance for collisional fluxes in $\mathbf{q}_e$:

$$\frac{2}{3n}(p_e \operatorname{div}\mathbf{V}_e + \operatorname{div}\mathbf{q}_e) \approx \frac{2}{3n}(nT_e(\mathbf{b}\nabla)V_{e\parallel} + 0.71(\mathbf{b}\nabla)nT_eV_{e\parallel}) \approx 1.14T_e(\mathbf{b}\nabla)V_{e\parallel},$$

$$V_{e\parallel} \approx -j_\parallel/en, \quad \chi_{e\parallel} = \frac{2}{3n}\left(3.16\frac{nT_{Se}\tau_e}{m_e}\right).$$

The rate with which the ions are heated by ion–electron collisions is $P_{ei} = \frac{2m_e}{M_i\tau_e}(T_e - T_i)$, where m_e is the mass of an electron, M_i is the mass of an ion, T is in units of eV, $\tau_e = 3.5\times 10^5 \frac{T_e^{3/2}}{\Lambda Z n}$ [s] is the electron time between collisions, Λ is the Coulomb logarithm, and n is in units of cm^{-3}.

If we evaluate the divergence of the flux,

$$\operatorname{div}(n\mathbf{V}_\perp) = \frac{c}{B}[\mathbf{b}\times\nabla\varphi]\nabla n - \frac{c}{B}\left(\frac{d\langle n\rangle}{dx} + \frac{n_S}{R}\right)\frac{\partial\varphi}{\partial y},$$

with allowance for the magnetic field line curvature in the expression for velocity, then the terms with the factor $1/R$ appear in the left-hand side of equations (A.6)–(A.8). Although $-\frac{d\langle n\rangle}{dx} \gg \frac{n_S}{R}$, the term with the radius of curvature should be incorporated in order for the energy in equations (1)–(4) to be conserved in the absence of dissipation.

To derive the four-field ETL model equations (10)–(17), first, we utilize expansion (5); second, multiply equations (1)–(4) by φ, T_i, T_e, and n, respectively; and then average the resulting equations over the TL, imposing periodic (in y) boundary conditions and assuming that $\varphi = 0$, $\partial\varphi/\partial y = 0$, $T_{i,e} = 0$, and $n = 0$ at $x = 0, L$:

$$\frac{dU}{dt} + \frac{1}{UL}\int_0^L W'\varphi_0' dx = -\frac{1}{U}\mu\langle\varphi_0''^2\rangle, \quad \text{(A.9)}$$

$$\frac{dI}{dt} - \frac{1}{L}\int_0^L W'\varphi_0' dx = g_B Q - \sigma(\langle\tilde{\varphi}^2\rangle - 1.71\langle\tilde{\varphi}\tilde{T}\rangle - \langle\tilde{\varphi}\tilde{n}\rangle) - \mu\langle\Delta\tilde{\varphi}^2\rangle, \quad \text{(A.10)}$$

$$\frac{d\Theta_i}{dt} + \frac{1}{\Theta_i L}\int_0^L Q_i' T_{i0} dx = -\frac{1}{\Theta_i}\chi_i\langle T_{i0}'^2\rangle - \hat{Q}_{ie}, \quad \text{(A.11)}$$

$$\frac{dJ_i}{dt} - \frac{1}{L}\int_0^L Q_i' T_{i0} dx = (g_{Ti} - g_B)Q_i - \chi_i\langle|\nabla\tilde{T}_i|^2\rangle, \quad \text{(A.12)}$$

$$\frac{d\Theta_e}{dt} + \frac{1}{\Theta_e L}\int_0^L Q_e' T_{e0} dx = -\frac{1}{\Theta_e}\chi_e\langle T_{e0}'^2\rangle + \hat{Q}_{ie}, \quad \text{(A.13)}$$

$$\frac{dJ_e}{dt} - \frac{1}{L}\int_0^L Q_e' T_{e0} dx = (g_{Te} - g_B) Q_e + 1.14\sigma(\langle\tilde{\varphi}\tilde{T}_e\rangle - 4.87\langle\tilde{T}_e^2\rangle - \langle\tilde{n}\tilde{T}_e\rangle) - \chi_e\langle|\nabla\tilde{T}_e|^2\rangle, \quad \text{(A.14)}$$

$$\frac{dN}{dt} + \frac{1}{NL}\int_0^L \Gamma' n_0 dx = -\frac{1}{N} D\langle n_0'^2\rangle, \quad \text{(A.15)}$$

$$\frac{dJ_n}{dt} - \frac{1}{L}\int_0^L \Gamma' n_0 dx = (g_n - g_B)\Gamma + \sigma(\langle\tilde{\varphi}\tilde{n}\rangle - 1.71\langle\tilde{T}_e\tilde{n}\rangle - \langle\tilde{n}^2\rangle) - D\langle|\nabla\tilde{n}|^2\rangle. \quad \text{(A.16)}$$

Here, $W(x) = -\frac{1}{L}\int_0^L \frac{\partial\tilde{\varphi}}{\partial x}\frac{\partial\tilde{\varphi}}{\partial y} dy$ is the y-averaged Reynolds shift; $Q(x) = Q_i(x) + Q_e(x) + \left(1 + \frac{T_{Si}}{T_{Se}}\right)\Gamma(x)$ is the y-averaged heat flux; the prime denotes the derivative with respect to x; the angle brackets stand for spatial averaging, $\langle\ldots\rangle = \frac{1}{L^2}\int_0^L\int_0^L \ldots dxdy$, a $Q_i(x) = -\frac{1}{L}\int_0^L \tilde{T}_i\frac{\partial\tilde{\varphi}}{\partial y} dy$, $Q_e(x) = -\frac{1}{L}\int_0^L \tilde{T}_e\frac{\partial\tilde{\varphi}}{\partial y} dy$, $\Gamma(x) = \frac{1}{L}\int_0^L \tilde{n}\frac{\partial\tilde{\varphi}}{\partial y} dy$, $Q = \frac{1}{L}\int_0^L Q(x) dx$, $U = \langle\varphi_0'^2\rangle^{1/2}$ is the amplitude of the sheared flow velocity; $I = \langle|\nabla\tilde{\varphi}|^2/2\rangle$ is the kinetic energy of the turbulent fluctuations; $\Theta_i = \langle T_{i0}^2\rangle^{1/2}$, $\Theta_e = \langle T_{e0}^2\rangle^{1/2}$, and $N = \langle n_0^2\rangle^{1/2}$ are the amplitudes of the deviations of the y-averaged temperature and density profiles from the linear profiles; $J_f = \langle\tilde{f}^2/2\rangle$; and $\tilde{f} = \tilde{T}_i, \tilde{T}_e, \tilde{n}$ is the thermal energy of the fluctuations. The nonlinear terms that describe energy exchange between the averaged-profile plasma and the fluctuations are evaluated by integrating by parts with allowance for the relationship $\int_0^L \frac{\partial}{\partial y}(\ldots) dy = 0$ under the periodic boundary conditions, e.g.,

$$\langle\varphi_0[\mathbf{e}_\zeta\times\nabla\tilde{\varphi}]\cdot\nabla\Delta\tilde{\varphi}\rangle = -\langle\tilde{\varphi}[\mathbf{e}_\zeta\times\nabla\varphi_0]\cdot\nabla\Delta\tilde{\varphi}\rangle = \left\langle\varphi_0'\frac{\partial\tilde{\varphi}}{\partial y}\frac{\partial^2\tilde{\varphi}}{\partial x^2}\right\rangle = -\frac{1}{L^2}\int_0^L\int_0^L \varphi_0'\frac{\partial}{\partial x}\left(\frac{\partial\tilde{\varphi}}{\partial x}\frac{\partial\tilde{\varphi}}{\partial y}\right) dxdy = \frac{1}{L}\int_0^L W'\varphi_0' dx. \quad \text{(A.17)}$$

Equations (A.9)–(A.16) manifest the energy conservation law even in the absence of dissipation:

$$\frac{d}{dt}\left(\frac{U^2}{2} + I + \frac{\Theta_i^2}{2} + J_i + \frac{\Theta_e^2}{2} + J_e + \left(1 + \frac{T_{Si}}{T_{Se}}\right)\left(\frac{N^2}{2} + J_n\right)\right) = g_{Ti}Q_i + g_{Te}Q_e + \left(1 + \frac{T_{Si}}{T_{Se}}\right) g_n\Gamma. \quad \text{(A.18)}$$

The finite-dimensional set of equations (10)–(17) was derived with the minimum number of harmonics (7) needed to describe the three-wave interaction and the generation of a sheared flow. In order to exactly satisfy the energy conservation law for a truncated Fourier expansion, we substituted the set of harmonics (7) into equations (A.9)–(A.16) rather than into (1)–(4). The solution to equations (1)–(4) is well approximated by a set of harmonics (7) such that the first harmonic is unstable, while the second harmonic, which ensures the stabilization of the first harmonic, is stable. In this case, the second (damped) harmonic serves as a sink of the energy released by the pressure gradient during the interchange instability. Of course, if the pressure gradient in the TL is far above the threshold, then there exists a "tail" of harmonics, which ensures cascading of the energy to small-scale fluctuations through which the energy is dissipated. In our model, energy dissipation by the "tail" harmonics is described by appropriately adjusting the numerical factor in front of the seed coefficients of viscosity, diffusivity, and thermal diffusivity. This factor was determined from the calibration calculations and their comparison with the experiment.

Let us present the estimates required for switching from equations (A.9)–(A.16) to the finite-dimensional set of equations (10)–(17):

$$W \approx (k_x k_y/k) X_c \varphi_{2s}(-0.5\cos k_x x \sin 2k_x x + \sin k_x x \cos 2k_x x), \quad \frac{1}{L}\int_0^L W'\varphi_0' dx \approx -\frac{3k_x^2 k_y}{8k} V X_c \varphi_{2s} \approx \frac{3k_x^2 k_y}{80k}\tau V^2 X_c^2 \equiv V_1 V^2 X^2, \quad \text{(A.19)}$$

where, to the lowest order, we have $X = X_c/2$. In (A.19), we also took into account the fact that the second harmonic is generated as a result of the nonlinear interaction between the first harmonic and the sheared flow. Then, from equation (1), we can estimate the amplitude of the second harmonic,

$$(4k_x^2 + k_y^2)\frac{\varphi_{2s}}{\tau} \propto -\frac{k_y^3}{2k} V X_c \text{ or } \varphi_{2s} \propto -\frac{\tau}{10} V X_c, \quad \text{(A.20)}$$

where τ is the decay time of the second harmonic. Because of truncation of the Fourier expansion, this time appears to be the parameter of the problem. Since the regular closure procedure is lacking, we are forced to introduce the coefficient V_1, which is determined from the calibration calculations and their comparison

with experiments. Under the assumption that the large-scale turbulence is self-organized, i.e., that $\Delta\varphi \propto -k^2\varphi$, we can use the estimates $\langle \tilde{\varphi}^2 \rangle \approx 2I/k^2$ and $\langle (\Delta\tilde{\varphi})^2 \rangle \approx 2Ik^2$. Recall that the phase shift between the fluctuations of the temperatures, density, and potential was assumed to be $\alpha_k = \pi/2$. Consequently, for correlations of the form $\langle \tilde{f}\tilde{\varphi} \rangle$, where $\tilde{f} = \tilde{T}_i, \tilde{T}_e, \tilde{n}$, we have $\langle \tilde{f}\tilde{\varphi} \rangle = 0$, so that the correlations between the temperature and density fluctuations can be estimated as $\langle \tilde{n}\tilde{T}_e \rangle = 2\sqrt{J_n J_e}$. We present the estimates of the flux and the related convective term for the case of density fluctuations:

$$\Gamma(x) = -\frac{1}{L}\int_0^L \tilde{n}\frac{\partial\tilde{\varphi}}{\partial y}dy \approx \frac{k_y}{2k}X_c Y_s \sin^2 k_x x,$$
$$\frac{1}{L}\int_0^L \Gamma' n_0 dx = \frac{k_x k_y}{4k}X_c Y_s Z = \frac{k_x k_y}{k}XY_n Z_n, \quad \text{(A.21)}$$

where $Y_n = Y_s/2$. Substituting the above estimates into equations (A.9)–(A.16) and switching to the variables V, X, Y, and Z such that $U = V$, $I = X^2/2$, $J_f = Y_f^2/2$, $\Theta_{i,e} = Z_{i,e}$, and $n = Z_n$, we arrive at the generalized Lorentz set of equations (10)–(17).

REFERENCES

1. R. J. Groebner, T. N. Carlstrom, K. H. Burrell, *et al.*, in *Proceedings of 16th International Conference on Fusion Energy, Montreal, 1996* (IAEA, Vienna, 1997), Vol. 1, p. 867.
2. Yu. N. Dnestrovskiĭ, M. V. Ossipenko, and S. V. Tsaun, Fiz. Plazmy **24**, 771 (1998) [Plasma Phys. Rep. **24**, 715 (1998)].
3. G. V. Pereverzev, P. N. Yushmanov, A. Yu. Dnestrovskiĭ, *et al.*, Preprint No. 5358/6, IAÉ (Kurchatov Institute of Atomic Energy, Moscow, 1991).
4. S. I. Braginskii, in *Reviews of Plasma Physics*, Ed. by M. A. Leontovich (Gosatomizdat, Moscow, 1963; Consultants Bureau, New York, 1965), Vol. 1.
5. M. I. Rabinovich and D. I. Trubetskov, in *Introduction to the Theory of Oscillations and Waves* (Nauka, Moscow, 1984), p. 379.
6. M. V. Ossipenko, Fiz. Plazmy **23**, 909 (1997) [Plasma Phys. Rep. **23**, 837 (1997)].
7. J. Q. Dong, W. Horton, R. D. Bengston, and G. X. Li, Phys. Plasmas **1**, 3250 (1994).
8. R. A. Moyer, J. W. Cuthbertson, T. E. Evans, *et al.*, J. Nucl. Mater **241**–**243**, 633 (1997).

Translated by O. E. Khadin

Plasma Physics Reports, Vol. 26, No. 6, 2000, pp. 477–483. Translated from Fizika Plazmy, Vol. 26, No. 6, 2000, pp. 511–518.

TOKAMAKS

Feedback Suppression of Resistive Wall Modes in a Tokamak

A. B. Mikhailovskii and V. D. Pustovitov

Russian Research Centre Kurchatov Institute, pl. Kurchatova 1, Moscow, 123182 Russia

Received September 9, 1999

Abstract—The possibility of feedback suppression of the external kink modes in a tokamak with a resistive wall is studied theoretically, assuming that the stabilizing conductors are located at a certain distance from the wall and without making any assumptions regarding the locations of the magnetic sensors that close the feedback circuit and the parameters (i.e., the particular components of the perturbed magnetic field or magnetic fluxes) measured by the sensors. It is shown that the efficiency of the stabilizing system can generally be analyzed within a two-parameter model. The parameters of the problem are the jump in the logarithmic derivative of the radial magnetic field in the region where the stabilizing conductors are positioned and the ratio of the minor radius of the torus on which the conductors are wound to the radius of the wall. However, specific calculations should be carried out with at least a three-parameter model: the final results should depend on the currents in the conductors and the locations of the conductors and magnetic sensors. The relation between the magnetic parameter in the criterion for the suppression of the resistive wall modes and the currents in the stabilizing conductors is clarified, and the current magnitudes required for the suppression are estimated. © *2000 MAIK "Nauka/Interperiodica".*

1. INTRODUCTION

Mikhailovskii and Kuvshinov [1] treated the problem of feedback suppression of the so-called resistive wall modes (RWMs) (specifically, external kink modes excited due to the wall resistivity [2]), assuming that the magnetic sensors measuring the local values of the perturbed magnetic field and the stabilizing conductors are located just behind the wall. In this study, we assume that the stabilizing conductors are placed at a certain distance from the wall and do not make any assumptions regarding the magnetic measurements and the locations of the magnetic sensors required to close the feedback circuit. The main objective of this paper is to analyze the condition for suppression of the external kink modes in a tokamak as a function of the distance between the stabilizing conductors and the wall. This problem is of current interest because RWMs may be a serious obstacle to confinement of high-pressure plasmas in tokamaks [3]; in particular, solving this problem is important for obtaining reliable estimates of the parameters in the ITER design [4].

The capabilities and efficiency of any stabilizing feedback system depend on the way in which it is arranged. Four versions of feedback systems for suppressing RWMs, which differ in the choice of the signal that initiates the system response, were considered in a recent paper by Okabayashi *et al.* [5]. Here, we do not restrict ourselves to treating particular versions but discuss the general physical criterion for suppressing RWMs, which is the starting point for choosing a scheme for stabilization by active external means. As an example of how to apply the general criterion to a feedback system, we will calculate the currents in the stabilizing conductors needed to suppress RWMs (in [1], the currents were characterized by a parameter whose physical meaning remained unspecified).

In [1, 2], the feedback stabilization problem was treated in cylindrical geometry, in which case the RWMs appeared because the longitudinal current density profile was not optimal. Such modes can be referred to as cylindrical RWMs. However, from the standpoint of the possibility of confining high-temperature plasmas in tokamaks, it is of interest to study another type of external kink modes, specifically, the modes that are driven by the plasma pressure gradient and that can be referred to as toroidal RWMs. The toroidal RWMs, which were first observed in the experiments performed by Turnbull *et al.* [6], limit the maximum possible β values in tokamaks. In contrast to cylindrical RWMs, which are perturbations with one poloidal mode number, toroidal RWMs are modes with different poloidal numbers, coupled to each other through the dependence of the magnetic field on the poloidal angle. This circumstance makes it difficult to analyze toroidal RWMs theoretically and, in particular, to study the feedback suppression of RWMs in which we are interested here.

To simplify the analytic description, Mikhailovskii and Kuvshinov [2] developed an approximate model of toroidal RWMs. In the approach taken in [2], one of the perturbation modes is regarded as fundamental, while the others are treated as satellites and are assumed to be important only in the plasma region. This makes it possible to describe the perturbations on the outside of the

1063-780X/00/2606-0477$20.00

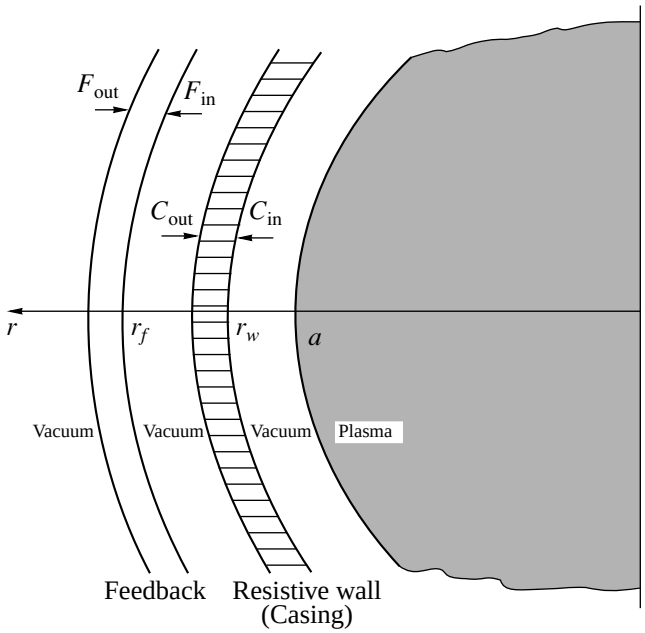

Fig. 1. Geometry of the problem and the main symbols.

wall in the cylindrical approximation. Here, we also apply this approach, treating the influence of the feedback system in the cylindrical approximation. In this case, the role of toroidal effects consists in determining the so-called dimensionless instability growth rate (which will be introduced below) in the absence of feedback. According to [7], this growth rate is governed by the equilibrium parameters of a particular discharge and can be obtained from one-dimensional simulations. We treat the dimensionless growth rate as a free parameter and, for illustration, explain its physical meaning in the case of cylindrical RWMs in a plasma with a step profile of the longitudinal current density [1, 2].

In Section 2, we formulate the problem and present the basic equations. In Section 3, we derive a dispersion relation [see (12) below] showing that the feedback efficiency can be characterized in terms of only two parameters, which will be denoted by W_m and y. The quantity W_m is proportional to the jump in the logarithmic derivative of the radial magnetic field in the region where the stabilizing conductors are located and is defined below by formula (9). The quantity y, whose definition is given after formula (13), is the ratio of the minor radius of the torus on which the conductors are wound to the radius of the wall.

Clearly, the parameter W_m is governed by the current in the stabilizing conductors, which is responsible for the jump in the derivative of the radial magnetic field. However, W_m is the ratio of this jump to the magnitude of the total radial magnetic field in the same region (i.e., in the region where the stabilizing conductors are positioned). Since the total radial field should be determined from magnetic measurements, the feedback efficiency is also governed by the type of magnetic detectors and their locations. Consequently, the problem of stabilizing the RWMs should involve at least three parameters: the final result should depend on both the coil currents and the location of the conductors and magnetic detectors. To simplify matters, in Section 4, we first analyze the problem in terms of two parameters, W_m and y. Then, in Section 5, we clarify the meaning of the quantity W_m as a function of the coil currents and the location of the active coils and magnetic detectors. We also present the results of particular calculations carried out with allowance for the third parameter. Final remarks and some estimates are given in Section 6.

2. FORMULATION OF THE PROBLEM AND BASIC EQUATIONS

We assume that the plasma column ($0 < r < a$, where r is the radial coordinate) is surrounded by a vacuum region ($a < r < r_w$) and a conducting wall ($r_w < r < r_w + d$). The thicknesses of both the vacuum gap and the wall ($r_w - a$ and d, respectively) are assumed to be small in comparison with a. The conductivity of the medium surrounding the wall is negligible, so, for simplicity, the surrounding medium can be regarded as a vacuum. Outside the wall, a set of helical stabilizing conductors is arranged in the region $r_f < r < r_f + \delta$. The transverse size δ of the conductor region is also assumed to be small compared to a. The magnetic detectors (sensors) are positioned somewhere between the wall and the feedback coils. At this point, we do not specify the type of sensors or their locations, which are to be determined after we formulate the physical requirements for the stabilization system. Figure 1 shows the geometry of the problem and the corresponding notation.

One of the key equations in our problem is the equation for the radial component $\tilde{B}_r$ of the magnetic field of the fundamental perturbation mode in the wall region (see equation (9) in [1] or equation (5) in [2]):

$$\tilde{B}_r'' = 4\pi\sigma\gamma\tilde{B}_r/c^2, \qquad (1)$$

where σ is the wall conductivity, γ is the instability growth rate, c is the speed of light, and the prime denotes the derivative with respect to r. We assume that the perturbations depend on time as $\exp(\gamma t)$ and that $\tilde{B}_r$ depends on the poloidal and toroidal angles, θ and ζ, as $\exp[i(m\theta - n\zeta)]$, where m is the number of the fundamental poloidal mode and n is the toroidal number of the perturbation. For simplicity, we usually omit the exponential factors in the perturbed quantities.

Assuming that $\tilde{B}_r$ changes insignificantly on spatial scales of about the wall thickness, we obtain from (1)

$$\left.\frac{r\tilde{B}_r'}{\tilde{B}_r}\right|_{C_{in}}^{C_{out}} = \hat{\gamma}, \qquad (2)$$

where $\hat{\gamma} = \gamma/\gamma_D$ is the dimensionless growth rate and $\gamma_D = c^2/(4\pi\sigma da)$ is the reciprocal of the skin time of the wall. In writing (2), we took into account the approximate equality $r_w \simeq a$. Here and below, C_{in} indicates that a function should be calculated at the inner surface of the wall ($r = r_w$) and C_{out} refers to the outer surface (see Fig. 1).

According to equation (9) in [2],

$$(\ln\tilde{B}_r)'_{r_w} \simeq (\ln\tilde{B}_r)'_{a+\varepsilon} = [\ln(\mu - n/m)X_m]'_{a-\varepsilon}, \quad (3)$$

where X_m is the mth harmonic of the radial displacement of the perturbed plasma, $\mu = 1/q$, q is the safety factor, and ε is an infinitesimal quantity. Hence, equation (2) reduces to

$$\hat{\gamma} = \Gamma + \left.\frac{r\tilde{B}'_r}{\tilde{B}_r}\right|_{C_{\text{out}}} + (m+1), \quad (4)$$

with Γ the dimensionless instability growth rate in the absence of feedback,

$$\Gamma = -(m+1) - a[\ln(\mu - n/m)X_m]'_a. \quad (5)$$

In particular, for a cylindrical plasma with a steplike current density profile (the current is nonzero only in the region $0 < r < a_0$), Γ has the form [1, 2]

$$\Gamma = -2m\frac{m - nq_0 - 1}{m - nq_0 - 1 + (a_0/r_w)^{2m}}, \quad (6)$$

where $q_0 = q(0)$. For a plasma described in toroidal geometry, Γ is determined by the right-hand side of formula (55) in [2].

With the approach adopted here, the problem of the influence of feedback on RWMs reduces to that of calculating the logarithmic derivative of the radial field component $\tilde{B}_r$ in (4) as a function of the location of the feedback coils and the amplification coefficient of the feedback system. This is the subject of Section 3.

3. DERIVATION OF THE DISPERSION RELATION

In the gap between the wall and the stabilizing conductors (a region free of coils and currents), the amplitude of the radial component of the perturbed magnetic field $\tilde{\mathbf{B}}$ depends on the radius as

$$\tilde{B}_r(r) = C(r^{m-1} + Dr^{-m-1}), \quad (7)$$

where C and D are constants. Consequently, at the inner surface of the conductor region (F_{in}, Fig. 1), we have

$$\left.\frac{r\tilde{B}'_r}{\tilde{B}_r}\right|_{F_{\text{in}}} = \frac{m - 1 - (m+1)Dr_f^{-2m}}{1 + Dr_f^{-2m}}. \quad (8)$$

To find D, we can specify the jump in the derivative of the radial component $\tilde{B}_r$, driven by the currents flowing in the stabilizing conductors, by the expression

$$\left.\frac{r\tilde{B}'_r}{\tilde{B}_r}\right|_{F_{\text{in}}}^{F_{\text{out}}} = 2mW_m, \quad (9)$$

which is analogous to (7) in [1] (namely, the quantity $2mW_m$ corresponds to W in [1]). We also take into account the relationship

$$\left.\frac{r\tilde{B}'_r}{\tilde{B}_r}\right|_{F_{\text{out}}} = -(m+1), \quad (10)$$

which is valid in the vacuum region surrounding the stabilizing conductors. The last three formulas yield

$$Dr_f^{-2m} = -\left(1 + \frac{1}{W_m}\right). \quad (11)$$

With (7) and (11), expression (4) becomes

$$\hat{\gamma} = \Gamma - 2mf_m, \quad (12)$$

where

$$f_m \equiv \frac{W_m}{y^{2m} + W_m(y^{2m} - 1)} \quad (13)$$

and $y = r_f/r_w$. Note that the dimensionless growth rate (12) can be rewritten as

$$\hat{\gamma} = -\left.\frac{r\tilde{B}'_r}{\tilde{B}_r}\right|_{C_{\text{in}}} - (m+1) - 2mf_m. \quad (14)$$

In the limit $W_m \longrightarrow 0$, expression (12) gives $\hat{\gamma} = \Gamma$. This explains why the quantity Γ was called the dimensionless instability growth rate in the absence of feedback.

4. ANALYSIS OF THE DISPERSION RELATION IN THE TWO-PARAMETER PROBLEM

According to (12), the condition for feedback suppression of the instability is

$$2mf_m > \Gamma. \quad (15)$$

For $y = 1$ (when the stabilizing conductors are positioned just behind the wall), condition (15) becomes $W_m > \Gamma/2m$, in accordance with the results of [1]. However, for $y \neq 1$, condition (15) can be satisfied not only in the range $W_m > 0$ (we regard this as the first operating mode of the feedback system) but also in the range $W_m < 0$ (which will be regarded as the second operating mode). In Section 4.1, we present the general results of the analysis of these two cases. In Section 4.2, we discuss the conditions under which one or another case would be beneficial.

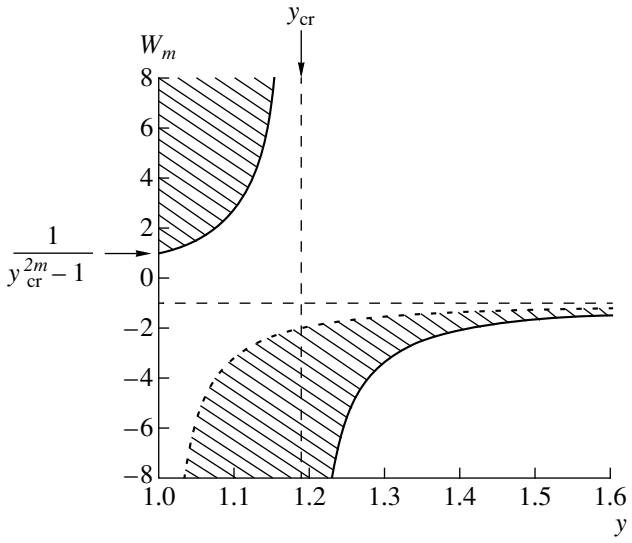

Fig. 2. Feedback stabilization of RWMs for $m = 2$ and $y_{cr}^{2m} = 2$ ($\Gamma = 2m$). The hatched regions in the ($W_m = y = r_f/r_w$) plane show the domains in which the instability can be suppressed. The domain boundaries (the branches of the curve $W_m = y^{2m}/(y_{cr}^{2m} - y^{2m})$) are shown by heavy lines. The dashed curve corresponds to $W_m = y^{2m}/(1 - y^{2m})$.

4.1. General Results

For $y \neq 1$ and $W_m > 0$, condition (15) can be rewritten as

$$W_m > \frac{\Gamma y^{2m}}{2m - \Gamma(y^{2m} - 1)}, \tag{16}$$

in which case the instability can be suppressed only if the gap between the wall and the stabilizing conductors is not too large,

$$y < y_{cr}, \tag{17}$$

where the critical value y_{cr} of y is defined as

$$y_{cr}^{2m} \equiv 1 + \frac{2m}{\Gamma}. \tag{18}$$

Condition (17) can also be represented as a restriction on the thickness of the gap between the conducting wall and the set of stabilizing conductors,

$$\frac{r_f - r_w}{r_w} = y - 1 < \left(1 + \frac{2m}{\Gamma}\right)^{\frac{1}{2m}} - 1. \tag{19}$$

For large values of Γ, the quantity y_{cr} is close to unity. Consequently, in this case, restrictions (17) and (19) appear to be fairly stringent.

Since the physical meaning of the problem implies that $\Gamma > 0$ and $y \geq 1$, condition (16) indicates that, for $y > 1$, the mode stabilization requires larger values of W_m and, accordingly, higher currents in the stabilizing coils in comparison with those analyzed in [1] for the case $y = 1$.

The quantity y is governed by the design of the device and should be fixed, while Γ can change depending on the discharge parameters. The higher the growth rate Γ, the smaller the critical value y_{cr}. As the quantity y_{cr} approaches y, condition (16) becomes progressively more difficult to satisfy. To see this, we rewrite (16) as

$$W_m > \frac{y^{2m}}{y_{cr}^{2m} - y^{2m}}. \tag{20}$$

Since, in practice, the parameter W_m can only be finite, requirement (20) is sometimes impossible to satisfy even when condition (17) holds.

Going over from $y = 1$ to larger values of y makes condition (20) more restrictive. On the other hand, for $y \neq 1$, there is another way to satisfy the stabilization condition (15): along with trying to satisfy (20), we can turn to the range $W_m < 0$. Recall that inequality (16) follows from (15) if the denominator in (13) is positive, which corresponds to positive values of W_m. However, expression (13) implies that, for $y > 1$, criterion (15) can also be satisfied when W_m is negative. For $y < y_{cr}$, criterion (15) holds in the range

$$W_m < -\frac{y^{2m}}{y^{2m} - 1}. \tag{21}$$

For $y > y_{cr}$, criterion (15) is satisfied for W_m lying in the interval

$$-\frac{y^{2m}}{y^{2m} - y_{cr}^{2m}} < W_m < -\frac{y^{2m}}{y^{2m} - 1}. \tag{22}$$

The two domains where RWMs can be stabilized are displayed in Fig. 2.

4.2. Comparison between Two Possible Operating Modes of the Feedback System

Mathematically, the two operating modes are described by the two branches of the function f_m shown in Fig. 3. The right branch reflects inequality (20), and the left branch corresponds to (21) and (22). In the limit $y \longrightarrow 1$ (as the distance between the stabilizing conductors and the wall tends to zero), the right branch degenerates into a straight line and the left branch approaches infinity; consequently, the only way to stabilize RWMs is that treated in [1].

For $y > 1$, in the operating mode described by the right branch, it is possible to suppress only the modes that grow at a rate

$$\Gamma < \Gamma_{cr}, \tag{23}$$

where

$$\Gamma_{cr} \equiv \frac{2m}{y^{2m}-1}. \quad (24)$$

The higher the growth rate Γ, the larger the required values of W_m. For the operating mode described by the left branch, the stabilization condition (15) can be satisfied at any value of Γ: it is sufficient to hold W_m close to the upper limit in (21) and (22), which is independent of y_{cr} and is finite. In contrast, for the operating mode described by the right branch, the values of W_m that are required to satisfy the stabilization condition for RWMs with high Γ (which should be, however, lower than the critical growth rate Γ_{cr}) may be infinitely large.

According to (9), the parameter W_m is proportional to the currents flowing in the stabilizing conductors of the feedback system, so that large W_m values are undesirable. Consequently, the left branch seems to be more attractive from the standpoint of stabilizing RWMs with

$$\Gamma > \Gamma_{cr}/2, \quad (25)$$

where Γ_{cr} is defined by (24), because the W_m values required for suppression are smaller than those on the right branch. In contrast, for $\Gamma < \Gamma_{cr}/2$, the more preferable operating mode appears to be that described by the right branch.

5. THE W_m PARAMETER

According to (9), the parameter W_m depends only on $\tilde{B}_r'$ and $\tilde{B}_r$. The jump in the derivative $\tilde{B}_r'$ is governed exclusively by the currents in the stabilizing conductors, which serve as a controlled active element of the feedback system. However, since the currents flowing in the plasma and in the wall also contribute to the total field $\tilde{B}_r$, it should be determined from measurements with magnetic detectors that close the feedback circuit.

Since the thickness of the layer where the stabilizing conductors are arranged is assumed to be small in comparison with r_f, the denominator in (9) should be taken with $\tilde{B}_r(r_f)$. We also assume that the magnetic probes positioned somewhere on the outside of the wall allow measurements of $\tilde{B}_r$ at the radius $r = r_s$, which generally differs from r_f (here, r_s is the radial coordinate of the magnetic sensors). The desired quantity $\tilde{B}_r(r_f)$ can be expressed in terms of $\tilde{B}_r(r_s)$ with the help of (7) and (11):

$$\left(\frac{r_s}{r_f}\right)^{m+1}\frac{\tilde{B}_r(r_s)}{\tilde{B}_r(r_f)} = W_m\left[1-\left(\frac{r_s}{r_f}\right)^{2m}\right]+1. \quad (26)$$

With this relationship, we obtain from (9)

$$\frac{1}{W_m} = \frac{\tilde{B}_r(r_s)}{Y}\left(\frac{r_s}{r_f}\right)^{m+1} - \left[1-\left(\frac{r_s}{r_f}\right)^{2m}\right], \quad (27)$$

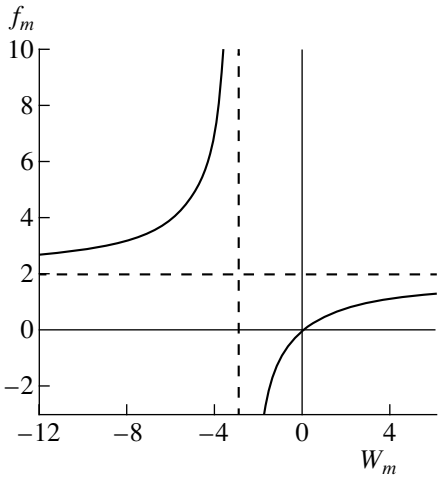

Fig. 3. Plot of the function $f_m(W_m)$ for $y^{2m} = 1.5$. The dashed lines show the horizontal ($f_m = 1/(y^{2m}-1)$) and vertical ($W_m = -y^{2m}/(y^{2m}-1)$) asymptotes.

where

$$Y \equiv \frac{1}{2m} r\tilde{B}_r'\Big|_{F_{in}}^{F_{out}}. \quad (28)$$

To evaluate Y in (27), we must specify the currents in the stabilizing conductors, which should produce the field $\tilde{B}_r \propto \exp[i(m\theta - n\zeta)]$. Such a field can be driven, e.g., by oppositely directed currents flowing in $2m$ helical coils that are wound around a torus of radius $r = r_f$ [8]:

$$i_\zeta^k = \frac{J_f}{r_f}(-1)^k\delta(r-r_f)\delta\left(\varphi-\alpha z-\frac{\pi k}{m}\right), \quad k = 0, 1, \ldots, 2m-1. \quad (29)$$

Here, i_ζ^k is the longitudinal current density in the kth coil; J_f is the current magnitude in each coil; and

$$\varphi - \alpha z = \theta - \frac{n}{m}\zeta - \theta_0, \quad (30)$$

where θ_0 is a constant, which will be used below in order to properly choose the phase of the stabilizing field $\tilde{B}_r$. The notation $\varphi - \alpha z$ is introduced for convenience in comparing our results with the results obtained by Morozov and Solov'ev [8] (we are working in conventional cylindrical coordinates r, φ, and z). The net current density can be obtained by summing up i_ζ^k over all of the coils:

$$i_\zeta = \frac{2mJ_f}{\pi r_f}\delta(r-r_f)\sum_{k=0}^{\infty}\cos[m(2k+1)(\varphi-\alpha z)]. \quad (31)$$

Retaining only the first term and setting $\theta_0 = 0$, we obtain the distribution i_ζ examined in [1]. However, below we will show that our problem requires another choice of θ_0.

The potential of the magnetic field produced by a set of coils with currents (29) was calculated in [8]. Using formula (5.59) from that paper, we obtain

$$r\tilde{B}_r'\Big|_{F_{\text{in}}}^{F_{\text{out}}} = C_0\sum_{k=0}^{\infty} N\alpha\left(\frac{N^2}{x_0^2}+1\right)\sin[N(\varphi-\alpha z)], \quad (32)$$

where

$$C_0 = \frac{8mJ_f\alpha r_f}{c}, \quad (33)$$

$$N = m(2k+1), \quad x_0 = N\alpha r_f. \quad (34)$$

In accordance with (29), we neglected the coil thickness in (32).

We only need the first harmonic in the exact equality (32) (in the approximation $\alpha r_f \ll 1$):

$$r\tilde{B}_r'\Big|_{F_{\text{in}}}^{F_{\text{out}}} = C_0\frac{m}{\alpha r_f^2}\sin[m(\varphi-\alpha z)]. \quad (35)$$

Up to this point, we assumed that $\tilde{B}_r \propto \exp[i(m\theta - n\zeta)]$. To keep this dependence in (35), we must set

$$\theta_0 = -\frac{\pi}{2m}, \quad (36)$$

in which case the fundamental harmonic of the quantity Y in (27) has the form

$$Y \equiv \frac{1}{2m}r\tilde{B}_r'\Big|_{F_{\text{in}}}^{F_{\text{out}}} = \frac{4J_f m}{cr_f}\cos(m\theta - n\zeta), \quad (37)$$

so that the parameter W_m can be found simply by substituting (37) into (27).

Now, we go over to a description of the suppression of RWMs in terms of the three-parameter problem mentioned above.

Equality (27) suggests that we can take the quantity

$$U = \frac{Y}{\tilde{B}_r(r_s)} \quad (38)$$

as one of the parameters of the problem. Physically, this is the ratio of the current in the stabilizing conductors to the perturbed magnetic field measured by the probes. Using (27), we express W_m through U and insert it into (13) to arrive at the following expression for the function f_m, which characterizes the operation efficiency of the feedback system:

$$f_m = \frac{U}{y^{m-1}s^{m+1} + U(s^{2m}-1)}, \quad (39)$$

where $s = r_s/r_w$ is the ratio of the radius at which the probes are located to the radius of the wall. The function f_m is seen to depend on the quantities U, y, and s, which are just the aforementioned three parameters of the problem.

Let us analyze formula (39) in the following two limiting cases.

A. The probes are positioned near the stabilizing conductors (s = y)

For $s = y$, relationship (39) reduces to

$$f_m = \frac{U}{y^{2m} + U(y^{2m}-1)}, \quad (40)$$

in which case U coincides with W_m. This indicates that, in the limiting case at hand, the general results obtained in Section 4 can be used directly in particular calculations.

B. The probes are positioned near the wall (s = 1)

For $s = 1$, formula (39) becomes

$$f_m = \left(\frac{r_w}{r_f}\right)^{m-1}U. \quad (41)$$

Clearly, under these conditions, the feedback system for suppressing RWMs can operate only in the first of the two possible operating modes discussed in Section 4.

Formula (41) makes it possible to determine the amount by which the current in the stabilizing conductors should be increased as the conductors are displaced away from the conducting wall, provided that the magnetic probes remain near the wall.

6. FINAL REMARKS AND ESTIMATES

Relationships (16), (20)–(22), (27), and (37) allow us to estimate the current in the stabilizing conductors that is required to suppress RWMs, and formulas (38)–(41) can be used to express the result obtained in terms of the perturbed magnetic field $\tilde{B}_r$ measured by the magnetic probes arranged at different radial locations.

Let us make some estimates for the above two limiting cases, in which the magnetic detectors are positioned either at the same radius as the stabilizing conductors (case A) or near the wall (case B).

A. Case $r_s = r_f$ (the probes are far from the wall)

We assume that the magnetic detectors (Mirnov probes) measuring the perturbed field $\tilde{B}_r$ are placed at the same radial position as the stabilizing conductors, in which case it is more convenient to operate with the

parameter W_m. Using (27) and (37), we can represent it in the form

$$W_m = 2m\frac{B_f}{\tilde{B}_r(r_f)}, \quad (42)$$

where

$$B_f \equiv \frac{2J_f}{cr_f} \quad (43)$$

is the field produced by the current J_f flowing in a straight conductor at a distance r_f from the conductor. Clearly, the currents required to suppress RWMs are governed by the discharge parameters (in our model, these currents are functions of the parameter Γ). According to (6), we estimate Γ as $\Gamma = 2m$, in which case the stabilization condition (16) for RWMs in the operating mode described by the right branch in Fig. 1 reduces to

$$\frac{W_m}{2m} = \frac{B_f}{\tilde{B}_r(r_f)} > \frac{1}{2m}\frac{y^{2m}}{2-y^{2m}}. \quad (44)$$

As an example, we take $y^{2m} = 1.5$ (or $\Gamma_{cr} = 4m$). This corresponds to the choice $r_f/r_w \simeq 1.11$ for $m = 2$ and the choice $r_f/r_w \simeq 1.07$ for $m = 3$. With these parameter values, criterion (44) becomes $W_m > 3$ for any value of m. For comparison, note that, in the case $y = 1$, which was considered in [1], condition (44) gives $W_m > 1$. Consequently, when there is a gap between the wall and the set of stabilizing conductors, the values of W_m should be several times larger than those in the absence of the gap ($y = 1$). However, for $y > 1$, the stabilization condition (44) remains rather modest: the field B_f should be approximately the same as the measured field $\tilde{B}_r(r_f)$.

Formulas (21) and (22) allow us to conclude that, for $y^{2m} = 1.5$, the stabilization condition at the left branch of the function f_m in Fig. 3 should have the form $W_m < -3$.

For $m = 2$, the value $|W_m| = 4$, at which both of the stabilization conditions in the example at hand are satisfied, is reached at $B_f = \tilde{B}_r(r_f)$. Setting this field to be equal to 2 G and taking $r_f = 200$ cm, we can see that the current in the stabilizing conductors should be as high as $J_f = 2$ kA.

B. Case $r_s = r_w$ (the probes are close to the wall)

For $r_s = r_w$, formulas (15) and (41) enable us to represent the condition for feedback suppression of the RWMs as

$$U > \frac{\Gamma}{2m}\left(\frac{r_f}{r_w}\right)^{m-1}, \quad (45)$$

where, with allowance for (37) and (43), the quantity U defined in (38) has the form

$$U = 2m\frac{B_f}{\tilde{B}_r(r_s)}. \quad (46)$$

For $\Gamma = 2m$, condition (45) reduces to

$$\frac{B_f}{\tilde{B}_r(r_s)} > \frac{y^{m-1}}{2m}, \quad (47)$$

(recall that $y = r_f/r_w$). A comparison with (44) shows that the ratio of the desired field B_f to the measured field $\tilde{B}_r(r_s)$ turns out to be smaller than that in the case in which the probes are located far from the wall. In particular, for $y^{2m} = 1.5$, the field B_f required for the suppression of RWMs is several times lower than $\tilde{B}_r(r_s)$.

ACKNOWLEDGMENTS

We are grateful to Y. Shimomura and V.S. Mukhovatov for bringing the stabilization problem to our attention and stimulating discussions. We also thank B.N. Kuvshinov for helping with the work. This work was supported in part by the Russian Foundation for Basic Research, project no. 96-15-96815 (under the program “Leading Scientific Schools”).

REFERENCES

1. A. B. Mikhailovskii and B. N. Kuvshinov, Fiz. Plazmy **22**, 188 (1996) [Plasma Phys. Rep. **22**, 172 (1996)].
2. A. B. Mikhailovskii and B. N. Kuvshinov, Fiz. Plazmy **21**, 835 (1995) [Plasma Phys. Rep. **21**, 789 (1995)].
3. T. S. Taylor, E. J. Strait, L. L. Lao, *et al.*, Phys. Plasmas **2**, 2390 (1995).
4. Y. Shimomura and V. S. Mukhovatov, private communication.
5. M. Okabayashi, N. Pomphrey, and R. E. Hatcher, Nucl. Fusion **38**, 1607 (1998).
6. A. D. Turnbull, T. S. Taylor, E. J. Strait, *et al.*, in *Proceedings of 15th International Conference on Plasma Physics and Controlled Nuclear Fusion Research, Seville, 1994* (IAEA, Vienna, 1995), Vol. 1, p. 705.
7. B. N. Kuvshinov and A. B. Mikhailovskii, Fiz. Plazmy **22**, 490 (1996) [Plasma Phys. Rep. **22**, 446 (1996)].
8. A. I. Morozov and L. S. Solov’ev, in *Reviews of Plasma Physics*, Ed. by M. A. Leontovich (Gosatomizdat, Moscow, 1963; Consultants Bureau, New York, 1966), Vol. 2.

Translated by I. A. Kalabalyk

Plasma Physics Reports, Vol. 26, No. 6, 2000, pp. 484–492. Translated from Fizika Plazmy, Vol. 26, No. 6, 2000, pp. 519–528.

MAGNETIC CONFINEMENT SYSTEMS

Pressure Profiles of a Plasma Confined by the Magnetic Field of a Ring Current

P. A. Popovich* and V. D. Shafranov**

**Moscow Engineering Physics Institute, Kashirskoe sh. 31, Moscow, 115409 Russia*

***Russian Research Centre Kurchatov Institute, pl. Kurchatova 1, Moscow, 123182 Russia*

Received September 23, 1999; in final form, December 23, 1999

Abstract—Pressure profiles $p(\psi)$ marginal with respect to convective instability in a toroidal tubular plasma confined by the magnetic field of an internal levitated ring current and external ring currents are studied as functions of the shape of the magnetic separatrix. Configurations are found in which the maximum plasma pressure in a finite-width layer near the plasma boundary decreases by two orders of magnitude at the expense of artificially raising the effective length (characterized by the integral $\oint dl/B$) of the magnetic field lines near the separatrix surface. It is shown that, in the case of a straight cylindrical tubular plasma, which is the limiting case of a toroidal configuration with an arbitrarily large aspect ratio, the sufficient condition for the plasma to be MHD stable against both convective and kink perturbations is satisfied for local values $\beta \le 0.4$. © *2000 MAIK "Nauka/Interperiodica".*

1. INTRODUCTION

Research on the creation of a thermonuclear reactor based on magnetic plasma confinement has been carried out for nearly fifty years. The most substantial progress toward achieving fusion parameters has come from experiments on tokamaks; the next are experiments on *steady-state* helical plasma confinement systems, the largest of which are the W7-AS stellarator in Garching (Germany) and the LHD stellarator in Toki (Japan). The advanced W7-X stellarator, which is being constructed in a new thermonuclear research center in Greifswald (Germany), is supposed to be capable of producing plasmas in which the average ratio of plasma to the magnetic field pressure $\langle\beta\rangle$ will be as high as 5%.

Magnetic systems in stellarators, which are fully three-dimensional nonaxisymmetric devices, are rather complicated: the stellarator magnetic field is generated either by continuous helical windings or by modular twisted solenoidal coils. An attractive feature of steady-state axisymmetric devices with no toroidal magnetic field is their simple geometry: the external, purely poloidal, confining magnetic field is created by unidirectional currents flowing in a set of coaxial ring coils (two coils in quadrupole configurations, four coils in octopole configurations, etc.) and the plasma carries only diamagnetic current. Various versions of confinement systems with internal levitated conductors have been reviewed in a recent paper by A.I. Morozov and V.V. Savel'ev [1]. The simplest version seems to be that developed by Akira Hasegawa [2, 3], who proposed to confine plasmas in the magnetic field of one ring coil (a dipole configuration). The magnetic field of a levitated dipole stabilizes kink modes with $m \ge 1$. The inner part of a toroidal tubular plasma is stable, because the magnetic field increases away from the plasma boundary. The pressure profile that forms in the outer part is marginally stable against convective instabilities, in accordance with the familiar Kadomtsev's criterion [4] $p \sim (\oint dl/B)^{-\gamma}$, where $\gamma = 5/3$. Since the profile is gradually decreasing, the volume of confined plasma is very large ($\sim 10^4$ m^3). The shape of the separatrix can be made elliptical by imposing a transverse magnetic field, which weakens the magnetic field of the ring coil in its central region. Because of the presence of the separatrix null points (at which the magnetic field vanishes), the integral $\oint dl/B$ diverges logarithmically, so that, in the vicinity of null points, the maximum pressure consistent with stability tends to zero at a finite plasma volume. This idea underlies the Mirage system proposed by Morozov, Pastukhov, and Sokolov [5].

However, for the configurations under discussion, the plasma pressure profile marginal with respect to convective instability has not yet been calculated, as was done, e.g., by Vabishchevich *et al.* for compact tori [6]. This will be the subject of our paper, which is aimed at studying how the marginal pressure profile depends on the prescribed shape of the separatrix in the presence of the imposed external magnetic field. We solve the equilibrium equation for a toroidal plasma numerically by using the specially devised TuTor (Tubular Toroidal plasma equilibrium) code; the nonlinear right-hand side $p'(\psi)r^2$ (where r is the distance from the major axis of the torus) of the equilibrium equation is determined by Kadomtsev's marginal stability condition. However, we first examine the main equilibrium properties of a tubular plasma, neglecting

1063-780X/00/2606-0484$20.00

the axis curvature and treating, as an example, a cylindrically symmetric plasma configuration.

2. CYLINDRICALLY SYMMETRIC TUBULAR PLASMA

2.1. Equilibrium

For a confinement system with a straight central axial current J_c, the simplest geometric configuration is a hollow circular plasma cylinder. In cylindrical coordinates (ρ, φ, z), the equilibrium equations have the form

$$\frac{dp}{d\rho} = -jB, \tag{1}$$

$$\frac{d(\rho B)}{\rho d\rho} = \mu_0 j \tag{2}$$

(in SI units, $\mu_0 = 4\pi \times 10^{-7}$, so that the magnetic field pressure is $p_m = B^2/2\mu_0$). In a hollow plasma cylinder with an inner radius ρ_1 and outer radius ρ_2, the pressure increases ($p' > 0$) from zero to the maximum value p_0 in the region $\rho_1 \le \rho \le \rho_0$ and falls ($p' < 0$) to zero in the region $\rho_0 \le \rho \le \rho_2$ (Fig. 1). Equation (1) implies that, at the peak of the plasma pressure profile, we have either $B(\rho_0) = 0$ or $j(\rho_0) = 0$. If a tubular Z-pinch is created in the absence of the central current, $J_c = 0$, then the magnetic field changes sign at the surface $\rho = \rho_0$, as in the case with a planar Z-pinch. If the plasma is created in the external magnetic field of the current J_c in the central rod without deliberately generating reverse currents (as is the case with confinement systems), then the magnetic field does not change sign and the density of the pressure gradient–driven diamagnetic current, $j = -(1/B)dp/d\rho$, is negative in the region $\rho < \rho_0$ and is positive in the region $\rho > \rho_0$. In the first region, in which the plasma pressure gradient is directed opposite to the magnetic field gradient, the plasma is stable against flute perturbations. As was shown by Kadomtsev for the case of an ordinary pinch, a gradually decreasing, marginally stable density profile exists in the second region, in which the pressure decreases toward the plasma boundary.

Clearly, the total electric current flowing in the region of radius $\rho > \rho_1$,

$$J(\rho) = 2\pi\rho B(\rho)/\mu_0, \tag{3}$$

is the sum of the rod current J_c and the plasma current $J_p(\rho)$:

$$J(\rho) = J_c + J_p(\rho). \tag{4}$$

In the region $\rho_1 < \rho < \rho_0$, the pressure gradient is positive, while the current density $j(\rho)$ and plasma current

$$J_p^-(\rho) = \int_{\rho_1}^{\rho} j(\rho')2\pi\rho' d\rho' \tag{5}$$

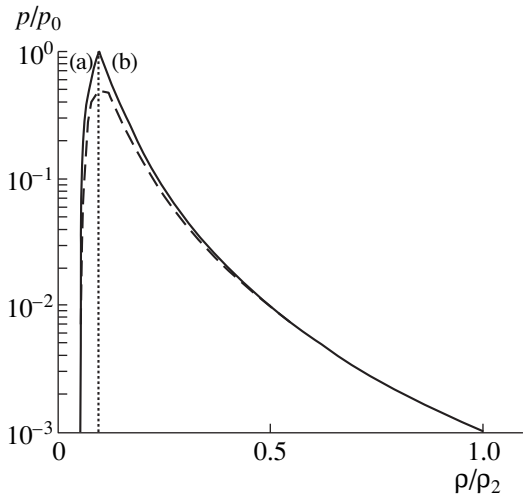

Fig. 1. Plasma pressure profiles in a cylindrical tubular pinch: (a) an arbitrarily increasing pressure profile in the inner part of a tubular plasma and (b) the pressure profile marginal with respect to flute instability (solid curve) in the outer region of a tubular pinch, where the pressure gradient is the largest (the dashed curve corresponds to a smoothed pressure profile, which also satisfies the stability condition).

are both negative, $J_p(\rho) = J_p^-(\rho) < 0$. In the outer region $\rho_0 < \rho < \rho_2$, where the pressure profile is decreasing, $p'(\rho) < 0$, the plasma current

$$J_p^+(\rho) = \int_{\rho_0}^{\rho} j(\rho')2\pi\rho' d\rho' \tag{6}$$

is positive and the total current is represented in the form of the sum in (4) with $J_p(\rho) = J_p^-(\rho_0) + J_p^+(\rho)$, so that we have $2\pi\rho B(\rho) = \mu_0[J_c + J_p^-(\rho_0) + J_p^+(\rho)]$.

In terms of the current $J(\rho)$ in (4), the equilibrium equation (1) becomes

$$p' = -\mu_0 \frac{JJ'}{4\pi^2\rho^2}. \tag{7}$$

Taking the product of (7) with $\pi\rho^2$ and integrating the resulting equation from ρ_1 to ρ_2 yields the Bennet relation for the averaged (over the plasma cross section) pressure $\langle p \rangle$ in a tubular plasma:

$$\begin{aligned} \langle p \rangle S &= \pi[p(\rho_2)\rho_2^2 - p(\rho_1)\rho_1^2] \\ &+ \frac{\mu_0}{8\pi}[J^2(\rho_2) - J^2(\rho_1)], \end{aligned} \tag{8}$$

where $S = \pi(\rho_2^2 - \rho_1^2)$ is the cross-sectional area of the plasma cylinder. Assuming that $p(\rho_1) = p(\rho_2) = 0$, we obtain

$$8\pi\langle p \rangle(\rho_2^2 - \rho_1^2) = \mu_0[J^2(\rho_2) - J^2(\rho_1)]. \tag{9}$$

We introduce the notation $J(\rho_2) = J_2$ and $B(\rho_2) = B_2 = \mu_0 J_2/2\pi\rho_2$ and the averaged parameter β, characterizing plasma confinement,

$$\beta_{av} = 2\mu_0\langle p\rangle/B_2^2 = 8\pi^2\langle p\rangle\rho_2^2/\mu_0 J_2^2. \quad (10)$$

With allowance for $J(\rho_1) = J_c$, we can relate the plasma beta (10) to the geometrical and physical parameters of a tubular plasma:

$$\beta_{av} = \frac{1 - J_c^2/J_2^2}{1 - \rho_1^2/\rho_2^2}, \quad (11)$$

where $J_2 = J_c + J_p$ and $J_p \equiv J_p(\rho_2)$.

The integral relationships derived for β_{av} apply both to the "passive-confinement" case (without externally generated currents), in which the magnetic field does not change sign and $J_2 > J_c$, and to the pinch case, in which the total plasma current can be either positive or negative. Formula (11) implies that the plasma can be in equilibrium ($\beta_{av} > 0$) for $J_2^2/J_c^2 > 1$, i.e., for $(2J_c + J_p)J_p > 0$, regardless of the sign of J_2. Assuming J_c to be positive, we can see that the equilibrium condition is always satisfied if the total plasma current is also positive, $J_p > 0$ (confinement systems). If the total plasma current is directed opposite to the rod current, $J_p < 0$, then the equilibrium condition is satisfied only for plasma currents that exceed the rod current at least by a factor of two, $|J_p| > 2J_c$ (for a tubular pinch with a skinned layer such that $\rho_2 - \rho_1 \ll \rho_2$, this result was obtained by Artsimovich [7]). If the negative plasma current is insufficiently high, $|J_p| < 2J_c$, then the plasma can be maintained in equilibrium only by a longitudinal magnetic field (the straight Hard Core Pinch device [8] and the toroidal Levitron [9, 10]).

Note that, for both cylindrical and toroidal tubular plasmas with a noncircular cross section, it is more convenient to characterize equilibrium by another parameter, specifically, the "invariant" plasma beta

$$\beta_{inv} = 1 - J_c^2/J_2^2. \quad (11a)$$

In the case of a cylindrical plasma, we have $\beta_{inv} = \beta_{av}(1 - \rho_1^2/\rho_2^2)$, so that, clearly, $\beta_{inv} < \beta_{av}$.

Below, we will be interested only in the confinement versions of tubular plasma systems with a current-carrying rod or ring internal to the plasma.

2.2. MHD Stability

Unstable modes are divided into two groups: compressible flute modes ($m = 0$ and $\nabla\cdot\boldsymbol{\xi} \neq 0$) and incompressible kink modes ($m \geq 1$ and $\nabla\cdot\boldsymbol{\xi} = 0$).

Kink perturbations ($m \neq 0$). According to [11, 12], the potential energy of incompressible kink perturbations with $\xi_\rho = \xi(\rho)\exp i\left(\frac{m}{\rho}\varphi + kz\right)$ has the form

$$W = \frac{\pi}{2\mu_0}\int\left\{\frac{1}{m^2 + k^2\rho^2}\left[(k\rho B_z + mB_\varphi)\frac{d\xi}{d\rho} + (k\rho B_z - mB_\varphi)\frac{\xi}{\rho}\right]^2 + \left[(k\rho B_z + mB_\varphi)^2 - 2B_\varphi\frac{d}{d\rho}(\rho B_\varphi)\right]\frac{\xi^2}{\rho^2}\right\}\rho d\rho. \quad (12)$$

For $B_z = 0$, we introduce the notation $X = \xi/\rho$, in terms of which (12) becomes

$$W = \frac{\pi}{2\mu_0}\int\left\{\frac{B^2\rho^2}{1 + k^2\rho^2/m^2}X'^2 + \left[B^2 - \frac{2}{m^2}B\frac{d}{d\rho}(\rho B)\right]X^2\right\}\rho d\rho \quad (13)$$

(here and below, we omit the subscript φ, so that $B = B_\varphi$). The second term in square brackets, $-2B(\rho B)' = -2\mu_0\rho jB$, shows that, if the current density is negative, then the ideal MHD modes are stable (the Rosenbluth criterion) [11]. Note that these formulas apply not only to regions filled entirely with a plasma but also to configurations with a vacuum gap between the plasma and, e.g., the metal chamber (see [12, 13]). In the vacuum region, ξ can be regarded as a fictitious displacement, which is related to the physical quantity—the perturbed radial magnetic field component B_1—by the complex relationship $B_1 = imB(\xi/\rho) = imBX$. The condition for B_1 to vanish at the boundaries of the confinement region coincides with the condition $\xi = 0$. The Euler–Lagrange equation for X is

$$\frac{d}{d\rho}\left(\frac{B^2\rho^2}{1 + k^2\rho^2/m^2}\frac{dX}{d\rho}\right) + \left[\frac{2}{m^2}B\frac{d(\rho B)}{d\rho} - B^2\right]X = 0. \quad (14)$$

From (13), we can see that the most dangerous perturbations are those with $m = 1$. A sufficient condition for plasma stability can be obtained by omitting the first positive term in (13), so that we have $W \geq W_1$, where

$$W_1 = \frac{\pi}{2\mu_0}\int\left[B^2 - 2B\frac{d}{d\rho}(\rho B)\right]X^2\rho d\rho. \quad (15)$$

Taking into account the equilibrium equation, the sufficient condition for local plasma stability, $B^2 > 2B(\rho B)'$, can be written as

$$-\frac{\rho p'}{p} < \frac{1}{\beta}. \quad (16)$$

Note that, in the presence of a longitudinal magnetic field, the last term in (12) contains, instead of m^2B^2, the factor $(mB_\varphi + k\rho B_z)^2$, which vanishes with m and k satisfying the equality $mB_\varphi + k\rho B_z = 0$. In this case, the kink modes can be stabilized only when the current density is negative (in a passive-confinement version, in which the magnetic field does not change sign). Recall that plasmas with a negative current lower (in absolute value) than the doubled rod current, $|J_p| < 2J_c$, can be maintained in equilibrium only by the longitudinal magnetic field B_z, in which case the sufficient condition for stability remains valid only when the magnetic field B does not change sign, i.e., when $|J_p| < J_c$.

Flute perturbations ($m = 0$). The profiles of the plasma pressure and, accordingly, the current density should also satisfy the condition for stability against flute perturbations with $m = 0$.

According to the condition for stability against flute modes (see the Introduction), the pressure profile in the outer part of a tubular plasma is determined by the relationship

$$p(\psi) = \text{const} \times (d\psi/dV)^\gamma, \tag{17}$$

where $\psi(V)$ is the poloidal magnetic flux and dV is the volume of the layer between the toroidal surfaces p = const and $p + dp$ = const. Given the flux and volume elements per unit length, $d\psi = Bd\rho$ and $dV = 2\pi\rho d\rho$, we can write (17) as

$$\frac{p(\rho)}{p_0} = \left(\frac{B\rho_0}{B_0\rho}\right)^\gamma = \left(\frac{(J_c + J_p^- + J_p)\rho_0^2}{J_0\rho^2}\right)^\gamma, \tag{18}$$

where the normalizing constants ρ_0, B_0, and J_0 are chosen so that $p_0 = p(\rho_0)$, $B_0 = B(\rho_0)$, and $J_0 = J(\rho_0)$. At low plasma pressures, when $J_p^- + J_p(\rho) \ll J_0$ (i.e., $J \approx J_c$), the pressure decreases according to the law $p(\rho) \propto \rho^{-2\gamma} = \rho^{-10/3}$. Since the local stability condition depends on the magnetic field magnitude at a given surface ρ (i.e., on the total current flowing in the region of radius ρ), the pressure profile marginal with respect to flute instability in the region $\rho > \rho_0$ coincides with the "outer" (in the region $\rho > \rho_K$) portion of the pressure profile obtained by Kadomtsev for an ordinary pinch in the form of two equations.[1] With the notation $Y = (p_i/p)^{1/5}$, it is convenient to represent these equations as

$$\frac{1}{\beta} = \frac{5}{4}(Y^2 - 1), \tag{19}$$

$$\left(\frac{\rho}{a}\right)^2 = \frac{Y}{\beta} \tag{20}$$

where p_i and a are scaling factors. As applied to a tubular plasma, it is necessary that the current $J_c + J_p^-(\rho_0)$ flowing inside a surface $\rho = \rho_0$ be equal to the pinch current in the region $\rho < \rho_K$ in Kadomtsev's solution. Since we deal with a hollow plasma column, the plasma pressure profile is peaked at a certain cylindrical surface $\rho = \rho_0$ (rather than at the axis of the system) and is decreasing in both directions away from this surface. In the region outside the surface $\rho = \rho_0$, the properly scaled pressure profile is exactly the same as the outer portion of the profile obtained by Kadomtsev, $p/p_i = P_K(\rho/a)$. To determine the boundaries $\rho_0/a = f_\rho(\beta_0)$ and $\rho_2/a = f_\rho(\beta_2)$ of this region from the prescribed ratios p_2/p_0 and ρ_2/ρ_0, it suffices to find the values of β_0 and β_2 from the two equations

$$\frac{p_2}{p_0} = \left(\frac{Y_0}{Y_2}\right)^5, \quad \left(\frac{\rho_2}{\rho_0}\right)^2 = \frac{Y_2(Y_2^2 - 1)}{Y_0(Y_0^2 - 1)}. \tag{21}$$

The decreasing portion of the marginally stable pressure profile is illustrated in Fig. 1. The dashed curve shows a more realistic smoothed profile, which is characterized by a smaller pressure gradient and is therefore also stable.

A comparison between the sufficient conditions for local stability of the modes with $m = 0$ [4] and $m = 1$ [see (16)],

$$-\rho\frac{p'}{p} < \frac{4}{\frac{6}{5} + \beta}, \quad -\rho\frac{p'}{p} < \frac{1}{\beta}, \tag{22}$$

allows us to conclude that, for Kadomtsev's profile, even the condition for local stability of the $m = 1$ mode is satisfied at $\beta < 0.4$, i.e., according to (19) and (20), at $p/p_i < 1/\sqrt{3}$ and $\rho/a > 2.08$.

3. TOROIDAL TUBULAR PLASMA

3.1. Stability of Kink Modes

A pithy sufficient condition for the stability of incompressible ($\text{div}\,\boldsymbol{\xi} = 0$) kink perturbations can also be derived for a *toroidal* tubular pinch. In fact, in the axisymmetric case under discussion and in the absence of a toroidal magnetic field (when the current flows across the magnetic field, $\mathbf{j} \cdot \mathbf{B} = 0$, and the local shear equals zero, $S = \dfrac{\mathbf{B} \times \nabla a}{(\nabla a)^2} \cdot \nabla \times \dfrac{\mathbf{B} \times \nabla a}{(\nabla a)^2} = 0$), the potential energy of incompressible perturbations, which is given by formula (6.39) in review [14], has the form

[1] Since, in the review by Kadomtsev [12], the denominator in one of the formulas for the pressure profile is misprinted, in the Appendix, we present the derivation of the plasma pressure profile in parametric form.

$$W = \frac{1}{2}\mu_0\int\left\{\frac{(\mathbf{B}\cdot\nabla\xi)^2}{(\nabla a)^2} + \frac{(\nabla a)^2}{B^2}(\mathbf{B}\cdot\nabla\eta)^2 + B^2T_3^2 - \frac{\nabla p\cdot\nabla(2\mu_0 p + B^2)}{B^2(\nabla a)^2}\xi^2\right\}d\mathbf{r}. \quad (23)$$

Here, a is an arbitrary toroidal magnetic surface label (the volume V enclosed by a surface, the toroidal or poloidal magnetic flux, etc.), ξ and η are the components of the displacement vector

$$\boldsymbol{\xi} = \xi\frac{\nabla a}{(\nabla a)^2} + \eta\frac{\mathbf{B}\times\nabla a}{B^2} + \mu\mathbf{B},$$

and $T_3 = \dfrac{\boldsymbol{\xi}\cdot\nabla(2\mu_0 p + B^2)}{B^2} - \dfrac{\mathbf{B}\cdot\nabla(\mathbf{B}\cdot\boldsymbol{\xi})}{B^2}$. Omitting the second and third positive terms gives

$$W > W_1 = \frac{1}{2}\mu_0\int\left\{(\mathbf{B}\cdot\nabla\xi)^2 - \frac{\nabla p\cdot\nabla(2\mu_0 p + B^2)}{B^2}\xi^2\right\}\frac{d\mathbf{r}}{|\nabla a|^2}. \quad (24)$$

Hence, the sufficient condition for plasma stability against kink perturbations is

$$(\mathbf{B}\cdot\nabla\xi)^2 > \frac{\nabla p\cdot\nabla(2\mu_0 p + B^2)}{B^2}\xi^2 = 2\mu_0(\mathbf{k}\cdot\nabla p)\xi^2, \quad (25)$$

where $\mathbf{k} = \dfrac{\nabla_\perp(2\mu_0 p + B^2)}{2B^2}$ is the magnetic field line curvature in an equilibrium plasma configuration $\left(\nabla_\perp = \nabla - \mathbf{B}\dfrac{\mathbf{B}\cdot\nabla}{B^2}\right)$. Using the estimates $\mathbf{B}\cdot\nabla \approx kB$, $\mathbf{k}\cdot\nabla p \approx kp/a$, we obtain a tentative stability criterion

$$\frac{2\mu_0 p}{B^2} < ka. \quad (26)$$

Since we are interested in configurations in which the radius of curvature is comparable with the transverse dimension of the system, this estimate gives the upper limit on the maximum possible local beta, $\beta \sim 0.5$. To obtain more exact estimates of the maximum plasma pressure consistent with kink instability requires special calculations. It is particularly important here to examine the stability condition in the presence of a separatrix.

3.2. Equilibrium Code at the Stability Boundary of Flute Modes

Assuming that the kink modes can be stabilized by an internal current, we investigate pressure profiles for a configuration with a sufficiently large drop in the plasma pressure: from the maximum pressure p_0 inside the tubular column to a pressure p_2 of about $10^{-3}p_0$ at the plasma boundary (separatrix). We substitute the derivative $p'(\psi)$ obtained from (17) into the equilibrium equation for an axisymmetric plasma and take into account the relationship $dV/d\psi = \oint dl/B$ to arrive at the desired plasma equilibrium equation for determining the pressure profile at the stability boundary of flute perturbations:

$$\frac{\partial^2\psi}{\partial r^2} - \frac{1}{r}\frac{\partial\psi}{\partial r} + \frac{\partial^2\psi}{\partial z^2} = -4\pi^2\mu_0 r^2\frac{d}{d\psi}\left\{p_0\frac{(\oint dl/B|_{p=p_0})^\gamma}{(\oint dl/B)^\gamma}\right\}, \quad (27)$$

where ψ is the poloidal magnetic flux outside a magnetic surface. The boundary conditions for the nondimensionalized equation (27) are $u|_{S_i} = 1$ and $u|_{S_e} = 0$, where $u = \psi/\psi_i$, S_i is the inner boundary of a tubular plasma column, S_e is its outer boundary, which coincides with the separatrix surface, and ψ_i is the poloidal flux at the inner boundary S_i. The poloidal flux S_e at the outer boundary is assumed to be equal to zero.

In solving the equilibrium equation, the derivative $p'(\psi)$ should be found by calculating the integral $\oint dl/B$ along closed magnetic field lines. If the mesh points of the grid on which the equation is solved do not lie on the magnetic surfaces, the accuracy with which the integral $\oint dl/B$ can be calculated is insufficient. To improve the computational accuracy, we solved the equilibrium equation iteratively on radial grids with mesh points on the lines of the poloidal coordinate by optimizing the grids with respect to the magnetic field line geometry: at each iteration step, the mesh points were adjusted to lie on the magnetic surfaces, in which case there was no need to additionally approximate the values of the flux ψ in calculating the integral $\oint dl/B$ over a magnetic surface. At each iteration step, equation (27) was solved by the finite-element method [15]; the derivative $p'(\psi)$ on the right-hand side was calculated from the function ψ found at the preceding iteration step. Such a code makes it possible to compute pressure profiles marginal with respect to flute instability in a plasma configuration with an arbitrarily shaped magnetic separatrix.

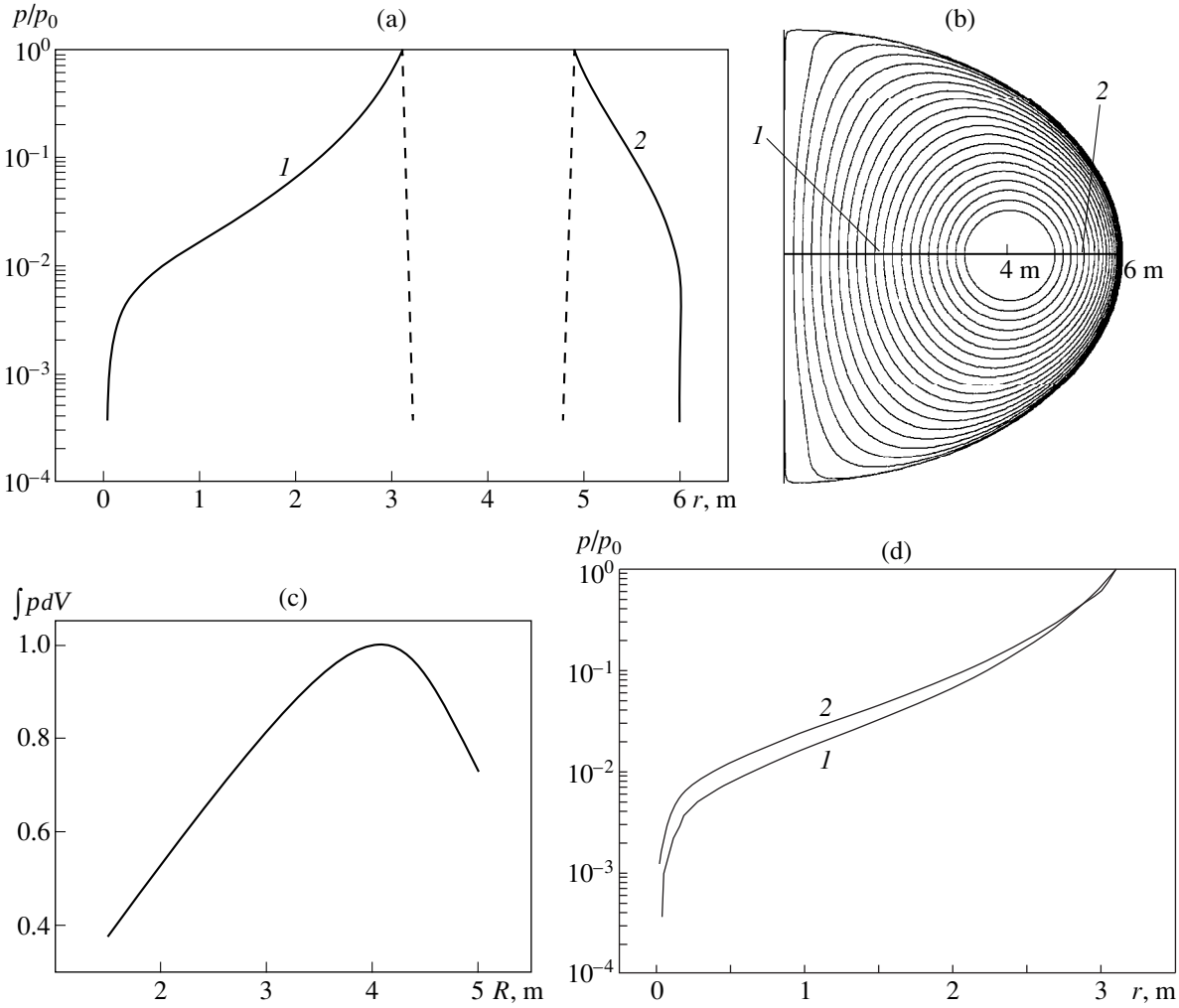

Fig. 2. Calculation of the equilibrium configuration marginal with respect to flute instability in a tubular plasma with a fixed elliptical boundary. (a) Plasma pressure profiles in the equatorial plane (on a logarithmic scale): (*1*) the pressure profile in the region between the *z*-axis and the inner side of the levitated ring and (*2*) the profile on the outside of the internal ring. Near the separatrix, the pressure falls off sharply because of the presence of magnetic null points. (b) The related family of magnetic surfaces. (c) The integral $\int pdV$ (one of the possible criteria for making the effective volume of confined plasma as large as possible) as a function of the major radius of a levitated ring (in arbitrary units) for a fixed shape of the plasma boundary and a fixed minor radius of the ring. (d) The inner portion of the plasma pressure profile *1* in Fig. 1a (on a logarithmic scale) for two different values of β_{inv}: β_{inv} = (*1*) 0 and (*2*) 0.35. Figures 1a–1c refer to the configuration proposed by Morozov, Pastukhov, and Sokolov [5] (the major and minor radii of a levitated ring are R = 4 m and a = 0.8 m). In Fig. 2d, R is a variable parameter.

We checked the accuracy of the numerical code in two ways. First, we compared the pressure profiles computed for large-aspect-ratio configurations without a separatrix (the cylindrical approximation) with the analytic profiles obtained from (21). Second, we carried out numerical calculations for configurations with a separatrix at $p'(\psi)$ = const, in which case the pressure profiles can also be evaluated analytically.

3.3. Magnetic Surfaces and Pressure Profiles at the Stability Boundary of Flute Modes]

We carried out a series of computations for the plasma configuration that was proposed by Morozov, Pastukhov, and Sokolov [5] and in which the separatrix has the shape of an ellipse. Figure 2a shows the plasma pressure profile marginal with respect to flute instability in the equatorial plane. The profile in the left part of the figure (curve *1*) corresponds to the inside of a levitated ring, and the right part (curve *2*) illustrates the pressure profile on the outside. Near the separatrix, the plasma pressure falls off sharply because of the presence of magnetic null points. Figure 2b presents the relevant family of magnetic surfaces.

We investigated the confinement efficiency as a function of the major radius R of a levitated ring, keeping both the minor radius and the shape of the outer boundary (separatrix) fixed. The value of the integral of

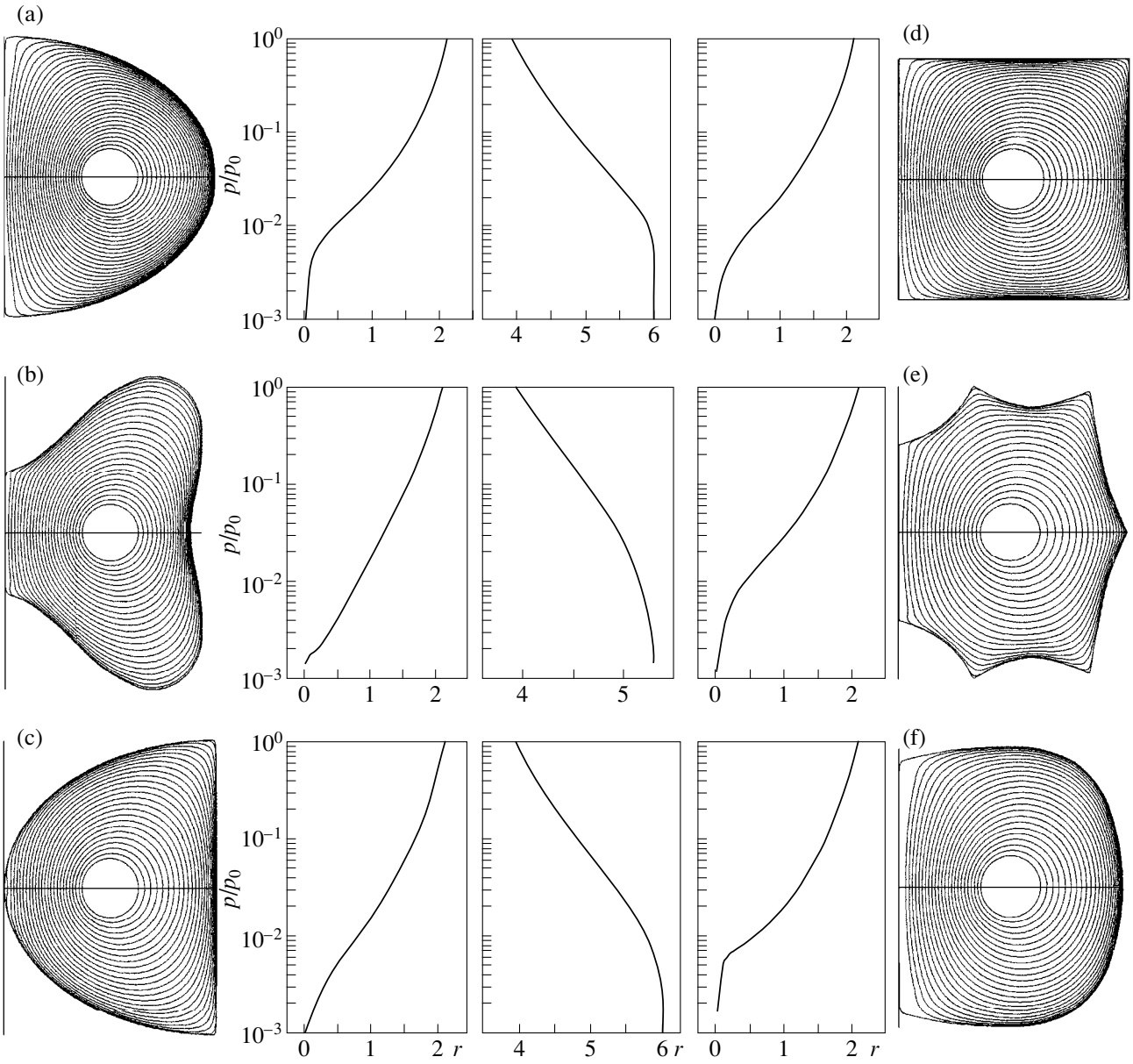

Fig. 3. Examples of configurations with different shapes of the separatrix: the pressure profiles in the equatorial plane and the related families of magnetic surfaces. The profiles are computed in the low β approximation.

the plasma pressure over the entire volume of the system, $\int pdV$, can serve as one of the possible criteria for making the effective volume of a confined plasma as large as possible. In Fig. 2c, different points on the profile of this integral correspond to systems with different major radii of a levitated ring. The profile is peaked at $R \approx 4$ m, which agrees with the estimates that governed the choice of the plasma configuration in [5]. Figure 2d shows inner portions of the pressure profiles obtained for this configuration at different values of the integral parameter $\beta_{inv} = 1 - J_e^2/J_2^2$. As in the case of a cylindrical configuration, the larger the parameter β, the broader the pressure profile.

Examples of configurations with different shapes of the plasma separatrix are illustrated in Fig. 3. One way of optimizing configurations is to search for a system in which the plasma pressure falls off sharply across a fairly broad layer near the separatrix, since it would hardly be possible to create configurations with a very abrupt drop in pressure across a thin layer (because of diffusion). According to the stability condition for flute modes, the plasma pressure is inversely proportional to $(\int dl/B)^\gamma$; consequently, it is expedient to reduce the

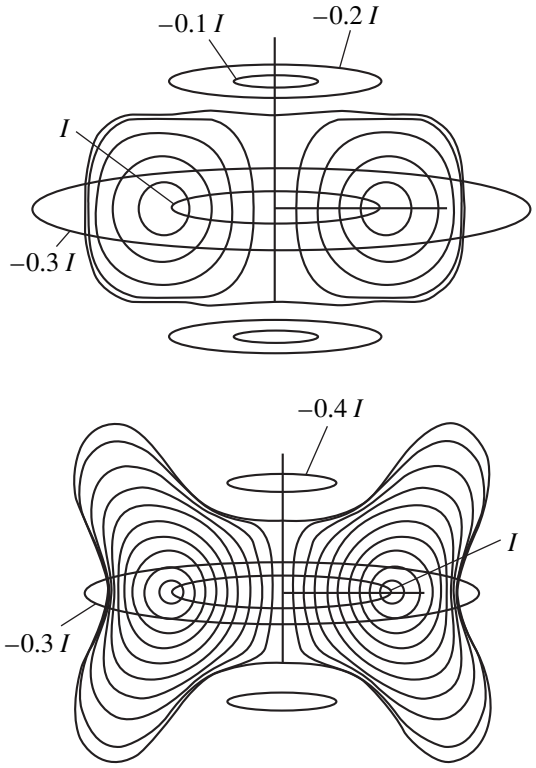

Fig. 4. Examples of the sets of ring currents capable of producing magnetic separatrices that are similar in shape to those in Fig. 3.

edge pressure by making the magnetic field lines near the separatrix longer, which is illustrated in Fig. 3b. This configuration appears to be the most beneficial, because the layer across which the pressure falls off is the narrowest.

Here, we have not attempted to search for a set of ring currents capable of producing a magnetic separatrix with the desired shape. However, as an example, Fig. 4 illustrates how to create separatrices whose shapes are similar to those examined above by means of several ring currents.

4. CONCLUSION

We have analyzed the equilibrium and stability of a cylindrical tubular plasma confined by the external azimuthal magnetic field of a current flowing in a hard core placed along the *z*-axis. In contrast to a hard-core pinch device with the "externally generated" currents, in the passive-confinement version under consideration, no external current is excited and the plasma carries only a diamagnetic current. We have shown that, in the outer region, the radially decreasing pressure profile marginal with respect to flute instability is exactly the same as the profile calculated by Kadomtsev for an ordinary pinch. It is also shown, unlike an ordinary pinch, a tubular plasma pinch can be stable against kink modes.

We have developed the two-dimensional TuTor code capable of computing equilibrium plasma pressure profiles that are marginally stable against flute perturbations in a toroidal tubular pinch with a central ring current. The simulations carried out for such systems under the assumption that the shape of the magnetic separatrix is prescribed showed that, as expected, the plasma pressure profile near the separatrix is sharply decreasing and the plasma remains MHD stable against flute modes. One of the optimization parameters—the width of the layer across which the pressure falls off sharply—can be controlled by varying the shape of the separatrix. In toroidal tubular pinches, it is possible to satisfy the criteria for MHD stability of kink modes, as in the case of cylindrical tubular pinches.

In this paper, we have not discussed the question of how to maintain an internal ring with current J_c. In the review by Morozov and Savel'ev [1], attention was focused on the idea of a levitated ring supported by a horizontal magnetic field, which was proposed as early as 1958 by Sakharov [16]. Another noteworthy idea proposed by Sakharov is that of maintaining a current-carrying ring mechanically. Along with the cables discussed in [16], it might be expedient to consider local supports connecting the internal ring to the external current-carrying ring. In this case, a strong magnetic field generated between the rings gives rise to "toroidal magnetic mirrors," which can reduce the energy flux to supports. Such a confinement system with toroidal magnetic mirrors and possibly with current-carrying supports requires a separate investigation.

ACKNOWLEDGMENTS

We are grateful to S.Yu. Medvedev for valuable advice concerning the optimization of computations and to M.A. Samitov for providing us with the code for calculating the vacuum field from the prescribed distribution of the ring currents. We also thank V.V. Arsenin for amending the manuscript. This work was supported in part by the Russian Foundation for Basic Research, project no. 97-02-17695.

APPENDIX

To refine expressions (4.4) in the review by Kadomtsev [12], we derive formulas that describe the pressure profile marginal with respect to flute instability in a cylindrically symmetric plasma, without making any assumptions regarding the parameter γ. We take the logarithmic derivative of (18), introduce the local parameter $\beta = 2\mu_0 p/B^2$, and eliminate B' using the equilibrium equation (1) to obtain

$$-\frac{d\ln p}{d\ln \rho} = -\frac{\rho p'}{p} = \frac{2\gamma}{1+\frac{\gamma}{2}\beta}. \qquad \text{(A.1)}$$

Analogously, we find the logarithmic derivative of β:

$$\frac{d\ln\beta}{d\ln\rho} = \frac{\rho p'}{p} - \frac{2\rho B'}{B} = \frac{\rho p'}{p}(1+\beta) + 2. \qquad \text{(A.2)}$$

These relationships give

$$\frac{d\ln p}{d\ln\beta} = \frac{4\gamma}{4(\gamma-1)+2\gamma\beta}. \qquad \text{(A.3)}$$

Integrating (A.3) over β, we arrive at a parametric representation of the marginal plasma pressure profile:

$$\frac{p}{p_i} = \left(\frac{\beta}{\beta + 2(\gamma-1)/\gamma}\right)^{\frac{\gamma}{\gamma-1}},$$
$$\frac{\rho}{a} = \frac{[\beta + 2(\gamma-1)/\gamma]^{\frac{2-\gamma}{2(\gamma-1)}}}{\beta^{1/2(\gamma-1)}}, \qquad \text{(A.4)}$$

where p_i and a are integration constants. With $\gamma = 5/3$, (A.4) becomes

$$\frac{p}{p_i} = \left(\frac{\beta}{\beta + \frac{4}{5}}\right)^{5/2}, \quad \frac{\rho}{a} = \frac{\left[\beta + \frac{4}{5}\right]^{1/4}}{\beta^{3/4}}. \qquad \text{(A.5)}$$

Note that there are misprints in the review by Kadomtsev [12]: in the formula corresponding to the second relationship in (A.5), the power index 1/4 in the numerator has been left out and the denominator contains the power index 5/4 instead of 3/4.

Instead of formulas (A.4) and (A.5) for $p(\beta)$ and $\rho(\beta)$, it is more convenient to use the formulas for $\beta(p)$ and $\rho(p)$. The dependence $\beta(p)$ can be obtained directly from the first relationship in (A.4):

$$\beta = \frac{2(\gamma-1)/\gamma}{(p_i/p)^{(\gamma-1)/\gamma} - 1} = \frac{4/5}{(p_i/p)^{2/5} - 1}, \qquad \text{(A.6)}$$

which also gives the representations

$$\beta + 2\frac{\gamma-1}{\gamma} = \beta\left(\frac{p_i}{p}\right)^{\frac{\gamma-1}{\gamma}},$$
$$\frac{1}{\beta} = \frac{\gamma}{2(\gamma-1)}\left[\left(\frac{p_i}{p}\right)^{\frac{\gamma-1}{\gamma}} - 1\right]. \qquad \text{(A.7)}$$

From the second relationship in (A.4), we find

$$\left(\frac{\rho}{a}\right)^2 = \frac{1}{\beta}\left(\frac{p_i}{p}\right)^{\frac{2-\gamma}{\gamma}} = \frac{\gamma}{2(\gamma-1)}\left[\left(\frac{p_i}{p}\right)^{\frac{\gamma-1}{\gamma}} - 1\right]\left(\frac{p_i}{p}\right)^{\frac{2-\gamma}{\gamma}}$$
$$= \frac{5}{4}\left[\left(\frac{p_i}{p}\right)^{\frac{2}{5}} - 1\right]\left(\frac{p_i}{p}\right)^{\frac{1}{5}}. \qquad \text{(A.8)}$$

The formulas derived describe the behavior of the stable marginal pressure profile on the outside of the surface at which the plasma pressure is maximum. For large values of ρ, the parameter β is small; specifically, for $\rho \sim 1/\beta^{1/2(\gamma-1)}$, we have $p \sim \beta^{\gamma/(\gamma-1)}$. In other words, as ρ increases, the plasma pressure falls off according to the law $1/\rho^{2\gamma} = 1/\rho^{10/3}$.

Note that the first equality in (A.8) gives $\frac{B^2}{2\mu_0 p_i} = \left(\frac{\rho}{a}\right)^2\left(\frac{p}{p_i}\right)^{\frac{2}{\gamma}}$, so that we have $\frac{p}{p_i} = \left(\frac{\mu_0 J^2(\rho)a^2}{8\pi^2 p_i \rho^4}\right)^{\frac{\gamma}{2}}$. We can see that, at a given surface ρ, the plasma pressure profile depends solely on the total current $J(\rho) = 2\pi\rho B(\rho)/\mu_0$.

REFERENCES

1. A. I. Morozov and V. V. Savel'ev, Usp. Fiz. Nauk **168**, 1153 (1998) [Phys. Usp. **41**, 1049 (1998)].
2. A. Hasegawa, Comm. Plasma Phys. Control. Fusion **1**, 147 (1987).
3. A. Hasegawa, L. Chen, and M. E. Mauel, Nucl. Fusion **11**, 2405 (1990).
4. B. B. Kadomtsev, in *Plasma Physics and the Problem of Controlled Nuclear Fusion* (Akad. Nauk SSSR, Moscow, 1958), Vol. IV, p. 380.
5. A. I. Morozov, V. P. Pastukhov, and A. Yu. Sokolov, in *Proceedings of Workshop on D–^{3}He Based Reactor Studies, Moscow, 1991*, p. 1C1.
6. P. N. Vabishchevich, L. M. Degtyarev, V. V. Drozdov, *et al.*, Fiz. Plazmy **7**, 981 (1981) [Sov. J. Plasma Phys. **7**, 536 (1981)].
7. L. A. Artsimovich, in *Controlled Nuclear Fusion* (Fizmatgiz, Moscow, 1963), Chap. 5.5, p. 188.
8. P. Reynolds, D. J. Lees, R. J. Bickerton, *et al.*, in *Proceedings of 2nd Conference on Plasma Physics and Controlled Nuclear Fusion Research, Culham, 1965* (IAEA, Vienna, 1966), Vol. 2, p. 329.
9. S. Yoshikawa, Nucl. Fusion **13**, 433 (1973).
10. B. Lehnert, J. Nucl. Energy C **1**, 40 (1959).
11. W. A. Newcomb, Ann. Phys. **10**, 232 (1960).
12. B. B. Kadomtsev, in *Reviews of Plasma Physics*, Ed. by M. A. Leontovich (Gosatomizdat, Moscow, 1963; Consultants Bureau, New York, 1966), Vol. 2.
13. V. D. Shafranov, Zh. Tekh. Fiz. **40**, 241 (1970) [Sov. Phys. Tech. Phys. **15**, 175 (1970)].
14. V. D. Pustovitov and V. D. Shafranov, in *Reviews of Plasma Physics*, Ed. by B. B. Kadomtsev (Énergoatomizdat, Moscow, 1987; Consultants Bureau, New York, 1990), Vol. 15.
15. L. M. Dyagterev, V. V. Drozdov, and S. Yu. Medvedev, *Numerical Modeling of Equilibrium and Stability of a Toroidal Plasma* (IPM Akad. Nauk SSSR, Moscow, 1989).
16. A. D. Sakharov, in *Plasma Physics and the Problem of Controlled Nuclear Fusion* (Akad. Nauk SSSR, Moscow, 1958), Vol. 1.

Translated by O. E. Khadin

Plasma Physics Reports, Vol. 26, No. 6, 2000, pp. 493–501. Translated from Fizika Plazmy, Vol. 26, No. 6, 2000, pp. 529–537.

PLASMA DYNAMICS

Magnetohydrodynamics of a Weakly Ionized Plasma: Ambipolar Magnetic Diffusion and Shock Front Structure

I. V. Sokolov[1, 2] and J. I. Sakai[1]

[1]*Laboratory of Plasma Astrophysics, Faculty of Engineering, Toyama University, 3190, Gofuku, Japan*
[2]*Institute of General Physics, Russian Academy of Sciences, ul. Vavilova 38, Moscow, 117942 Russia*

Received February 11, 1999; in final form, November 2, 1999

Abstract—Kinetic equations with the BGK collision integral are used to derive MHD equations for a weakly ionized plasma that are applicable over a broad range of magnetic field strengths. In strong magnetic fields, a substantial contribution to the transverse diffusion of the magnetic field comes from the ambipolar magnetic diffusion, which is associated with the motion of both the charged component and the magnetic field against the background of the neutral plasma component. The problems of the magnetic field diffusion in a weakly ionized plasma and the shock wave structure are solved. © *2000 MAIK "Nauka/Interperiodica".*

1. INTRODUCTION

Numerous experiments on the propagation of shock waves in weakly ionized plasmas in shock tubes (as well as recent experiments with gas-dynamic tubes) have revealed a number of effects that are not completely clear. One of them is the formation of a precursor, which overtakes the gas-dynamic shock wave and propagates as the wave of the perturbed ion density, almost without driving neutrals into motion.

The experiments motivated theoretical studies of the structure of shock waves in a weakly ionized plasma [1] (see also [2]) with allowance for the possible motion of the charged component against the background of the neutral gas upstream of the hydrodynamic shock. We think that it will be of interest to consider the problem of the shock wave structure again and to examine shock waves in a weakly ionized plasma with such a strong magnetic field that its pressure should be incorporated into the equations of motion.

We will show that, although in laboratory plasmas the magnetic field pressure is usually lower than the neutral pressure (if an especially strong magnetic field is not created intentionally) and, accordingly, the magnetic field has an insignificant impact on the propagation of gas-dynamic shock waves, the magnetic field energy density can be comparable with the energy density of the charged component, so that, in our opinion, the magnetic field may be responsible for a number of experimentally observed effects associated with the motion of the charged component against the background of neutrals at the shock fronts.

In various plasma phenomena in the universe (from the formation of stars to the processes in the Earth's ionosphere), the magnetic field energy density is usually comparable with the pressure of the neutral component of a weakly ionized plasma, in which case the motion of the charged component with respect to the neutral gas is especially important and can give rise to qualitatively new effects [3–5]. That is why the problems we are considering here may also be of interest for astrophysical applications.

In this paper, we use the kinetic equations for charged particles with the Bhatnagar–Gross–Krook (BGK) model collision integral [6] in order to derive a set of MHD equations that describe motions in a weakly ionized plasma and apply them to a broad range of magnetic field strengths, including such strong magnetic fields that both the electrons and ions are magnetized in collisions with neutrals; i.e., the electron and ion gyrofrequencies are higher than the collision frequencies, which is typical of space and astrophysical plasmas. An analysis of the MHD equations derived demonstrates the possibility of significant enhancement of the transverse diffusion of a strong magnetic field.

We will solve the problems of the structure of a weak shock wave and the nonlinear diffusion of the external magnetic field in a weakly ionized plasma.

2. KINETIC EQUATIONS FOR CHARGED PARTICLES AND THEIR SOLUTIONS

We treat the motion of neutral gas in the hydrodynamic approximation, which applies to the processes occurring on long time scales such that the characteristic frequency Ω is much lower than the neutral–neutral collision frequency,

$$\Omega \ll \nu_{nn}. \tag{1}$$

We describe charged particles interacting with an electromagnetic field in the kinetic approximation because we do not assume that gyrofrequencies are small in comparison with the collision frequencies. However, since the ion–neutral and electron–neutral

1063-780X/00/2606-0493$20.00

collision frequencies, ν_{in} and ν_{en}, satisfy the conditions $\nu_{in} \geq \nu_{nn}$ and $\nu_{en} \gg \nu_{nn}$, inequality (1) allows us to neglect the time and space derivatives in the kinetic equations,

$$e_a\left(\mathbf{E} + \frac{[\mathbf{v}\times\mathbf{H}]}{c}\right)\frac{\partial f_a}{\partial \mathbf{p}} + \nu_{an}\left(f_a - \frac{f_{aM}}{n}\int d\mathbf{p}\, f_a\right) = 0, \quad (2)$$

where $a = e, i$; f_{aM} are Maxwellian distribution functions with a temperature equal to that of the neutral gas; and n is the density of the electrons and ions in a plasma, which is assumed to be quasineutral. The rest of the notation is standard. The degree of ionization is assumed to be weak,

$$\chi = n/N \ll 1 \quad (3)$$

(N is the neutral density), so that we can neglect collisions among the charged particles. This implies that $\chi \leq 10^{-4}$–10^{-2}, because the cross sections for collisions among the charged particles differ greatly from the cross sections for collisions between charged and neutral particles. Equations (2) with the BGK collision integral and with constant collision frequencies are written for each of the small spatial regions of a weakly ionized plasma in the frames of reference in which the neutral gas is at rest.

We solve equations (2) in the first-order approximation in the electric field $\mathbf{E}$, which is driven inductively in the course of motion of a weakly ionized plasma in a magnetic field. Accordingly, we represent the electron and ion distribution functions as the sum of Maxwellian distribution functions and small corrections,

$$f_a = f_{aM} + \delta f_a, \quad (4)$$

$$e_a\mathbf{E}\frac{\partial f_{aM}}{\partial \mathbf{p}} + \frac{e_a[\mathbf{v}\times\mathbf{H}]}{c}\frac{\partial \delta f_a}{\partial \mathbf{p}} + \nu_{an}\left(\delta f_a - \frac{f_{aM}}{n}\int d\mathbf{p}\,\delta f_a\right) = 0. \quad (5)$$

We seek a solution to kinetic equations in the form

$$\delta f_a = -(\mathbf{p}\mathbf{U}_a)\frac{\partial f_{aM}}{\partial \varepsilon}, \quad \varepsilon = \frac{\mathbf{p}^2}{2m_a}, \quad (6)$$

where $\mathbf{U}_a$ are constant vectors independent of the particle momenta. Expressions (6) turn equations (5) into identities if the constant vectors satisfy the condition

$$e_a\left(\mathbf{E} + \frac{1}{c}[\mathbf{U}_a\times\mathbf{H}]\right) = m_a\nu_{an}\mathbf{U}_n, \quad (7)$$

where m_a are the electron and ion masses.

Substituting (4) and (6) into the integral $\int d\mathbf{p}\, f_a\mathbf{v}$, we can readily see that $\mathbf{U}_a$ are the mean directed velocities of the electrons and ions with respect to the neutral gas. Consequently, equations (7) for the electrons and ions are merely two-fluid hydrodynamic equations in which the terms of the form $\frac{\partial \mathbf{U}_a}{\partial t} + (\mathbf{U}_a\nabla)\mathbf{U}_a$ are omitted by virtue of condition (1). Using the equation for the quasisteady magnetic field in which the displacement current is discarded,

$$\operatorname{curl}\mathbf{H} = \frac{4\pi n\sum_a e_a\mathbf{U}_a}{c}, \quad (8)$$

we can obtain from (7) the following expression for the bulk force with which the charged component acts upon the neutral gas (i.e., the density of the momentum transferred from charged particles to neutrals per unit time):

$$n\sum_a m_a\nu_a\mathbf{U}_a = \frac{\operatorname{curl}\mathbf{H}\times\mathbf{H}}{4\pi}. \quad (9)$$

Using (8), we eliminate $\mathbf{U}_e$ from (9) to obtain $\mathbf{U}_i$:

$$\mathbf{U}_i = \frac{cm_e\nu_{en}}{4\pi e_i m_i\tilde{\nu}_{in}n}\operatorname{curl}\mathbf{H} + \frac{\operatorname{curl}\mathbf{H}\times\mathbf{H}}{4\pi n\tilde{\nu}_{in}m_i}, \quad \tilde{\nu}_{in} = (m_i\nu_{in} + m_e\nu_{en})/m_i \approx \nu_{in}. \quad (10)$$

Inserting (10) into (7), we express the electric field in terms of curl$\mathbf{H}$ and $\mathbf{H}$:

$$\mathbf{E} = \frac{c}{4\pi}\rho_{ik}(\operatorname{curl}\mathbf{H})_k + \frac{\hat{\nu}_{in}}{\hat{\nu}_{in}}\frac{\operatorname{curl}\mathbf{H}\times\mathbf{H}}{4\pi n e_i}, \quad \hat{\nu}_{in} = (m_i\nu_{in} - m_e\nu_{en})/m_i \approx \nu_{in}, \quad (11)$$

$$\rho_{ik} = \frac{1}{\sigma}\left[\delta_{ik} + \frac{\sigma H^2}{nm_i\tilde{\nu}_{in}c^2}\left(\delta_{ik} - \frac{H_iH_k}{H^2}\right)\right], \quad \sigma = \frac{e^2n\tilde{\nu}_{in}}{m_e\nu_{en}\nu_{in}}. \quad (12)$$

We also need the expression for the density of the power loss due to Joule heating of the neutral gas:

$$\frac{c}{4\pi}(\mathbf{E}\operatorname{curl}\mathbf{H}) = \frac{e^2}{(4\pi)^2\sigma}(\operatorname{curl}\mathbf{H})^2 + nm_i\nu_{in}\left(\frac{\operatorname{curl}\mathbf{H}\times\mathbf{H}}{4\pi nm_i\tilde{\nu}_{in}}\right)^2. \quad (13)$$

3. MHD EQUATIONS OF MOTION FOR A WEAKLY IONIZED PLASMA

We write the complete set of MHD equations of motion in the common frame of reference, in which the velocity $\mathbf{U}$ of motion of the neutral component depends on time and coordinates (above, for each local spatial plasma region, we introduced its own frame, in which

the neutral gas was at rest, and the MHD equations were written in these frames). With allowance for Lorentz transformations, we must make the replacements $\mathbf{E} \longrightarrow \mathbf{E} - \frac{1}{c}[\mathbf{U} \times \mathbf{H}]$ and $\mathbf{U}_i \longrightarrow \mathbf{U}_i + \mathbf{U}$. We use the hydrodynamic approximation for the neutral component with allowance for (9) and substitute the transformed ion velocity (10) into the continuity equation for the charged component and the transformed electric field into the induction equation:

$$-\frac{1}{c}\frac{\partial \mathbf{H}}{\partial t} = \mathrm{curl}\mathbf{E}. \tag{14}$$

As a result, we obtain

$$\frac{\partial N}{\partial t} + \mathrm{div}(\mathbf{U}N) = 0, \tag{15}$$

$$\frac{\partial n}{\partial t} + \mathrm{div}(\mathbf{U}n + \mathbf{U}_d n) = 0,$$
$$\mathbf{U}_d = \frac{\mathrm{curl}\mathbf{H} \times \mathbf{H}}{4\pi n m_i \tilde{\nu}_{in}}, \tag{16}$$

$$m_i N\left(\frac{\partial \mathbf{U}}{\partial t} + (\mathbf{U}\nabla)\mathbf{U}\right) = -\mathrm{grad}\,P_n + \frac{\mathrm{curl}\mathbf{H} \times \mathbf{H}}{4\pi}, \tag{17}$$

$$\frac{\partial \mathbf{H}}{\partial t} = \mathrm{curl}[\mathbf{U} \times \mathbf{H}] - \frac{c^2}{4\pi}\mathrm{curl}[\rho_{ik}(\mathrm{curl}\mathbf{H})_k] - \frac{\hat{\nu}_{in} m_i c}{e_i}\mathrm{curl}\mathbf{U}_d, \tag{18}$$

$$\frac{\partial P_n}{\partial t} + \mathbf{U}\,\mathrm{grad}\,P_n + \gamma P_n \mathrm{div}\,\mathbf{U} = (\gamma - 1)\left[\frac{1}{\sigma}\left(\frac{c\,\mathrm{curl}\mathbf{H}}{4\pi}\right)^2 + n m_i \tilde{\nu}_{in} U_d^2\right], \tag{19}$$

where P_n is the neutral pressure and γ is the adiabatic power-law index for the neutral gas.

4. AMBIPOLAR MAGNETIC DIFFUSION

Equation (16) accounts for ambipolar magnetic diffusion [9], whose rate is proportional to Ampére's force [replace $\mathrm{curl}\mathbf{H} \times \mathbf{H}$, rather than ordinary ambipolar diffusion [7, 8], whose rate is proportional to the gradient of the charged-particle density, –grad$n$. Comparing ambipolar magnetic diffusion with ordinary diffusion (which is ignored in our analysis), we can see that magnetic diffusion dominates under the condition

$$\frac{H^2}{8\pi} \gg nT, \tag{20}$$

which implies that the magnetic field energy density (more precisely, the characteristic amplitude of its spatial variations) exceeds the charged-particle energy density. Inequality (20) is often satisfied for space plasmas and for weakly ionized laboratory plasmas (even in experiments in which the magnetic field in a device is controlled so that it is aligned with the Earth's magnetic field, plasma densities on the order of $n \leq 10^{10}$ cm^{-3} are sufficient for this inequality to hold). Hence, we can say that, in many interesting problems, instead of following the hydrodynamic approach to a weakly ionized plasma, we should take an MHD approach or, at least, a hydrodynamic approach with allowance for ambipolar magnetic diffusion.

The physical meaning of ambipolar magnetic diffusion is quite clear: a drop in the magnetic field pressure $\delta H^2/8\pi$ over the spatial scale L accelerates the charged component to the velocity $U_d \sim \delta H^2/(8\pi L n \tilde{\nu}_{in} m_i)$ relative to the neutral component, thereby giving rise to a diffusion with the coefficient

$$D_{am} \sim L U_d \sim \frac{H^2}{8\pi n m_i \tilde{\nu}_{in}}. \tag{21}$$

In the case of ambipolar magnetic diffusion, both the magnetic field and the charged component drift with respect to the neutral component. We emphasize that, in a weakly ionized plasma, this process, which is accompanied by friction between the charged and neutral particles, is the only mechanism for the interaction between the magnetic field and neutral gas (of course, if the magnetic properties of neutrals are neglected). In contrast to a fully ionized plasma, in which all of the plasma particles can interact with the magnetic field either directly or via the charge-separation electric field (which, in particular, makes magnetic confinement possible and is responsible for the existence of equilibrium configurations), the majority of particles in a weakly ionized plasma are insensitive to both the magnetic field and the magnetic pressure gradient. Remember that the magnetic field can indirectly affect the neutral particles only via the charged component propagating against the background of neutral gas; however, in this case, the forces acting on the neutral component [see equation (17)] inevitably give rise to the convection of the magnetic field and charged component [see the related terms in equations (16) and (18)]. Under the assumptions adopted, a weakly ionized plasma cannot be in equilibrium with the magnetic field.

Unlike the conventional one-fluid hydrodynamic equations, the above equation for the magnetic field contains a Hall term that accounts for the induction effects associated with the charge-separation electric fields, which are always present in a plasma with ambipolar magnetic diffusion because the friction force of electrons on neutrals differs from that of ions on neutrals. However, the most interesting effect from the standpoint of astrophysical applications is the nonlinear (in H) growth of the plasma resistivity in the directions transverse to the magnetic field, in which case the related growth in the magnetic field diffusion coefficient in the transverse directions is again a direct con-

sequence of the ambipolar magnetic diffusion. The nonlinear terms in the plasma resistivity become dominant under the condition

$$\frac{e^2H^2}{m_i m_e \nu_{en}\nu_{in}c^2} \gg 1. \quad (22)$$

This condition can also be derived as the requirement for ambipolar magnetic diffusion to dominate over ordinary magnetic diffusion, which is described by the H-independent coefficient $c^2/(4\pi\sigma)$. For estimates, we take (22) with the frequencies $\nu_{an} \sim N\sigma_{an}(T/m_a)^{1/2}$ and cross sections $\sigma_{an} \sim 10^{-16}$ cm^2 and introduce the ratio of the neutral pressure to the magnetic field pressure, $\beta_n = 8\pi NTH^{-2}$. As a result, we obtain

$$N\beta_n \ll 10^{19}\ \text{cm}^{-3}. \quad (23)$$

Condition (23) usually holds for weakly ionized space plasmas, in which the energy is considered to be equally distributed between the magnetic field and the plasma particles, $\beta_n \sim 1$.

In such plasmas, neutral gas heating via collisions between current-carrying electrons and neutrals plays a lesser role than heating via the friction between charged particles (mainly, the ions) and neutrals due to ambipolar magnetic diffusion, which is represented by the last term in equation (19) for neutral heating.

We again emphasize that it is the ambipolar magnetic diffusion in a weakly ionized plasma with a large number of neutrals that is responsible for the appearance of the new effects under discussion here, which are absent, e.g., in a plasma with two ion species (ions with different charges and/or masses). In the latter case, the solutions to the problems of magnetic field diffusion in a plasma [10] and the shock wave structure [11] are known.

5. DIFFUSION OF A MAGNETIC FIELD IN A WEAKLY IONIZED PLASMA

We study the possible effect of ambipolar magnetic diffusion on the magnetic field evolution in a weakly ionized plasma by treating the problem of the diffusion of a magnetic field in a plasma.

Let a plasma with the parameters $N = N_0$, $n = n_0$, and $\mathbf{H} = \mathbf{H}_0$ occupy the half-space $x > 0$ (we work in Cartesian coordinates x, y, and z) by the time $t = 0$. For simplicity, we assume that the magnetic field is parallel to the plasma boundary and is directed along the y-axis. We consider the case in which the magnetic field $\mathbf{H} = \mathbf{H}_1 = \alpha\mathbf{H}_0$ with $\alpha > 1$ originates at the boundary $x = 0$ at the time $t = 0$ and thereafter is maintained to be constant (the interesting case $\alpha = 0$, which corresponds to the magnetic field reconnection at the plasma boundary and can be treated in a similar manner, will be analyzed in a separate study). In the initial stage (whose characteristic duration will be estimated below), the motion of neutral gas can be ignored. In this stage, the magnetic field penetration into the region $x > 0$ is governed exclusively by the convection of both the charged plasma component and the magnetic field, which is frozen in this component, against the background of neutral gas; moreover, the neutrals can be assumed to be immobile, because their inertia is large and they are not directly affected by the magnetic field. Let us follow the magnetic field evolution during the initial stage.

Assuming that the neutral density is constant, we write the equations for the dimensionless magnetic field and charged-particle density, $Y = H_y/H_0$ and $Z = n/n_0$, in the form

$$\frac{\partial Y}{\partial t} + \frac{\partial}{\partial x}(U_d Y) = \tilde{D}_M \frac{\partial}{\partial x}\left(\frac{1}{Z}\frac{\partial Y}{\partial x}\right), \quad (24)$$

$$\frac{\partial Z}{\partial t} + \frac{\partial}{\partial x}(ZU_d) = 0, \quad (25)$$

where

$$U_d = -\tilde{D}_{am}\frac{Y}{Z}\frac{\partial Y}{\partial x}, \quad (26)$$

and

$$\tilde{D}_M = \frac{c^2 m_e \nu_{en}\nu_{in}}{4\pi e^2 n_0 \tilde{\nu}_{in}}, \quad \tilde{D}_{am} = \frac{H_0^2}{4\pi n m_i \tilde{\nu}_{in}} \quad (27)$$

are the coefficients of the magnetic field diffusion and ambipolar magnetic diffusion, respectively. The collision frequencies should be taken with $N = N_0$.

Equations (24) and (25) can be somewhat simplified by transforming to the Lagrangian variables [12] associated with the elements of the charged component. As a new spatial coordinate, we introduce the following variable describing the mass motion:

$$\xi(x, t) = \int_{x_0(t)}^{x} dx' Z(x', t). \quad (28)$$

The magnetic field pressure causes the left boundary $x_0(t)$ of the region occupied by the charged component to displace to the right. Transforming equation (25) into Lagrangian variables, we obtain, in the usual way,

$$\left(\frac{\partial x}{\partial t}\right)_\xi = U_d; \quad (29)$$

i.e., the ξ = const contours in the (x, t) plane coincide with the trajectories of the fluid elements of the charged plasma component (different values of the Lagrangian label ξ refer to different fluid elements). We change the derivatives, $(\partial/\partial t)_\xi = (\partial/\partial t)_x + U_d(\partial/\partial x)_t$ and $(\partial/\partial\xi)_t =$

$Z^{-1}(\partial/\partial x)_t$, to convert equations (24) and (25) with (26) to the form

$$\frac{\partial}{\partial t}\left(\frac{Y}{Z}\right) = \tilde{D}_M \frac{\partial^2 Y}{\partial \xi^2}, \quad (30)$$

$$\frac{\partial}{\partial t}\left(\frac{1}{Z}\right) = -\tilde{D}_{am}\frac{\partial}{\partial \xi}\left(Y\frac{\partial Y}{\partial \xi}\right). \quad (31)$$

Without allowance for ordinary dissipation of the magnetic field, the quantity Y/Z is a Lagrangian invariant; i.e., it is frozen in the charged plasma component and is carried by it.

We begin the analysis of (30) and (31) by treating two limiting cases. For $\tilde{D}_M \ll \tilde{D}_{am}$ (i.e., without allowance for magnetic field diffusion), equation (30) gives $Y = Z$ and equation (31) reduces to the nonlinear heat conduction equation

$$\frac{\partial}{\partial t}\left(\frac{1}{Z}\right) = \tilde{D}_{am}\frac{\partial}{\partial \xi}\left(Z^3\frac{\partial(1/Z)}{\partial \xi}\right). \quad (32)$$

The method for solving this equation (in particular, with the above boundary conditions) and its interesting exact solutions are presented in [13]. The magnetic field carried by the charged component diffuses (more precisely, propagates in a diffusive manner) in a plasma with the velocity $\sim \tilde{D}_{am}^{1/2} t^{-1/2}$.

In the opposite limiting case ($\tilde{D}_M \gg \tilde{D}_{am}$), setting $Z = 1$ in (30) provides a linear heat conduction equation, whose solutions are well known. The magnetic field is no longer frozen in the charged plasma component and penetrates diffusively into a plasma with the velocity $\sim \tilde{D}_M^{1/2} t^{-1/2}$. The charged component diffuses in the same direction as the field but with a lower velocity $\sim \tilde{D}_{am}\tilde{D}_M^{-1/2} t^{-1/2}$.

For an arbitrary ratio $R = \tilde{D}_{am}/\tilde{D}_M$ between the diffusion coefficients, we seek solutions to equations (30) and (31) in the form of dimensionless functions of the only possible dimensionless combination of the spatial coordinate and time, $\lambda = x/(D_M t)^{1/2}$. This combination converts equations (30) and (31) to the ordinary differential equations

$$Y'' + \frac{1}{2}\lambda\left(\frac{Y}{Z}\right)' = 0, \quad R(YY')' - \frac{1}{2}\lambda\left(\frac{1}{Z}\right)' = 0,$$
$$Y, Z|_{\lambda\to\infty} = 1, \quad Y|_{\lambda = 0} = \alpha > 1, \quad (33)$$

where the prime denotes the derivative with respect to λ.

The solutions shown in Fig. 1 illustrate the qualitative tendencies described above.

Now, we determine the conditions under which the neutral component can be assumed to be immobile. The boundary of the region occupied by the charged component moving with the characteristic velocity U_d is displaced with respect to the neutral gas by the distance $U_d t$ over the time t. The neutral gas through which this boundary passes is affected by the bulk force $\tilde{\nu}_{in} n m_i U_d$ over the time t; as a result, the neutral particles acquire the velocity $U \sim \tilde{\nu}_{in} n m_i U_d t/(m_i N) = \tilde{\nu}_{in} n U_d t/N$. The condition for the entrainment of neutral gas by the charged component, $U \sim U_d$, starts to hold only after a fairly long time interval $t \sim N/(\tilde{\nu}_{in} n)$, over which the neutral component can be assumed to be immobile. However, we must keep in mind that, over a very short time interval at the beginning of the initial stage, one of the main conditions for the applicability of the initial

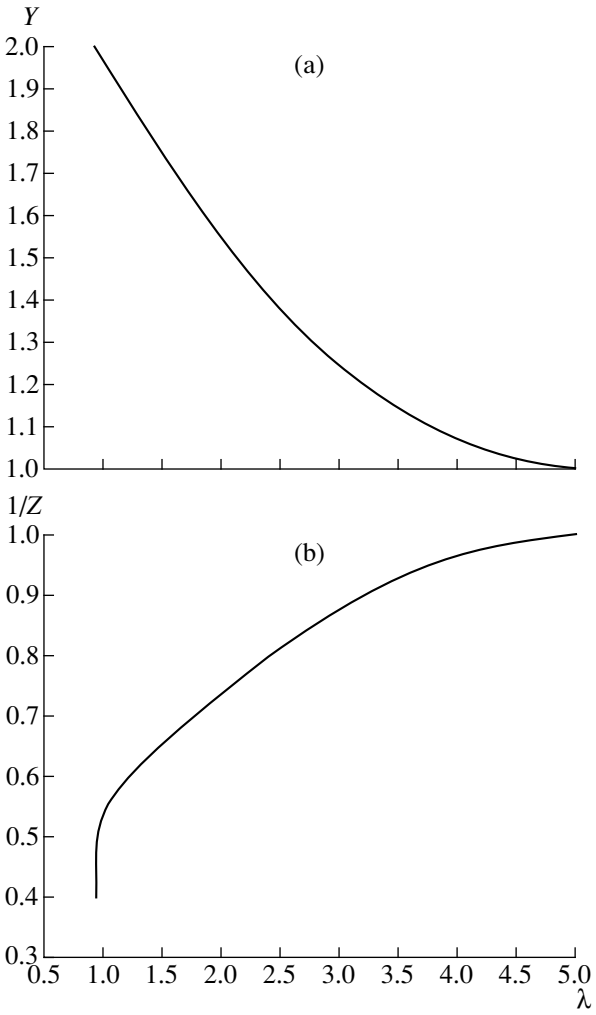

Fig. 1. Self-similar penetration of the magnetic field into a weakly ionized plasma: (a) distribution of the magnetic field normalized to that deep in the plasma and (b) distribution of the specific volume $1/Z$. At an arbitrary time, the spatial coordinate refers to the distance from the boundary of the region occupied by the charged component moving into the plasma. The magnetic field penetrating into the plasma is seen to be two times stronger than that deep in the plasma.

equations (15)–(19) may fail to hold: the linearization of the kinetic equation and the BGK model itself imply that the velocity of the charged component with respect to the neutral gas should be low in comparison with the thermal velocities, whereas, at the very beginning of the initial stage, the relative velocity evaluated from the diffusion equation behaves as $t^{-1/2}$.

6. STRUCTURE OF SHOCK WAVES IN A WEAKLY IONIZED PLASMA

Now, we describe the structure of shock waves in a weakly ionized plasma. It is of interest to note that, under condition (20), which implies that the magnetic energy density exceeds the energy density of the charged particles, the shock wave structure can be described without regard to such a specific plasma process as the energy transfer in the charged plasma component (which was a key problem in previous investigations [1, 2]); in this way, it is sufficient to exploit equations (15)–(19). The reason is that the processes of the energy and momentum transfer in the charged component are unimportant because the energy and momentum of the charged component are both negligible and the role played by the ambipolar magnetic diffusion, which is incorporated into equations (15)–(19), in the momentum transfer from charged particles to the neutral component is greater than that of ordinary ambipolar diffusion: the ambipolar magnetic diffusion coefficient (and even more so the total diffusion coefficient, which includes the ordinary magnetic diffusion coefficient) is larger than the ordinary ambipolar diffusion coefficient.

For simplicity, we restrict ourselves to considering a longitudinal shock wave, such that the magnetic field vector is parallel to the shock front. We write equations (15)–(19) in the frame in which the shock front is at rest. We assume that the velocity is aligned with the positive x-axis, which is directed from the region upstream of the shock front to the region downstream of the front; i.e., when moving along the x-axis from $-\infty$ toward $+\infty$, the gas velocity decreases, while the density, pressure, and magnetic field increase. We denote by the subscripts 0 and 1 the plasma states upstream and downstream of the shock front, respectively. In the steady-state case, equations (15)–(19) with the magnetic field configuration adopted can be written as

$$U = U_0 N_0/N, \tag{34}$$

$$n = \frac{n_0 u_0}{U} + \frac{HH'}{4\pi m_i \tilde{\nu}_{in0} U_0}, \tag{35}$$

$$m_i N_0 U_0 U + P + \frac{H^2}{8\pi} = m_i N_0 U_0^2 + P_0 + \frac{H_0^2}{8\pi}, \tag{36}$$

$$UH - U_0 H_0 = \tilde{D}H', \quad \tilde{D} = \frac{c^2}{4\pi\sigma_0} + \frac{UHH_0}{4\pi m_i \tilde{\nu}_{in0} U_0}, \tag{37}$$

where the prime indicates the derivative with respect to x. Except for equation (35), which was already used to derive (37), these are one-fluid MHD equations with the refined total magnetic field diffusion coefficient. We also restrict ourselves to treating weak shocks, $N_1 - N_0 \ll N_0$. In the problem as formulated, the jump in entropy at the shock front is a small third-order quantity [12] and we can set

$$\begin{aligned} P - P_0 &= P_0[(N/N_0)^\gamma - 1] \\ &\approx P_0\left[\gamma\left(1 - \frac{U}{U_0}\right) + \frac{\gamma(\gamma+1)}{2}\left(1 - \frac{U}{U_0}\right)^2\right]. \end{aligned} \tag{38}$$

For a weak shock, we can also put $\tilde{D}$ = const and introduce the dimensionless variable $x = \tilde{D}\lambda/U_0$. As a result, we arrive at the following two differential equations, describing the shock front structure:

$$\begin{aligned} (u_0^2 - v_{s0}^2)(u-1) + \frac{\gamma+1}{2} v_{s0}^2 (u-1)^2 \\ + v_{A0}^2 \frac{h^2 - 1}{2} = 0, \end{aligned} \tag{39}$$

$$\frac{dh}{d\lambda} = hu - 1, \tag{40}$$

where $u = U/U_0$, $h = H/H_0$, $v_{s0} = [\gamma P_0/m_i N_0)]^{1/2}$ is the speed of sound and $v_{A0} = [H_0/(4\pi m_i N_0)]^{1/2}$ is the Alfvén velocity upstream of the front. In the plane (u, h), the points corresponding to the states at the shock front lie on ellipse (39) and above the curve $hu = 1$, which is a hyperbola, because the right-hand side of (40) is positive in the shock (compression) wave. Since the points at which the hyperbola intersects the ellipse correspond to the initial and final states, we can take (39) with

$$u = u_1, \quad h_1^2 - 1 = u_1^{-2} - 1 \approx 2(1 - u_1) + 3(1 - u_1)^2 \tag{41}$$

in order to obtain the final parameter values:

$$I = h_1 - 1 \approx 1 - u_1 \approx \frac{u_0^2 - v_{s0}^2 - v_{A0}^2}{\frac{3}{2} v_{A0}^2 + \frac{\gamma+1}{2} v_{s0}^2}. \tag{42}$$

As usual, the quantity I will be referred to as the shock wave intensity. From (42), we can see that the shock wave is supersonic with respect to the gas upstream of the wave front:

$$u_0^2 - v_{s0}^2 - v_{A0}^2 > 0. \tag{43}$$

Since the curve defined by (39) is an ellipse, the function $u(h)$ along this curve may be non-single-valued. Depending on the relative positions of the hyperbola and ellipse, we can distinguish between two radi-

cally different cases (Fig. 2). The first case is illustrated in Fig. 2a. When moving from the point corresponding to the state upstream of the front to the point corresponding to the state downstream of the front along the ellipse (this portion of the ellipse corresponds to the states at the front), together with the condition $h = h_1$, the condition $u = u_1$ turns out to be satisfied. This result indicates the possibility of a continuous transition from the initial state to the final state inside the shock front, so that the front structure is continuous (Fig. 3a). The second case is illustrated in Fig. 2b. When moving along curve (39), we can see that, when the magnetic field reaches the value h_1, the velocity does not approach the value u_1, because this value lies on the other branch of the function $u(h)$. In this situation, the velocity can take the value u_1 only via a gas-dynamic jumplike transition. The spatial scale on which this transition occurs is governed by processes that were not included in our analysis. Owing to diffusion, the magnetic field is continuous on arbitrarily short spatial scales and, therefore, remains constant within this jump. Thus, ahead of the gas-dynamic jump, the magnetic field increases continuously up to h_1 and the velocity also grows to a certain value. Within the jump, the velocity increases instantaneously from this value up to u_1 (Fig. 3a). The sign of the derivative dH/du along curve (39) at the point (u_1, h_1) serves as a criterion for distinguishing between the two cases. The condition for this derivative to be positive (and, accordingly, for a continuous solution to exist) has the form

$$I\left[\frac{\gamma(\gamma+1)}{6}-1\right]<\frac{2}{3}. \qquad (44)$$

(Recall that the quantity $\beta_n = 2v_{s0}^2/\gamma v_{A0}^2$ was introduced as the ratio of the neutral pressure to the magnetic field pressure upstream of the front.)

If the magnetic field pressure is higher than the thermal pressure (the parameter β_n is small), then the left-hand side of (44) is negative and the shock front structure is continuous. If the magnetic field pressure is low ($\beta_n \longrightarrow \infty$), then, naturally, there is a gas-dynamic jump at the shock front, because, in the absence of a field, the shock wave is nothing more than a gas-dynamic jump. In a weak magnetic field, only very weak shocks (with intensities $I \le \beta_n^{-1}$) can have a continuous structure.

To describe the continuous structure of a shock wave, we expand the quantity $1 - u$ in powers of $h - 1$ with the help of (39), retaining terms up to the second order. Then, we substitute the resulting expansion in (40) and expand the right-hand side of (40) with the same accuracy to obtain

$$\frac{dh}{d\lambda} = \frac{3}{2}\left[1+\frac{\gamma(\gamma+1)}{6}\beta_n\right](h-1)(h_1-h). \qquad (45)$$

Equation (45) has the solution

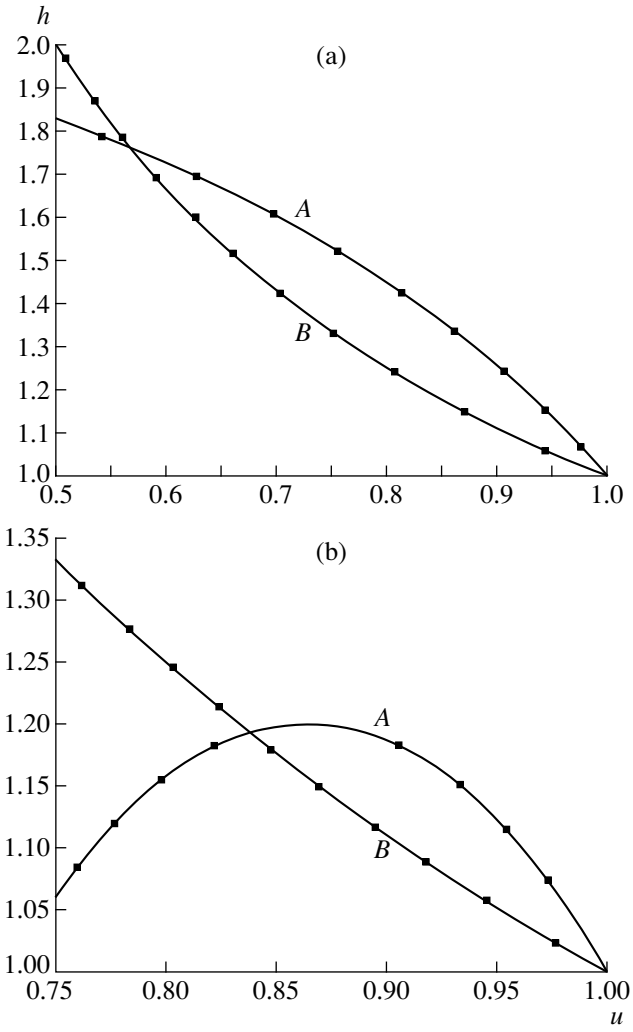

Fig. 2. Two cases of relative positions of curve (39) (marked by *A*) and curve (40) (marked by *B*). Case (a) corresponds to a shock wave with a continuous structure (for the parameter values $v_{s0}/v_{A0} = 1$ and $u_0/v_{A0} = 2$), and case (b) corresponds to the front structure with a gas-dynamic jump (for $v_{s0}/v_{A0} = 3$ and $u_0/v_{A0} = 3.5$).

$$h-1 = \frac{I}{2}\left\{1+\tanh\left[\left(\frac{3}{4}+\frac{\gamma(\gamma+1)\beta_n}{8}\right)I\lambda\right]\right\}. \qquad (46)$$

To describe a precursor ahead of the gas-dynamic jump at a shock front with a discontinuous structure, we can assume that the velocity in the precursor region is constant, so that

$$\frac{dh}{d\lambda} = h-1, \quad h-1 = I\exp\lambda. \qquad (47)$$

In dimensional variables, the characteristic width Δ_c of the front with a continuous structure and the width Δ_d

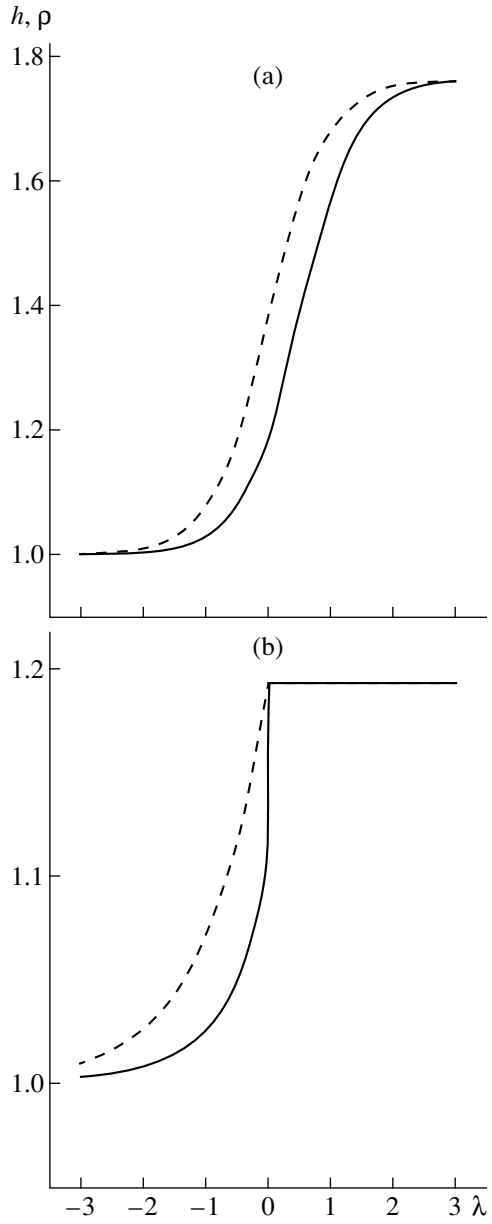

Fig. 3. Profiles of the density (solid curve) and magnetic field (dashed curve) inside the shock front normalized to their values ahead of the shock front. Cases (a) and (b) correspond to the parameters of Figs. 2a and 2b, respectively.

of the precursor upstream of the front with a discontinuous structure are as follows:

$$\Delta_c = \frac{\tilde{D}}{I\left[\frac{3}{4} + \frac{\gamma(\gamma+1)}{8}\frac{v_{s0}^2}{v_{A0}^2}\right]\sqrt{v_{s0}^2 + v_{A0}^2}}, \qquad \Delta_d = \frac{\tilde{D}}{\sqrt{v_{s0}^2 + v_{A0}^2}}. \tag{48}$$

7. DISCUSSION OF THE RESULTS AND CONCLUSIONS

First, we discuss the applicability of our results to the analysis of shock waves in tubes that are prefilled with a weakly ionized plasma. Simple estimates show that the magnetic field diffusion is dominated by ordinary magnetic diffusion, while the contribution of ambipolar magnetic diffusion is insignificant. In this case, the diffusion coefficient is very large. To obtain rough estimates, we set $\nu_{en} \sim 10^{-7}N$ [s^{-1}]] and express the diffusion coefficient in terms of the degree of ionization, $\tilde{D} \sim 3 \times 10^4 \chi^{-1}$ [cm^2/s]. This indicates that, if a precursor has enough time to form in the course of experiments in which the plasma is weakly ionized and shock waves propagate with a typical velocity of about $\sim 10^5$ cm/s, then it may become as wide as several tens or even hundreds of meters. Such a precursor will have essentially no impact on the shock wave, because the magnetic energy density is low compared to the neutral pressure, so that the wave structure will remain discontinuous and the gas-dynamic jump will remain almost unchanged.

However, the magnetic field redistribution may lead to the redistribution of the charged-particle density upstream of the shock front. The density redistribution should be described by the above set of equations supplemented with fairly complicated boundary conditions for the magnetic field. Here, we leave out of account the unpleasant fact that, during probe measurements of the charged-particle density, the magnetic field redistribution gives rise to inductive electric fields, which, in turn, may induce probe currents that are completely unrelated to the plasma density variations.

The conclusions regarding astrophysical applications can be summarized as follows. First, in a weakly ionized plasma, transverse magnetic diffusion turns out to be inherently nonlinear and is closely related to ambipolar magnetic diffusion. This indicates in particular that, in zero field regions (magnetic null points and lines), the magnetic field diffusion sharply reduces (the ambipolar diffusion coefficient vanishes) and ordinary diffusion, associated with electron–neutral collisions, comes into play.

Second, in weakly ionized space plasmas, the front width of the shock waves is very sensitive to both the direction of the magnetic field and its strength. In a finite-β_n plasma, a purely transverse shock wave, in contrast to a purely longitudinal wave, may have a continuous structure and its front width is governed by the ambipolar magnetic diffusion coefficient, which is nonlinearly dependent on the magnetic field. In the regions where the magnetic field is zero and β_n values are arbitrarily large, the width of the shock fronts is small and the parameter range in which shock waves with a continuous structure can exist is narrow.

We should say a few words about papers [14, 15], which appeared when we were preparing this work for

publication. Bulanov and Sakai [14] presented a comprehensive review of the research that has been carried out on ambipolar magnetic diffusion, beginning with the paper by Mestel and Spitzer [16]. Smolyakov and Khabibrakhimov [15] considered the penetration of an alternating magnetic field into the column of a weakly ionized plasma with allowance for ambipolar magnetic diffusion; the problem as formulated has much in common with the problem treated in Section 5 of our paper.

REFERENCES

1. R. F. Avramenko, A. A. Rukhadze, and S. F. Teselkin, Pis'ma Zh. Éksp. Teor. Fiz. **34**, 485 (1981) [JETP Lett. **34**, 463 (1981)].
2. V. A. Pavlov, Fiz. Plazmy **22**, 182 (1996) [Plasma Phys. Rep. **22**, 167 (1996)].
3. M. Suzuki and J. I. Sakai, Astrophys. J. **465**, 393 (1996).
4. M. Suzuki and J. I. Sakai, Astrophys. J. **487**, 921 (1997).
5. M. Ryutova, R. Shine, A. Title, and J. I. Sakai, Astrophys. J. **492**, 402 (1998).
6. A. F. Alexandrov, L. S. Bogdankevich, and A. A. Rukhadze, *Principles of Plasma Electrocdynamics* (Vysshaya Shkola, Moscow, 1978; Springer-Verlag, Berlin, 1984).
7. S. I. Braginskii, in *Reviews of Plasma Physics*, Ed. by M. A. Leontovich (Gosatomizdat, Moscow, 1963; Consultants Bureau, New York, 1963), Vol. 1.
8. E. M. Lifshitz and L. P. Pitaevskii, *Physical Kinetics* (Nauka, Moscow, 1979; Pergamon, Oxford, 1981).
9. F. H. Shu, Astrophys. J. **273**, 202 (1983).
10. L. Rudakov, Phys. Plasmas **2**, 2940 (1995).
11. A. V. Gordeev, Fiz. Plazmy **13**, 1235 (1987) [Sov. J. Plasma Phys. **13**, 713 (1987)].
12. L. D. Landau and E. M. Lifshitz, *Fluid Mechanics* (Nauka, Moscow, 1986; Pergamon, Oxford, 1987).
13. Ya. B. Zel'dovich and Yu. P. Raizer, *Elements of Gas Dynamics and the Classical Theory of Shock Waves* (Nauka, Moscow, 1966; Academic, New York, 1968).
14. S. V. Bulanov and J. I. Sakai, Astrophys. J., Suppl. Ser. **117**, 599 (1998).
15. A. L. Smolyakov and I. Khabibrakhimov, Phys. Rev. Lett. **81**, 4871 (1998).
16. L. Mestel and L. Spitzer, Mon. Not. R. Astron. Soc. **116**, 505 (1956).

Translated by O. E. Khadin

Plasma Physics Reports, Vol. 26, No. 6, 2000, pp. 502–506. Translated from Fizika Plazmy, Vol. 26, No. 6, 2000, pp. 538–542.

PLASMA DYNAMICS

Simulation of the Formation of Accelerating Structures and Ion Acceleration in the Collision of Magnetosonic Shock Waves

G. N. Dudkin, B. A. Nechaev, and V. N. Padalko

Research Institute of Nuclear Fusion, Tomsk Polytechnic University, pr. Lenina 2a, Tomsk, 634050 Russia

Received July 20, 1999; in final form, November 9, 1999

Abstract—Results are presented from numerical calculations of the maximum energy of accelerated deuterons as a function of the magnetic field for two models of the formation of the accelerating field in the region where two magnetosonic shock waves collide. The numerical results are compared with the similar experimental dependence. *© 2000 MAIK "Nauka/Interperiodica".*

1. INTRODUCTION

One of the processes accompanying high-power energy deposition in a plasma is the excitation of magnetosonic shock waves (MSWs). These waves have been actively studied both theoretically and experimentally because they are among the main sources of high-energy particles in cosmic plasma and play an important role in plasma heating in laboratory experiments.

Theoretical investigations [1–5] show that a fairly high electric field generated at the MSW front can accelerate charge particles to high energies with a high acceleration rate.

Laboratory experiments [6, 7] demonstrate that ions can be accelerated by MSWs both along and perpendicularly to the shock front. In both cases, the accelerated particles move across the magnetic field.

Taking into account the collisions between MSWs even more widens the spectrum of nonlinear plasmadynamic effects due to the sharp increase in the energy density (including electric and magnetic energies) in narrow space and time intervals.

In experiments [8–10], the possibility of accelerating plasma ions along an external magnetic field during the interaction of two MSWs propagating quasi-perpendicularly to the magnetic field toward each other was demonstrated for the first time. It was shown experimentally that, when two MSWs (with the magnetic Mach number $M_A \sim 1.7$ and extended plane fronts of length $l \sim 8$ cm) propagating toward each other in deuterium plasma with the density $N \sim 2.5 \times 10^{13}$ cm^{-3} at an angle of $\Theta \sim 12°$ to the external magnetic field ($B_0 = 1.0$ T) collided, a pulsed flux of accelerated deuterons ($\tau \approx 150$ ns and $I_{max} \approx 10^5$–10^6 particle/pulse) with a maximum energy of ~10 MeV was generated along the magnetic field. This means that, in the region where two MSWs collide, a traveling electric field directed along the external magnetic field is produced.

Two models were proposed to interpret the experimental results. According to the first model [8, 9], the generation of an accelerating electric-field wave propagating along the magnetic field is a result of the summation of the longitudinal (with respect to the magnetic field) components of the electric fields occurring at the MSW fronts. The other model [10] suggests that an ion-acoustic wave propagating along the external magnetic field is generated in the region where the MSWs collide and the ions are accelerated by the electric field at the front of this ion-acoustic wave. However, both models fail to adequately describe the process of trapping particles in the acceleration regime, to explain long-term confinement of ions in the phase with the accelerating wave, or to predict the maximum energy of the accelerated particles. In both models, it is assumed that the plasma density is constant along the magnetic field.

Detailed investigations of the plasma density distribution carried out in [11] by a method based on the measurements of the Hall potential during the passage of a controlled probing current showed that the plasma density distribution along the magnetic field is approximately described by the expression $N(z) = N_0(0.74 + 0.26\cos(kz))$, where $k = 0.255$ cm^{-1} and N_0 is the plasma density at $z = 0$. In [12], the spectra of the accelerated deuterons for the given density distribution were calculated under the assumption that the accelerating field resulted from the summation of the longitudinal components of the electric fields at the MSW fronts. The calculations show that the initial plasma density distribution substantially affects the spectrum and number of accelerated ions.

In this paper, we present the results of calculations carried out to test (and choose one of) the two models describing the dependence of the energy of the accelerated ions on the initial magnetic field, the other parameters being fixed. The results obtained are compared with the similar experimental dependence.

In calculations, we take into account the shape of the plasma density distribution along the magnetic field, the finite plasma pressure, and the degree to which the plasma is magnetized.

1063-780X/00/2606-0502$20.00 © 2000 MAIK "Nauka/Interperiodica"

The paper is organized as follows. In Section 2, we describe the MSW formation. In Section 3, we specify the physical parameters for the two models of ion acceleration. Section 4 gives a brief description of the experiment. Section 5 presents the procedure and results of numerical calculations of acceleration for both models.

2. FORMATION OF AN MSW

Let the plasma drifting from the region with the electric field $\mathbf{E}_p$ (discharge region), which is directed perpendicularly to the magnetic field, move along the *X*-direction (across the magnetic field **B**) with the velocity $V_d \simeq cE_p/B$, where c is the speed of light. When the plasma flow arrives at the region where $E_p \longrightarrow 0$ (outside the discharge), the drift velocity vanishes ($V_d \longrightarrow 0$). The increase in the ion velocity with respect to the electron velocity (due to the difference in the Larmor radii) leads to the charge separation along the *X*-axis; i.e., the field E_x emerges. This field accelerates the electrons and decelerates the ions, so that the kinetic energy of the plasma flow is transferred to the electrons, which drift in the *Y*-direction with the velocity $V_y \simeq \beta_e V_d$ under the action of the Lorenz force [13] (here, $\beta_e = \omega_{Be}/\nu_{ei}$ is the degree to which the electrons are magnetized, ω_{Be} is the electron cyclotron frequency, and ν_{ei} is the electron–ion frequency).

The charge separation in the *Y*-direction is accompanied by the polarization current. On the spatial scale $\delta x \sim R_i$ (where R_i is the ion Larmor radius), the polarization current density is $j \simeq eN\beta_e V_d$. Taking into account the dielectric permittivity of a magnetized plasma ($\varepsilon \simeq 4\pi m_i N c^2/B^2$), we obtain the time $t \simeq 1/\beta_e\omega_{Bi}$ during which the current flows [11]. During the same time, the *Y*-component of the electric field in the plasma increases to $E_y \leq E_p$ and the plasma begins drifting again. For small values of β_e (large values of ν_{ei}), which corresponds to a relatively cold plasma ($\nu_{ei} \sim 1/T^{3/2}$), the polarization current is small and the plasma moves across the magnetic field almost without deceleration. (This regime was used to fill the working volume with an initial plasma.) As β_e and V_d increase (which corresponds to an increase in the temperature and/or the drift velocity), the increased polarization current substantially increases the Joule loss and the plasma flow is decelerated. The polarization current produces an additional magnetic field (magnetic perturbation) [11]

$$\Delta B \simeq \frac{2\pi m_i c^2 N \beta E_p^2}{B_0^3}.$$

Here, B_0 is the external (unperturbed) magnetic field. If the polarization current rapidly increases, the magnetic perturbation is detached from the decelerated flow and, propagating through the initial plasma, transforms into an MSW. We assume that the magnetic perturbation transforms into a magnetoacoustic soliton. Then, the perturbation front should steepen from an initial width of $l \sim tV_A \sim c/\beta\omega_{pi}$ (where V_A is the Alfvén velocity and ω_{pi} is the ion plasma frequency) to

$$\Delta_{\text{sol}} \simeq c/\omega_{pe}[2(M_A - 1)]^{1/2}, \quad (1)$$

where ω_{pe} is the electron plasma frequency. Such a front can form when a freely propagating magnetic perturbation covers a distance of $L \sim c(2M_A - 1)/\beta\omega_{pi}(M_A - 1)$. Thus, the rapid change in E_p (which corresponds to a rapid energy deposition in the plasma) can result in the formation of a soliton with the Mach number

$$M_A \simeq \frac{\pi N m_i c^2 E_p^2}{B_0^4}\beta + 1 \quad (2)$$

(here, we take into account that $((\Delta B + B_0)/B_0 = (2M_A - 1))$ and the electric field at the front [2]

$$E_{\text{sol}} = \frac{m_i V_A^2 [2(M_A - 1)]^{3/2}\omega_{pe}}{ce}. \quad (3)$$

Further, we will consider an MSW with parameters corresponding to a magnetic soliton.

3. ACCELERATING FIELDS

Let two symmetric plane MSWs move toward each other in a uniform plasma. The MSW fronts are inclined at a certain small angle Θ to a uniform magnetic field. Then, the region where the MSWs collide moves along the *Z*-axis with the velocity $V_{ph} = M_A V_A/\sin\Theta$. We assume that, in the region where the MSWs collide, all of the components of the MSW electric field, except $E_z = 2E_{\text{sol}}\sin\Theta$, cancel each other; i.e., there is an electrostatic quasi-wave with the front width $\Delta_{\text{sol}}/\sin\Theta$ propagating at a fixed velocity V_{ph} along the magnetic field. The charge particles are accelerated in the field of the quasi-wave. If the electrostatic wave moves uniformly, the ratio of the maximum energy of the accelerated particles to their initial energy is at best ~2 under the condition that the initial particle velocity is comparable with the wave phase velocity and is directed in the direction of the wave propagation. In this case, the accelerated particle (ion) overtakes the wave and quits the acceleration regime. Consequently, in order to prolong the time the particle stays in the acceleration regime, it is necessary to provide conditions for the accelerating potential to propagate with increasing velocity along the *Z*-axis. Such conditions exist, e.g., in the presence of a plasma density gradient in the *Z*-direction (along the magnetic field). In this case, $V_{ph}(z) \sim M_A(z)V_A(z)/\sin\Theta(z)$ and, for small angles, we have [12]

$$\sin\Theta(z) \simeq \frac{d + z\tan\Theta_0}{2N(z)}\frac{dN}{dz} + \tan\Theta_0, \quad (4)$$

where Θ_0 is the initial angle between the MSW front and the magnetic field and d is the distance of the center of the MSW front from the axis along which two shock waves collide. Thus, in the case of the accelerated motion of the quasi-wave, both the width of the region occupied by the accelerating field and the field value are functions of Z:

$$\Delta_{\text{sol}}(z) \simeq \frac{c}{\omega_{pe}(z)[2(M_A-1)]^{1/2}\sin\Theta(z)}, \quad (5)$$

$$E_{\text{sol}}(z) = \frac{2m_i V_A^2(z)[2(M_A(z)-1)]^{3/2}\omega_{pe}(z)}{ce}\sin\Theta(z). \quad (6)$$

If $N(z)$ has a maximum, so that grad$N$ on both sides of the maximum has opposite directions, we have two electrostatic quasi-waves (collision regions) propagating from opposite directions with increasing velocities [12].

It should be noted that the accelerated propagation of the quasi-wave is also possible in the presence of magnetic field gradients in both the X- and Z-directions.

In the region where two MSWs collide, the plasma is additionally heated through compression by the magnetic fields ("walls") of the solitons. For the instantaneous equilibrium state, under the condition that the characteristic time of the density variation is $t_N > 1/\beta\Omega_{ci}$ (where $\Omega_{ci} = eB_0(2M_A(z)-1)/cm_i$ is the ion cyclotron frequency in the soliton magnetic field B_{sol}), we have

$$\frac{B_{\text{sol}}^2(z)}{8\pi} - \frac{B_p^2(z)}{8\pi} \simeq M_A(z)N(z)T_e(z)(1/\alpha + 1). \quad (7)$$

Here, B_p is the initial magnetic field in the plasma and $\alpha = T_e/T_i$ is the ratio between the electron and ion temperatures. For a Maxwell distribution (with the temperature T_i) in longitudinal (with respect to the magnetic field) ion velocities, a fraction of the particles is trapped in the regime of acceleration by the field $E_{\text{sol}}(z)$.

We also consider another mechanism for the formation of the accelerating field. Let us assume that, in the region where the MSWs collide, the thermal electron velocity is higher than the ion velocity ($V_{Te} > V_{Ti} \geq V_{ph}$) and the electrons are magnetized. Then, the charge separation proceeds along the magnetic field on the spatial scale on the order of the Debye length

$$\Delta_D(z) \simeq (T_e(z)/4\pi N(z)e^2)^{1/2}. \quad (8)$$

The electric field in this region is

$$E_D(z) \simeq B_p(z)\left(\frac{2(M_A(z)-1)\alpha}{1+\alpha}\right)^{1/2}. \quad (9)$$

Below, when calculating the spectra of accelerated ions, we use expressions (6) and (9) for the accelerating field.

4. EXPERIMENT

In order to test the above concepts of the formation of the accelerating field and the acceleration process, we carried out experiments in which we determined the final energy of the accelerated ions as a function of the magnetic field, the other parameters remaining almost unchanged. We chose the initial value of the magnetic field as an independent parameter, because the investigations showed that, when the magnetic field was varied (within a certain range), the longitudinal (with respect to the magnetic field) distributions of the energy density and plasma density in the plasma flow changed only slightly.

Experiments were carried out with the Temp plasma device described in greater detail in [8, 10]. Two pairs of 30-cm-long and 4-cm-wide electrodes with a gap distance of ≈2 cm were positioned in a ceramic chamber (with an inner diameter of 18 cm and length l = 150 cm) at a small angle to the symmetry axis of the longitudinal magnetic field. Two plasma flows produced in a "fast" discharge (characterized by a rapid increase in E_p and the deposited power) in the crossed **E** and **B** fields propagated toward each other across the magnetic field with the drift velocity V_d. Decelerated in the background plasma, these waves excited shock waves, whose collision at the varying angle $\Theta(z)$ resulted in the acceleration of deuterons along the magnetic field.

A beam of accelerated ions was formed in a 100-cm-long ion-transport line, which was connected coaxially to the discharge chamber. The guiding magnetic field in the line was 0.3 T. A scintillator detector was positioned at the end of the ion-transport line. The energy of accelerated ions was measured by the time-of-flight technique. The stop signal for the time-of-flight system was generated by the above scintillator detector. The start signal was generated by one of two optical detectors viewing the region where two MSWs collided, the spatial resolution being 0.8 mm. Signals from the detectors were fed to an S8-14 storage oscillograph. Since the base distance between the light and scintillator detectors was known (175 cm), we could reconstruct the maximum energy of the bunch of accelerated ions by processing the oscillograms. In the experiment, the maximum number of ions per pulse varied from 10^5 to 10^6. The experiments were carried out at a constant electric field $E_p \simeq 9$ kV/cm, fixed density $N_0 \simeq 2.5 \times 10^{13}$ cm^{-3}, and different magnitudes of the magnetic field, which provided different MSW Mach numbers [see (2)]. The measurement procedure was as follows. A series of shots was produced at the same initial parameters of the device. By analyzing the delay time for the detector signals in this series, we selected the event corresponding to the maximum energy and intensity of the flux of accelerated ions. This procedure was repeated for each new value of the magnetic field.

The experimental results are shown in Fig. 3. The error bars reflect only the error of determining the ion energy by the delay of the storage oscillograph signal.

The experiment is described in more detail in [14].

5. CALCULATIONS

The numerical calculation procedure is described in greater detail in [12]. Here, we restrict ourselves to its basic aspects.

We solve the problem of the one-dimensional motion of a particle in the electric field produced in the region where the MSWs collide. In calculations, we consider this field to be a potential step with the width (the region occupied by the field) determined by expressions (5) and (8) for the first and second models, respectively.

Within the potential step, the ions were accelerated, and, outside the step, they moved at a constant velocity. In each discretization interval over Z, the particles had a Maxwellian energy distribution corresponding to the equality between the gas-dynamic and magnetic pressures in the region where the MSWs collided. In accordance with this distribution, certain initial velocities and densities were assigned to the groups of particles. Then, we studied the interaction of each of these groups with the potential step.

Acceleration of a group of ions comes to an end when the group either leaves the step through its back boundary or reaches the Z boundary of the 8-cm-long integration region.

The validity of the model was tested for the case $N(z) = \text{const}$, for which an analytical solution is known.

Calculations were carried out for a deuterium plasma with the use of relations that express the final plasma and MSW parameters through the initial parameters B_0 and E_p, which can be controlled in the experiment:

$$\frac{B_p^2(z)}{8\pi} + \frac{N(z)m_i c^2 E_p^2}{2}\frac{}{B_0^2} = \frac{B_0^2}{8\pi}, \qquad (10)$$

$$M_A(z) \simeq \frac{\pi N(z) m_i c^2 E_p^2}{B_0^2 B_p^2(z)}\beta(z) + 1, \qquad (11)$$

$$\beta(z) = \frac{1}{4\pi N(z)}\left(\frac{m_i}{m_e}\right)^{1/2}\left(\frac{eB_p(z)}{m_i c}\right)\frac{m_e^2 c^3 E_p^3}{e^4 B_0^3}\frac{1}{\Lambda}, \qquad (12)$$

$$B_{\text{sol}}(z) \simeq B_p(z)(2M_A(z) - 1), \qquad (13)$$

where Λ is the Coulomb logarithm (in calculations, we take $1/\Lambda = 0.09$). Calculations were carried out for the experimentally measured distribution of the deuterium plasma density that was presented in the Introduction.

For the Mach numbers in the range from $M_A \geq 1$ to a supercritical value of $M_A \sim 3$, we calculated the values of E_p and B_0 for which M_A falls in the range in question (Fig. 1). It is seen from the figure that, under particular experimental conditions, the value of M_A depends strongly on the relation between E_p and B_0. However, in further calculations, we only varied B_0. The choice of

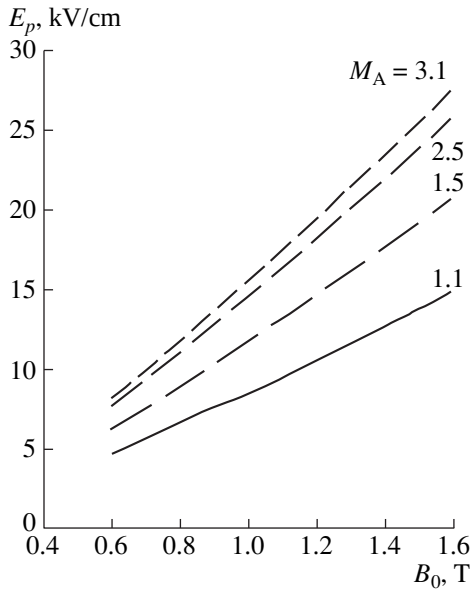

Fig. 1. Calculated values of B_0 and E_p for the given values of the magnetic Mach number M_A at $N_0 = 2.5 \times 10^{13}$, $\Theta_0 = 12°$, and $\alpha = 2$.

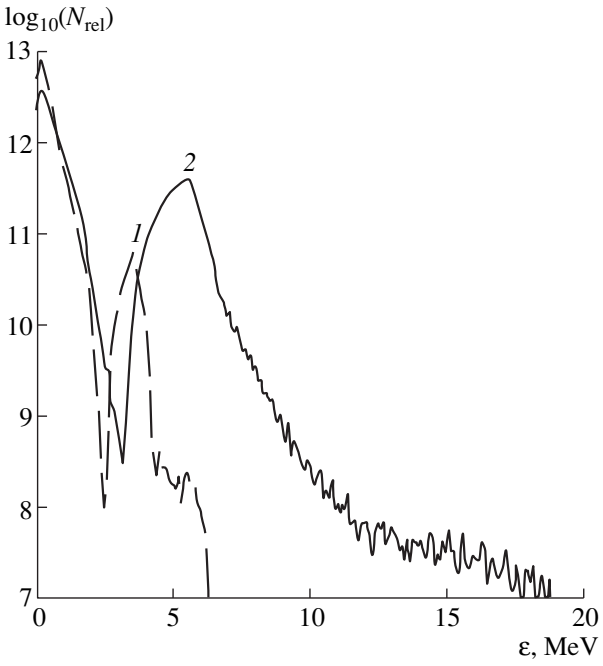

Fig. 2. Spectra of the accelerated deuterons calculated by expression (6) for E_{sol} (curve *1*) and expression (9) for E_D (curve *2*) at $N_0 = 2.5 \times 10^{13}$, $E_p = 9$ kV/cm, $\Theta_0 = 12°$, $\alpha = 2$, and $B_0 = 0.8$ T.

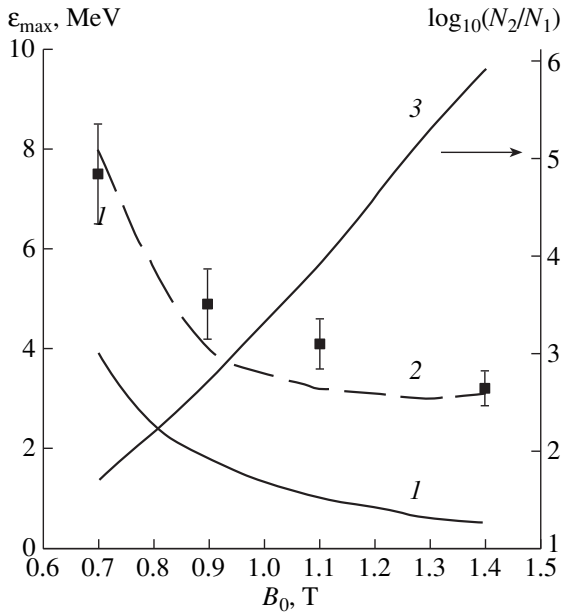

Fig. 3. The calculated energy of the accelerated deuterons (in the maximum of the spectral distribution) as a function of the initial magnetic field for the accelerating electric fields described by expressions (6) (curve *1*) and (9) (curve *2*). Squares show the experimental data. Curve *3* shows the calculated ratio between the number of accelerated ions for the two models (indices by *N* correspond to curves *1* and *2*). The values of the parameters are the same as in Fig. 2.

the initial magnetic field as an independent variable is determined by the fact that, as the experiments show, the change in E_p leads to the redistribution of the density in the plasma flow, which is difficult to control, because any probe placed in the region where the MSWs collide terminates the acceleration process.

For both models, the maximum energies of accelerated deuterons taken from the calculated spectra (Fig. 2) are presented in Fig. 3 as functions of B_0 (at $E_p \simeq$ const). The coefficient α was estimated from the bremsstrahlung intensity and was taken to be $\alpha \simeq 2$. The experimental results are presented in the same figure.

In conclusion, we note that, although the dynamic processes were calculated using the drift approximation, we obtained a satisfactory qualitative agreement between the calculated and experimental data for the Debye accelerating field. In the future, we also plan to investigate MHD processes, which, according to estimates, dominate in experiments with the discharge current density above a certain value.

ACKNOWLEDGMENTS

This work was supported in part by the Russian Foundation for Basic Research (project no. 97-02-17175) and the Russian Universities–Fundamental Research Program (project no. 241).

REFERENCES

1. L. P. Artsimovich and R. Z. Sagdeev, *Plasma Physics for Physicists* (Atomizdat, Moscow, 1979).
2. Y. Ohsawa, Phys. Fluids **28**, 2130 (1985).
3. Y. Ohsawa, Phys. Fluids **29**, 1844 (1986).
4. S. V. Bulanov and A. S. Sakharov, Pis'ma Zh. Éksp. Teor. Fiz. **44**, 421 (1986) [JETP Lett. **44**, 543 (1986)].
5. G. N. Kichigin, Zh. Éksp. Teor. Fiz. **101**, 1487 (1992) [Sov. Phys. JETP **74**, 793 (1992)].
6. N. A. Strokin, Zh. Éksp. Teor. Fiz. **88**, 2005 (1985) [Sov. Phys. JETP **61**, 1187 (1985)].
7. A. T. Altyntsev, G. N. Kichigin, I. V. Lebedev, and N. A. Strokin, Zh. Éksp. Teor. Fiz. **96**, 574 (1989) [Sov. Phys. JETP **69**, 324 (1989)].
8. G. N. Dudkin, B. A. Nechaev, A. V. Peshkov, *et al.*, Zh. Éksp. Teor. Fiz. **105**, 1606 (1994) [JETP **78**, 865 (1994)].
9. G. N. Dudkin, V. Yu. Egorov, B. A. Nechaev, *et al.*, Pis'ma Zh. Éksp. Teor. Fiz. **61**, 617 (1995) [JETP Lett. **61**, 633 (1995)].
10. G. N. Dudkin, V. Yu. Egorov, V. K. Kononov, *et al.*, Izv. Vyssh. Uchebn. Zaved., Fiz., No. 4, 119 (1998).
11. G. N. Dudkin, B. A. Nechaev, and V. N. Padalko, Fiz. Plazmy **23**, 258 (1997) [Plasma Phys. Rep. **23**, 237 (1997)].
12. G. N. Dudkin, B. A. Nechaev, V. N. Padalko, and A. S. Shlapakovskiĭ, Fiz. Plazmy **25**, 441 (1999) [Plasma Phys. Rep. **25**, 398 (1999)].
13. A. G. Belikov and N. A. Khizhnyak, Fiz. Plazmy **15**, 474 (1989) [Sov. J. Plasma Phys. **15**, 275 (1989)].
14. G. N. Dudkin, B. A. Nechaev, and V. N. Padalko, Fiz. Plazmy **26**, 142 (2000) [Plasma Phys. Rep. **26**, 129 (2000)].

Translated by A. D. Smirnova[†]

[†] Deceased.

Plasma Physics Reports, Vol. 26, No. 6, 2000, pp. 507–511. Translated from Fizika Plazmy, Vol. 26, No. 6, 2000, pp. 543–547.

PLASMA DYNAMICS

Ion-Acoustic "Houston's Horse" Effect

V. A. Pavlov

St. Petersburg State University, Universitetskaya nab. 7/9, St. Petersburg, 199164 Russia

Received March 16, 1999; in final form, July 20, 1999

Abstract—The structure of an ion-acoustic forerunner excited by a shock wave in a weakly ionized plasma is studied. It is shown that, when the shock velocity exceeds the ion-acoustic speed, a soliton bunch is produced at the perturbation front. The increase in the shock velocity to a certain critical value is accompanied by an increase in the soliton amplitude. A further increase in velocity leads to an explosive-like collapse of the bunch, which results in a decrease in the medium resistance. This phenomenon is analogous to the "Houston's horse" effect in narrow-channel hydrodynamics. © *2000 MAIK "Nauka/Interperiodica".*

1. The formulation of the problem is similar to that in [1]. We study a steady-state perturbation in a weakly ionized nonisothermal plasma ahead of the shock front. The perturbed quantities are assumed to be functions of $\xi = x - ct$, where x and t are the coordinate and time and c is the shock velocity. The plasma is characterized by the electron temperature T_e, ion temperature T_i, and the temperature T_n of neutrals. The stepwise shock of the neutral component is assumed to be strong.

We begin with the simplest problem and ignore the viscosity and heat conduction. In this case, the processes in the plasma are described by the set of equations

$$\begin{gathered}\frac{\partial n_i}{\partial t} + \frac{\partial}{\partial x}(n_i v_i) = 0, \quad \frac{\partial n_e}{\partial t} + \frac{\partial}{\partial x}(n_e v_e) = 0,\\ m_i\left(\frac{\partial}{\partial t} + v_i\frac{\partial}{\partial x}\right)v_i = |e|E - m_i\nu_{in}[v_i - v_n(\xi)],\\ 0 = -|e|E - kT_{0e}\frac{\partial \ln n_e}{\partial x},\\ \varepsilon_0\frac{\partial E}{\partial x} + |e|(n_e - n_i) = 0, \quad T_{0e} = \text{const},\\ v_n(\xi) = 0 \quad \text{for} \quad \xi > 0,\end{gathered} \tag{1}$$

where n and v are the electron density and velocity, e is the electron charge, m_i is the ion mass, E is the electric field, ε_0 is the permittivity of a vacuum, $\nu_{in} = \nu_{in}(\xi)$ is the collision frequency, and k is the Boltzmann constant.

The electric field in (1) can be represented in the potential form

$$E = -m_i v_s^2|e|^{-1}\frac{\partial \psi}{\partial x}, \quad v_s \equiv (kT_{0e}m_i^{-1})^{\frac{1}{2}}.$$

Since the process is steady, system (1) can be reduced to a single nonlinear equation for the potential

$$\begin{gathered}\frac{d}{d\xi}[F^{-2}(\psi) + 2M^{-2}\psi]\\ + 2\nu_{in}c^{-1}[1 - F^{-1}(\psi) - c^{-1}v_n(\xi)] = 0,\end{gathered} \tag{2}$$

where $F \equiv \exp\psi - 2D^2\psi''(\xi)$, $D \equiv (\varepsilon_0 kT_{0e}e^{-2}n_0^{-1})^{\frac{1}{2}}$, and $M \equiv cv_s^{-1}$ is the ion Mach number. Hereafter, the prime denotes the derivative with respect to the argument.

The fields are related by

$$\begin{gathered}n_e n_0^{-1} = \exp\psi, \quad n_i n_0^{-1} = \exp\psi - 2D^2\psi'',\\ v_i c^{-1} = 1 - F^{-1}, \quad E = -m_i v_s^2|e|^{-1}\psi'.\end{gathered} \tag{3}$$

Previously, equation (2) was investigated in two limiting cases: $D = 0$ and $\nu_{in} = 0$. The case $D = 0$ was studied in [1]. In this case, equation (2) can be transformed into the equation for v (below, the index by v is omitted):

$$v'[(c - v)^2 - v_s^2] - \nu_{in}(c - v)(v - v_n) = 0. \tag{4}$$

For $M > 1$, the solution to equation (4) has a discontinuity at the point $\xi = \xi_d$ [1] with the jump $c(1 - M^{-2})$.

The second limiting case $\nu_{in} = 0$ is well studied. From (2), we obtain Sagdeev's equation

$$2D^2\psi'' = -\frac{d\Phi(\psi)}{d\psi}, \tag{5}$$

$$\Phi(\psi) = 1 - \exp\psi + M^2\left[1 - (1 - 2M^{-2}\psi)^{\frac{1}{2}}\right]. \tag{6}$$

Since we are interested only in the real solutions, we have $\psi \le \psi_*$, where $\psi_* = 0.5M^2$. The "potential

energy" $\Phi(\psi)$ has a maximum at $\psi = 0$. For $M \le M_*$, where M_* satisfies the equation

$$1 - M_*^2 - \exp(0.5M_*^{-2}) = 0, \quad M_* \approx 1.6 \tag{7}$$

the equation $\Phi(\psi) = 0$ has a positive solution. For $1 < M \le M_*$, equation (5) has both periodic solutions and a nonperiodic (soliton) solution.

For $M > M_*$, equation (5) has only periodic solutions. When going over from $M = 1$ to $M = M_*$, the soliton amplitude increases from 0 to ψ_*, which corresponds to the velocity $v_* = M_* v_s$. For $M > M_*$, there is no soliton solution. The value $M = M_*$ is the bifurcation point for the soliton.

For weak dispersion, from (2) and (3), we obtain the equation intermediate between the two limiting cases described by (4) and (5). According to (3), ψ and v are related by

$$\exp(-\psi) = (1 - vc^{-1})(1 - \delta_1), \qquad \delta_1 \equiv 2D^2 \exp(-\psi)\psi'' . \tag{8}$$

We assume δ_1 to be a small parameter, $|\delta_1| \ll 1$. We make use of the representation

$$\psi|_{D=0} = -\ln(1 - vc^{-1})$$

to obtain

$$\delta_1 \approx 2D^2[c^{-1}v'' + c^{-2}(v')^2(1 - vc^{-1})] \approx 2D^2[c^{-1}v'' + c^{-2}(v')^2]. \tag{9}$$

Relations (8) and (9) yield the representation for $\psi \approx \psi(v)$:

$$\psi \approx -\ln(1 - vc^{-1})[1 - 2D^2c^{-1}v'' - 2D^2c^{-2}(v')^2].$$

Taking into account the relations

$$\psi' \approx c^{-1}v'(1 - vc^{-1})^{-1} + 2D^2c^{-1}v'''\left[1 + 0\left(\frac{v}{c}\right)\right],$$

$$F^{-1} = 1 - vc^{-1},$$

we transform equation (9) into the approximate equation for the velocity $v(\xi)$:

$$-v'''2D^2v_s^2(1 - vc^{-1}) + v'[(c - v)^2 - v_s^2] - \nu_{in}(c - v)(v - v_n) \approx 0. \tag{10}$$

In equation (10), we retained the second-order terms with respect to v and the first-order terms with respect to the parameter D^2. If we set $\nu_{in} = 0$ in equation (10), we obtain qualitatively the same dependences as those described by the solution to Sagdeev's equation (5): there is a bifurcation value of the Mach number for the soliton, $M_* = \sqrt{3}$; the maximum possible soliton amplitude is $v_* = \sqrt{3}\, v_s$.

Equation (16) for $v(\xi)$ that involves the ion viscosity and electron heat conduction was obtained in [1]. From (10) and (16), we obtain the equation describing v in the problem in question:

$$-v'''2D^2v_s^2(1 - vc^{-1}) + v''\eta c\rho_0^{-1}(1 - vc^{-1})^2 + v'[(c - v)^2 - v_s^2] - \nu_0(c - v)(v - v_n) \approx 0, \qquad \nu_0 \equiv \nu_{in}[1 - v_n(\xi)v^{-1}] + \kappa^{-1}v_s^2kn_0, \tag{11}$$

where κ is the electron thermal conductivity and η is the dynamic viscosity.

Thus, equation (11) involves the nonlinear terms to the third order in vc^{-1}, elastic ion–neutral collisions, electron heat conduction (this leads to the replacement $\nu_{in} \longrightarrow \nu_0$ in the region $\xi > 0$, where $v_n(\xi) = 0$), ion viscosity, and dispersion. The factors by the higher order derivatives v''' and v' contain small parameters proportional to D^2 and η, respectively. This means that we have a singularly perturbed problem.

The first term of the inner expansion can be obtained by setting $D = 0$ and $\eta = 0$ in (11). As was noted above, for $M > 1$, $v(\xi)$ has a discontinuity at the point $\xi = \xi_d(M)$ and the function $\xi_d(M)$ is monotonic [1]: for $M \longrightarrow (\gamma + 1)^{\frac{1}{2}}(\gamma - 1)^{-\frac{1}{2}}$, we have $\xi_d \longrightarrow 0$ (for $\gamma = 1.4$ $\xi_d \longrightarrow 0$ with $M \longrightarrow \sqrt{6}$). This corresponds to the merging of the ion-acoustic front with the front of the shock of the neutral component. In the vicinity of $\xi = \xi_d$, the velocity $v(\xi)$ described by (11) changes sharply. Hence, it is necessary to take into account the higher derivatives. Three cases are possible: (i) dispersion is more important than viscosity, (ii) dispersion is less important than viscosity, and (iii) the effects of dispersion and viscosity are of the same order of magnitude.

The first case is of greater interest; therefore, we restrict ourselves to consideration of only this problem.

2. Let us derive an approximate representation of the solution to equation (11) in the vicinity of the point $\xi = \xi_d$ (inner expansion) for $1 < M \le M_*$, when the dispersion is more important than the viscosity.

We will assume that the small dimensionless parameters δ_2 and δ_3,

$$\delta_2 \equiv D^2\lambda^{-2}(M), \quad \delta_3 \equiv \eta c(\rho_0 v_s^2 \lambda)^{-1}, \tag{12}$$

are of the same order of magnitude, $\delta_2 \simeq \delta_3$. Here, $\lambda = \lambda(M)$ is the spatial scale of the perturbations at $\xi \approx \xi_d$.

We construct the representation (inner expansion for the singular problem [2])

$$v(\xi, D) \approx U_0(y) + \delta_2 U_1(y) + \delta_2^2 U_2(y) + \ldots,$$
$$\delta_2(D) \longrightarrow 0, \quad D \longrightarrow 0 \qquad (13)$$
$$y \equiv (\xi - \xi_d) D^{-1}, \quad y \sim 1, \quad D \longrightarrow 0.$$

The condition $\delta_2 \approx \delta_3$ allows us to obtain the set of equations for $U_n(y)$. The leading term in (13) satisfies the equation

$$4 v_s^2 c^{-1} U_0'' = -\frac{dW(U_0)}{dU_0}, \qquad (14)$$

where

$$W(U_0) = 3^{-1} U_0^3 - U_0^2 c + 2 U_0 v_s^2 + 2 c v_s^2 (1 - U_0 c^{-1}) \ln(1 - U_0 c^{-1}). \qquad (15)$$

Figure 1 shows dependence (15) for different values of M. At the point $U_0 = 0$, $W(U_0)$ has a maximum. For $1 < M \le M_* = \sqrt{3}$, there are both periodic solutions (13) and a nonperiodic (soliton) solution. The soliton amplitude increases from 0 to $\sqrt{3}\, v_s$ with increasing M from 1 to $M_* = \sqrt{3}$. The ion density n_i is related to the velocity v by the expression

$$n_i = n_0 c (c - v)^{-1}.$$

As $M \longrightarrow M_*$, v tends to $c = \sqrt{3}\, v_s$; hence,

$$\max n_i \longrightarrow \infty \quad \text{при} \quad M \longrightarrow M_*.$$

Therefore, the amplitude of the soliton bunch exhibits an explosive-like behavior: the finite increase in the velocity of the neutral-component shock leads to an infinite increase in the amplitude of the soliton of the ion density n_i. The value $M = M_*$ is the bifurcation point for the soliton: for $M > M_*$, the soliton is absent and equation (13) has only periodic solutions. Integrating (13) over dU_0, we obtain the relation between U_0' and U_0 that describes the phase-plane portrait

$$v_s \sqrt{2 c^{-1}}\, U_0' = \pm \sqrt{W_0 - W(U_0)}, \quad W_0 = \text{const}.$$

Nonperiodic solutions correspond to $W_0 = 0$. The matching of the inner and outer expansions is shown in Fig. 2, where we take the soliton as the outer expansion. This allows us to describe the transition $v(\xi) \longrightarrow 0$ as $\xi \longrightarrow \infty$. For

$$\eta = k T_{0i} n_{0i} \nu_{in}^{-1},$$

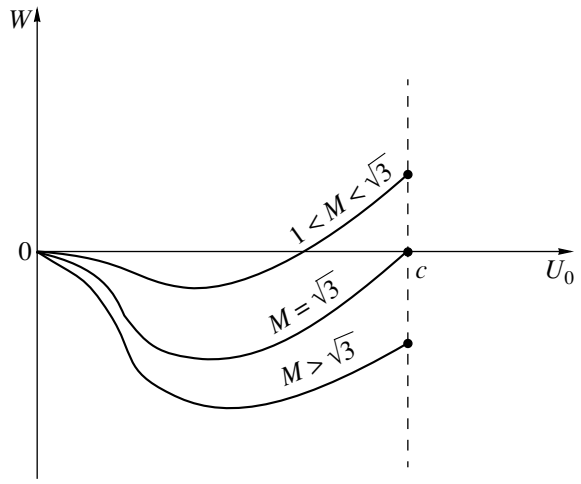

Fig. 1. The "potential energy" W as a function of U_0 for different values of the ion Mach number M.

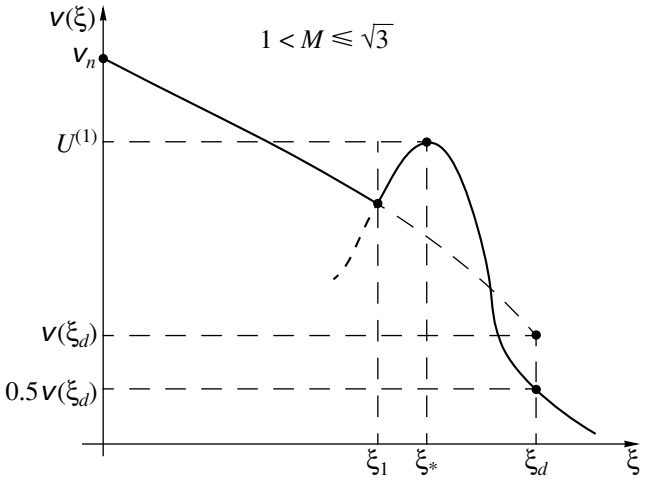

Fig. 2. Matching of the inner ($\xi > \xi_1$) and outer ($\xi < \xi_1$) representations for the velocity of the ion plasma component for $1 < M \le \sqrt{3}$.

the above condition $\delta_2 \approx \delta_3$ gives the criterion of the validity of expansion (13):

$$T_{0e} T_{0i}^{-1} \approx c \lambda(M) (D^2 \nu_{in})^{-1} \gg 1. \qquad (16)$$

When M increases to M_*, the soliton bunch collapses: in the model in question, we have $\eta = 0$ at the point $\xi = \xi_* \lambda(M) \longrightarrow 0$ for $M \longrightarrow M_*$; i.e., the assumptions adopted here [in particular (16)] are violated. In this case, viscosity becomes more important than dispersion.

3. We construct an approximate representation of the solution to equation (11) in the vicinity of the $\xi = \xi_d$ (inner expansion) for $M \geqslant M_*$ with allowance for vis-

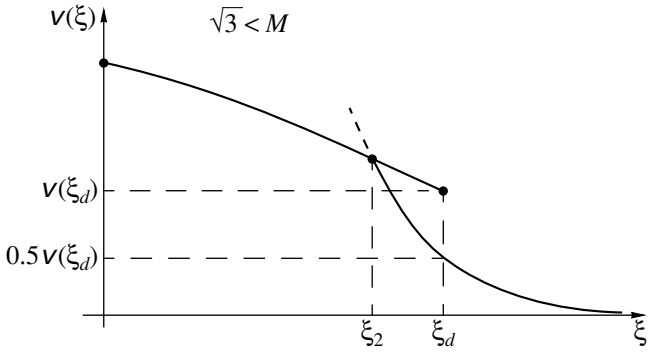

Fig. 3. Matching of the inner ($\xi > \xi_2$) and outer ($\xi < \xi_2$) representations for the velocity of the ion plasma component for $M > \sqrt{3}$.

cosity and with $\delta_2 \approx \delta_3^3$. The expansion is constructed in the form

$$v(\xi, \eta) \approx \varphi_0(z) + \left(\frac{\eta}{\eta_0}\right)\varphi_1(z) + \left(\frac{\eta}{\eta_0}\right)^2 \varphi_2(z) + \ldots,$$

$$\eta\eta_0^{-1} \ll 1,$$

$$\eta_0 \equiv \rho_0 c^{-1} v_s^2 \lambda(M), \quad z \equiv (\xi - \xi_d)\eta_0\eta^{-1},$$

$$z\lambda^{-1}(M) \sim 1, \quad \eta \longrightarrow 0.$$

For φ_n, we obtain the set of the coupled equations; φ_0 is described by the first-order equation

$$\varphi_0'\eta_0(c\rho_0)^{-1} + \varphi_0 + v_s^2(\varphi_0 - c)^{-1} + v_s^2 c^{-1} = 0, \quad (17)$$

which gives the relation between ξ and φ_0 in the form

$$-(\xi - \xi_d)\rho_0\eta_0^{-1}\varphi_* = \ln Q(\varphi_0),$$

$$\varphi_* \equiv (c^2 - v_s^2)c^{-1},$$

$$Q(\varphi_0) \equiv \frac{\varphi_0}{\varphi_{00}}\left(\frac{\varphi_* - \varphi_0}{\varphi_* - \varphi_{00}}\right)^{(\varphi_* c^{-1} - 1)}, \quad (18)$$

$$\varphi_{00} = \varphi_0(z)|_{z=0}.$$

The function $\varphi_0(\xi)$ decreases monotonically. The matching of $\varphi_0(\xi)$ and the outer representation of $v(\xi)$ is shown in Fig. 3 for $\varphi_0(0) = 0.5v(\xi_d)$. According to (18), the spatial scale of variations in $v(\xi, \eta)$ in the vicinity of $\xi = \xi_d$ is

$$\lambda \approx \eta[\rho_0 c(1 - M^{-2})]^{-1}.$$

The linear approximation for $\varphi_0(\xi)$ is described by

$$\varphi_0(\xi) \approx \varphi_{00}\exp\left[-\frac{c\rho_0}{\eta}(\xi - \xi_d)\right],$$

which allows evaluation of the field.

4. We obtain the intermediate representation for $v(\xi)$ in the vicinity of $\xi = \xi_1$ for the case of Section 2 and in the vicinity of $\xi = \xi_2$ for the case of Section 3. We denote $v_0 \equiv v(\xi_{1,2})$ and linearize equation (11) in the vicinity of $v \approx v_0$:

$$-v_1'''2D^2 v_s^2(1 - v_0 c^{-1}) + v_1''\eta(c\rho_0)^{-1}(c - v_0)^2 \quad (19)$$
$$+ v_1''[(c - v_0)^2 - v_s^2] - \nu_0 v_1(c - 2v_0) \approx \nu_0 v_0(c - v_0),$$

where $v_1 \equiv v - v_0$ and $|v_1| \ll v_0$.

The general solution to nonuniform equation (19) in the region $\xi \geq 0$ is

$$v_1 = -v_0(c - v_0)(c - 2v_0)^{-1} + \sum_{n=1}^{3} \mathrm{Re}[A_n \exp(q_n \xi)],$$

where q_n are the roots of the dispersion equation.

The intermediate representation and the representations in the adjacent regions can be matched at the points $\xi_{1,2} \pm \lambda(M)$. At one of these points, it is possible to provide the continuity of both the function and its first derivative.

5. The ion-acoustic shock-wave forerunner possesses the following properties. If $\delta_2 \approx \delta_3$ for $1 < M < M_* = \sqrt{3}$, then the soliton amplitude increases from zero to $\sqrt{3}\,v_s$ with increasing the Mach number from 1 to $\sqrt{3}$. At $M = M_*$, the bifurcation occurs; i.e., the soliton bunch collapses and the resistance of the medium sharply decreases. Smoothing of $v(\xi)$ in the vicinity of $\xi = \xi_d$ at $M_* > \sqrt{3}$ is due to viscosity. An abrupt disappearance of the soliton on the front of the forerunner corresponds to the "Houston's horse" effect. The hydrodynamic analogue of this effect was first observed in the nineteenth century. Below, we retell the description by Thomson presented in [3] (for the first time, this phenomenon was described in [4]).

"This effect was accidentally observed in a small channel between Glasgow and Ardrossan. A 'clever' horse drew the barge of William Houston, esquire. Suddenly the owner of the horse saw in wonder that the barge was moving unusually rapidly. The horse made much less efforts to draw it than usually, because it ran with a velocity equal to the velocity of the wave propagation. The wake wave, which usually splashed out on the bank, disappeared. Mr. Houston realized what benefit the company owning the channel transport can draw from the 'horse's' discovery. Since that time, the barges were towed through the channel at a higher velocity."

In [3], this effect was characterized somewhat inadequately: the formation of the wake wave was called the "Houston's horse" effect. In fact, the effect consists

in an abrupt disappearance of the wake wave when the boat velocity exceeds a certain critical velocity, rather than in the formation of a wake wave (soliton). In [3], it was stated that, "when the boat velocity v approaches the wave velocity c_{ph}, a boat in a narrow channel can climb up the crest of the wake wave, where it does not need to perform the work on the water by elevating or lowering its level." However, in reality, the boat cannot climb up the crest of its own wake wave; it can climb up only the crest of the "alien" wake wave (the wake wave of another boat or some other naturally or artificially created wave); it is also possible to slide down the alien wake wave (an example of this is surfing).

This effect is easily realized in a narrow sloping gutter (e.g., in a gutter for log floating). The barge can be replaced with a canoe, and the horse can be replaced with a man drawing the canoe against the water flow. The analogy between the ion-acoustic effect and the hydrodynamic one is the following: the parameter ν_0 characterizes the dragging against the bottom and the walls of the channel, η is the viscosity of the water, and D is the dispersion coefficient of the surface wave. In a narrow channel, the effect is due to strong nonlinearity; the "potential energy" $W(U)$ is described by either (15) or Sagdeev's approximation (5). In the Appendix, we present a model equation in which $W(U)$ is a fourth-order polynomial with $M_* = \sqrt{3}$. If $W(U)$ is described by a third-order polynomial, there is no critical Mach number: the soliton amplitude monotonically increases with increasing M. Presumably, such a regime exists in open shallow reservoirs. The "Houston's horse" effect has hysteresis: the decrease in the Mach number from $M > M_*$ to $M = 1$ does not lead to the appearance of a soliton at $M = M_*$, because the viscosity continues to smooth perturbations also at $M < M_*$.

APPENDIX

From (11), we will derive the model equation describing the "Houston's horse" effect. For this purpose, we linearize the terms with the higher order derivatives

$$-v'''2D^2v_s^2 + v''\eta c\rho_0^{-1} + v'[(c-v)^2 - v_s^2] - \nu_0 v(c-v) = 0. \quad (20)$$

For $D = 0$, $\eta = 0$, and $M = cv_s^{-1} > 1$, there is a discontinuous solution satisfying the condition $v(\xi) = 0$ for $\xi > \xi_d$ [1]. An analogue of equation (14) is

$$6v_s^2U_0'' = -\frac{dW(U_0)}{dU_0},$$
$$W(U_0) = -\frac{1}{4}U_0^2(U_0 - U^{(1)})(U_0 - U^{(2)}), \quad (21)$$
$$U^{(1,2)} \equiv 2c \mp \sqrt{6v_s^2 - 2c^2}.$$

The "potential energy" $\Phi(U_0)$ has extremes at the points

$$U = 0, \quad U^{(3,4)} = \frac{c}{2}[3 \mp \sqrt{3(4M^{-2} - 1)}].$$

Equation (21) has a nonperiodic solution only under condition $1 < M \le M_* = \sqrt{3}$; the soliton amplitude increases from 0 to $2\sqrt{3}\,v_s$ as M increases from 1 to $\sqrt{3}$. The value $M = \sqrt{3}$ is the bifurcation point for the soliton.

An analogue of equation (17) is

$$\varphi_0'3\eta_0 c\rho_0^{-1} + \varphi_0(\varphi_0 - \varphi^{(1)})(\varphi_0 - \varphi^{(2)}) = 0,$$
$$\varphi^{(1,2)} = \frac{c}{2}[3 \mp \sqrt{12M^{-2} - 3}]. \quad (22)$$

In the range $0 < \varphi < \varphi^{(1)}$, there exists a solution to equation (22) that monotonically decreases as $\xi \longrightarrow \infty$.

Model equation (20) qualitatively describes the "Houston's horse" effect: as M increases from 1 to $\sqrt{3}$, the soliton amplitude increases to $2\sqrt{3}\,v_s$; then, the soliton collapses. For $M > \sqrt{3}$, viscosity is more important than dispersion in the vicinity of $\xi = \xi_d$.

REFERENCES

1. V. A. Pavlov, Fiz. Plazmy **22**, 182 (1996) [Plasma Phys. Rep. **22**, 167 (1996)].
2. J. Colle, *Perturbation Methods in Applied Mathematics* (Blaisdell, Waltham, 1968; Mir, Moscow, 1972).
3. B. B. Kadomtsev and V. I. Rydnik, *Waves around Us* (Znanie, Moscow, 1981).
4. J. S. Russel, in *Reports of 14th Meeting of the British Association for Advancement of Science*, 1844, p. 311.

Translated by A. D. Smirnova[†]

[†] Deceased.

Plasma Physics Reports, Vol. 26, No. 6, 2000, pp. 512–518. From Fizika Plazmy, Vol. 26, No. 6, 2000, pp. 548–555.

PLASMA INSTABILITIES

Ion Larmor Radius Effects in Collisionless Reconnection[1]

D. Grasso[1], F. Califano[2], F. Pegoraro[2, 3], and F. Porcelli[1]

[1]*Istituto Nazionale Fisica della Materia and Dip. di Energetica, Politecnico di Torino, Italy*
[2]*Istituto Nazionale Fisica della Materia, Sez. A, Dip. Fisica, Università di Pisa, Italy*
[3]*Dip. di Fisica, Università di Pisa, Italy*

Received August 31, 1999; in final form, December 8, 1999

Abstract—The nonlinear evolution of collisionless magnetic field line reconnection is investigated numerically in plasma regimes where the effects of the electron and ion temperatures are important. These effects modify the structure of the current and vorticity layers that are formed during the onset of the reconnection instability. The results of investigations in a two-dimensional periodic configuration including ion Larmor radius effects to all orders are presented and compared with the results obtained in regimes with a large sound Larmor radius. It is found that, while the roles of the sound Larmor radius and the ion Larmor radius are interchangeable as far as the nonlinear reconnection rate is concerned, the structure of the vorticity and current density layers is different in the two cases. © *2000 MAIK "Nauka/Interperiodica".*

1. INTRODUCTION

In recent years, the problem of magnetic reconnection in collisionless regimes has been investigated extensively [1–10]. In these regimes, the decoupling of the plasma motion from the magnetic field is caused by the finite electron inertia [11–13]. The natural scale length associated with this process is the inertial skin depth, $d_e = c/\omega_{pe}$. Within the two-fluid model, the effects of the finite electron temperature in the generalized Ohm's law have also been considered [2]. These effects are important when the sound Larmor radius, $\rho_s = (m_i c^2 T_e/e^2 B^2)^{1/2}$, is comparable with d_e. On the other hand, ion Larmor radius effects were left aside. Since the ion Larmor radius is proportional to the sound Larmor radius through the relation $\rho_i = (T_i/T_e)^{1/2}\rho_s$, the results presented so far in the literature are valid in the cold ion limit, $T_i \ll T_e$ (such that $\rho_i < d_e$, while allowing $\rho_s \sim d_e$). Ion Larmor radius effects normally require full kinetic treatment of the ion species. However, the model proposed in [14], based on a Padé approximation of the ion response, allows us to consider these effects within a "modified fluid" description. The objective of this article is to investigate ion Larmor radius effects to all orders within the mentioned "modified fluid" approximation and to compare the results with those obtained when taking into account sound Larmor radius effects only. Previously, this analysis was limited in the nonlinear phase to a special class of self-similar solutions [15].

In the strictly collisionless (i.e., dissipationless) limit, the two-fluid model including finite temperature effects admits a Hamiltonian structure [14, 16, 17] with two infinite sets of conserved Casimirs. The Casimirs are arbitrary functionals of the fields that are conserved by the Hamiltonian in the Lagrangian sense. These Lagrangian invariants generalize the topological invariants that are found in the so-called reduced magnetohydrodynamics, as discussed in [14, 16]. Thus, the topology of these fields is frozen in the course of the dynamical evolution of the reconnection process, at least as long as the velocity fields with which the conserved fields are advected are smooth functions of space and time. Depending on whether electron and/or ion temperature effects are retained, different Lagrangian invariants and, thus, different Casimirs are conserved.

The linear theory of collisionless reconnection with finite electron temperatures and ion Larmor radius effects to all orders was developed in [18–21]. The following statements summarize the results of main interest here. When the tearing mode stability parameter Δ' is positive (Δ' is the jump of the logarithmic derivative of the perturbed magnetic flux across the reconnection layer), the growth rate and structure of the perturbed current density depend on the parameter $\rho_\tau = (\rho_i^2 + \rho_s^2)^{1/2}$, i.e., the geometric mean between the ion and sound Larmor radii. In particular, when $\rho_\tau > d_e$ and $\Delta' d_e \gg (d_e/\rho_\tau)^{1/3}$, the linear growth rate approaches the asymptotic value $\gamma_L \approx (2 d_e \rho_\tau^2/\pi)^{1/3}$ and the perturbed current density is mainly distributed over the inertial skin depth, with a tail extending up to distances of order ρ_s; the vorticity also exhibits a rapid variation over the scale d_e and a milder variation over the scale ρ_s (scale lengths are normalized to a macroscopic equilibrium length L, and the growth rate is normalized to the equilibrium Alfvén time τ_A). On the other hand, the profile of the stream function φ is very different when the ion temperature is smaller or larger than the electron one. When $T_i \ll T_e$, φ varies smoothly across the reconnec-

[1] This article was submitted by the authors in English.

tion layer over the scale length ρ_s. By contrast [21], when T_i exceeds T_e, the stream function, like the vorticity, varies rapidly over the distance d_e and approaches a constant amplitude over a distance of order ρ_τ. This behavior reflects the decoupling of the electron and ion flows at distances $x < \rho_i$. Linear theory also indicates that diamagnetic effects are important and can lead to complete stabilization with positive Δ' when $\omega_{*i,e} \geq \gamma_L$, where $\omega_{*i,e} = (cT_{i,e}/eBLn)dn/dx$ is evaluated at the reconnection layer [20]. In this paper, we neglect diamagnetic effects; i.e., we consider the limit of a weak density gradient such that $\omega_{*i,e} < \gamma_L$.

In the cold ion limit ($\rho_i/d_e \longrightarrow 0$), it was shown in [1] that the reconnection rate is faster than exponential in an early nonlinear phase, where the island width is still small compared to the macroscopic convection cells. This rate is even faster [2] when finite electron temperature effects are considered and $\rho_s > d_e$. In addition, for finite values of ρ_s/d_e, the current density and vorticity layers develop with a characteristic cross-shape structure [2]. In this paper, the two main questions we address relate to the nonlinear reconnection rate and to the structure of the current density and vorticity layers when ion Larmor radius effects are considered to all orders.

2. MODEL EQUATIONS

We adopt the generalized two-fluid model [14], in which electrons and ions are treated as two different species. This set of equations governs the evolution of plasma phenomena with frequencies below the ion cyclotron and magnetosonic frequencies and above the ion-acoustic frequency. We consider a two-dimensional configuration characterized by a strong magnetic field in the z-direction and neglect the coordinate along this direction. The magnetic field is $\mathbf{B} = B_0\mathbf{e}_z + \nabla\psi \times \mathbf{e}_z$, where B_0 is constant and $\psi(x, y, t)$ is the magnetic flux function.

The governing equations normalized to the Alfvén time τ_A and the equilibrium scale length are [14]

$$\frac{\partial F}{\partial t} + [\varphi, F] = \rho_s^2[U, \psi] + \nu_e\nabla^2 J, \tag{1}$$

$$\frac{\partial U}{\partial t} + [\varphi, U] = [J, \psi] + \nu_i\nabla^2 U, \tag{2}$$

$$F = \psi + d_e^2 J, \tag{3}$$

$$J = -\nabla^2\psi, \tag{4}$$

$$U - \rho_i^2\nabla^2 U = \nabla^2\varphi, \tag{5}$$

where φ is the stream function (which is proportional to the electrostatic potential) and $[A, B] = \mathbf{e}_z \cdot \nabla A \times \nabla B$. Here, a strong uniform magnetic field is assumed to be directed along the z-axis.

Electron inertia enters (1)–(5) through the electron skin depth d_e, and the electron and the ion temperatures enter through ρ_s and ρ_i, respectively. Equation (1) describes the motion of the electrons along the field lines, while (2) originates from the continuity equation, and U is related to the electron density variation. The latter is set equal to the ion density variation because of the quasineutrality condition. The ion density is expressed in terms of the electrostatic potential (which is proportional to the stream function φ) through a Padé approximation of the nonlinear ion response, valid to all orders in the ion Larmor radius ρ_i, as introduced in [14].

In the cold ion limit, $\rho_i \longrightarrow 0$, equation (5) coincides with the usual definition of the vorticity as the Laplacian of the stream function of the plasma. Here, we will consider the opposite limit by taking $\rho_s \longrightarrow 0$. In this case, φ is still related to the $\mathbf{E} \times \mathbf{B}$ drift of the electrons but it is no longer related to the fluid vorticity of the plasma. In particular, in the large Larmor radius limit, we see that the first term on the left-hand side of (5) can be neglected and φ is proportional to U [15].

Since we are interested in the numerical integration of (1)–(5) in the nonlinear phase, when the energy cascade to the small scales becomes significant, we have introduced a small artificial viscosity into (1) and (2) by means of two diffusive terms. Then, during the simulations, the values of the dissipation coefficients ν_e and ν_i have been chosen in order to dissipate only the unphysically very small scales well below the electron skin depth.

Neglecting the diffusive terms, the Hamiltonian structure of the model equations can be revealed [14, 16, 22]. The two fluxes $G_\pm = F \pm d_e\rho_s U$ are advected by the velocity fields $\mathbf{v}_\pm = \mathbf{e}_z \times \nabla\varphi_\pm$ (where $\varphi_\pm = \varphi \pm (\rho_s/d_e)\psi$), and equations (1) and (2) can be cast in a Lagrange invariant form:

$$\frac{\partial G_\pm}{\partial t} + [\varphi_\pm, G_\pm] = 0. \tag{6}$$

Moreover, if we introduce the new variables,

$$\begin{aligned} \xi_1 &= F, \\ \xi_2 &= d_e\rho_s U, \end{aligned} \tag{7}$$

we can cast our system of equations in noncanonical Hamiltonian form

$$\frac{\partial \xi_i}{\partial t} = \{\xi_i, H\} \quad i = 1, 2, \tag{8}$$

where the generalized Poisson's brackets [17] are defined as

$$\{P, Q\} = \int d^2x \mathcal{J}^{ij}\left[\frac{\delta P}{\delta \xi_i}, \frac{\delta Q}{\delta \xi_j}\right] \tag{9}$$

and

$$\mathcal{J}^{ij} = -\begin{pmatrix} \xi_2 & \xi_1 \\ \xi_1 & \xi_2 \end{pmatrix}.$$

The Hamiltonian is

$$H = \frac{1}{2}\int d^2x(|\nabla\psi|^2 + d_e^2 J^2 + \rho_s^2 U^2 + |\nabla\varphi|^2). \quad (10)$$

In (10), we recognize the magnetic energy, the kinetic energy due to the motion of the electrons along filed lines, the electron potential energy, and the ion kinetic energy.

This system of equations admits two infinite sets of Casimirs (functionals of the two Lagrangian invariant fields, $G_\pm$):

$$C_\pm = \int d^2x h_\pm(\xi_1 \pm \xi_2) = \int d^2x h_\pm(G\pm), \quad (11)$$

with $h_\pm$ arbitrary functions. In (6), we have assumed that the velocity fields $v_\pm$ remain smooth during the evolution of the system. We note that the absence of finite time singularities has been shown in the case of zero ion temperature in [6]. Expanding $h_\pm$ to first order in ρ_s, we find from (11) the Casimirs in the cold electron limit ($\rho_s \longrightarrow 0$)

$$C_1 = \int d^2x h_1(F), \quad C_2 = \int d^2x U h_2(F). \quad (12)$$

In this case, only the generalized magnetic flux F admits a conservative equation.

3. A BRIEF SUMMARY OF NONLINEAR RESULTS WITH $T_i = 0$

In ideal magnetohydrodynamics, the frozen-in law forces the magnetic field lines to move with the plasma. Electron inertia leads to a violation of this law over distances of the order of the inertial skin depth from the magnetic surface where $\mathbf{B_{eq}} \cdot \nabla v_x = 0$, with $\mathbf{B_{eq}}(x)$ the equilibrium field. In this sense, electron inertia is responsible for magnetic reconnection in the collisionless limit. However, electron inertia is not a dissipative process and the inertial skin depth is not a dissipative scale length (similar remarks apply to the ion and sound Larmor radii). Thus, the question may be raised of whether a significant amount of magnetic flux can indeed be reconnected in the absence of dissipation. The answer to this question requires nonlinear considerations.

In [1], where temperature effects were neglected ($T_i = T_e = 0$), it was shown that collisionless reconnection due to electron inertia is indeed a significant nonlinear process. In the large Δ' limit, the inertial skin depth still sets the scale of the nonlinear parallel current channel. However, a structure develops below d_e. The width of this structure keeps shrinking in time with apparently no lower limit cut-off. This should not come as a surprise, given the absence of dissipation. The current density tends to become singular, although it was clearly shown in [6] that no singularity develops in finite time, at least when temperature effects are neglected. It is important to note that this microscale below the inertial skin depth carries a negligible current (the current density is mainly distributed over d_e). Thus, the occurrence of this microscale does not play a role in the dynamic evolution of the magnetic island, which is found to grow in a quasi-explosive manner and to reach a macroscopic width over a time scale of the order of γ_L^{-1}. The quasi-explosive behavior terminates and the island width saturates when this width becomes comparable with the equilibrium scale length [7].

A similar phenomenology was found when finite electron temperature effects were included in the model [2, 3]. In addition, with ρ_s comparable with or larger than d_e, the current density and vorticity layers were found to split into two branches crossing at the stagnation point of the flow. These cross-shaped structures were interpreted on the basis of the Hamiltonian Casimirs.

The development of a microscale below the inertial skin depth poses a challenge to numerical simulations. However, since the microscale carries a negligible current, the reconnection rate remains unaffected by the inclusion of additional, microscale limiting (e.g., dissipative) terms in the model, as long as these terms do not modify the structure of the reconnection region over the inertial skin depth scale length. Indeed, we have verified numerically that the reconnection rate does not depend on viscosity in the limit where the viscosity coefficient tends to zero. In this limit, the role of viscosity is similar to coarse-graining, which is known to introduce irreversibility in processes such as Landau damping of electrostatic waves or continuous damping of Alfvén waves in inhomogeneous plasmas. As we remarked in the previous section, we also consider dissipation in this paper in order to facilitate numerical integration, with the values of the dissipation coefficient chosen so as to introduce a lower scale cut-off well below the inertial skin depth.

4. NUMERICAL RESULTS

Having in mind a comparison with the results obtained in the cold ion limit in [3], we choose a two-dimensional doubly periodic magnetic configuration, focusing on the so-called "large Δ'" regime characterized by $\Delta' d_e \gg (d_e \rho_{i,s})^{1/3}$ and by macroscopic flow cells. In this limit, when $\rho_{i,s} > d_e$, the linear growth rate $\gamma_L \approx (2 d_e \rho_T^2/\pi)^{1/3}$ is obtained [20].

The simulations have been carried out with a spectral code that uses standard Fourier transforms to calculate the spatial derivatives. The equations are integrated in the domain $[-L_x, L_x] \times [-L_y, L_y]$ with periodic boundary conditions in both directions. In order to follow the

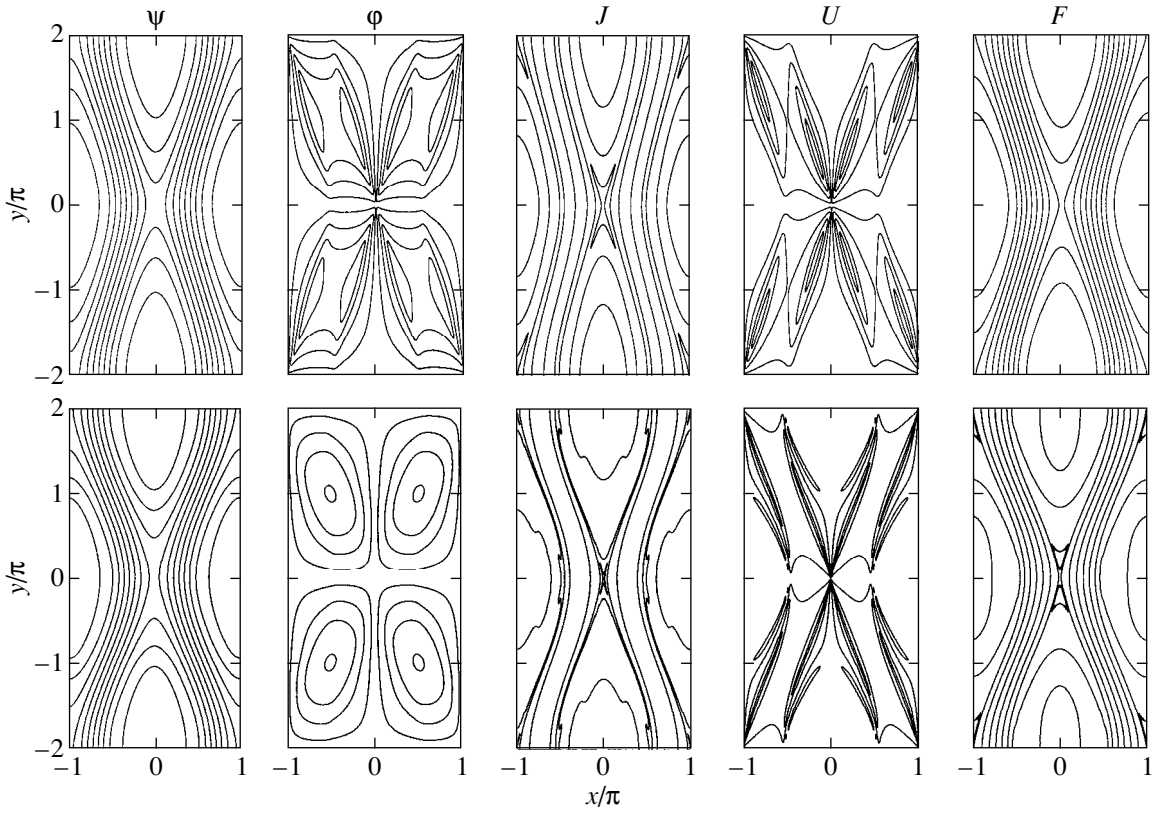

Fig. 1. Contour plots of the fields ψ, φ, *J*, *U*, and *F* for two simulations with $d_e = 0.08$. The first row corresponds to a case with $\rho_i = 3d_e$, $\rho_s = 0$, and $w = 8.5d_e$. The second row corresponds to a case with $\rho_i = 0$, $\rho_s = 3d_e$, and $w = 8d_e$. The *x* and *y* coordinates are normalized on the scale length L_x.

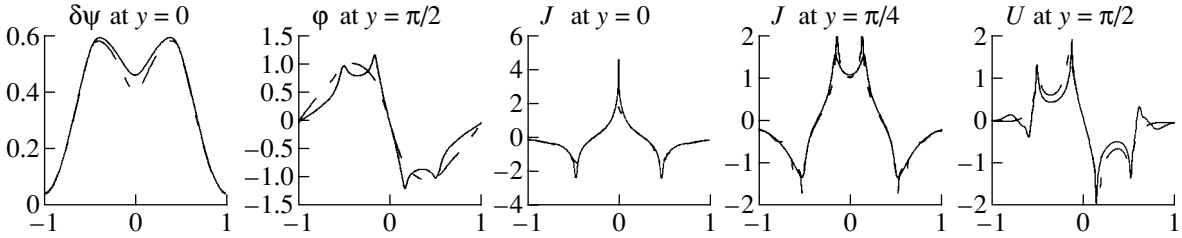

Fig. 2. Profiles of the fields δψ, φ, *J*, and *U* as functions of x/L_x at different values of the *y* coordinate. The solid lines correspond to the case $\rho_i = 3d_e$ and $\rho_s = 0$; the dashed lines correspond to the case $\rho_i = 0$ and $\rho_s = d_e$.

nonlinear evolution, we choose the viscosity coefficients $\nu_i = 4 \times 10^{-4}$ and $\nu_e = 3 \times 10^{-4}$, such that the associated dissipative scale lengths are of the order of $d_e/4$. The equilibrium configuration is given by $\psi_{eq} = \cos(x)$, $\psi_{eq} = 0$, with $L_x = \pi$, $\epsilon = L_x/L_y = 0.5$, and $d_e = 0.08L_x$. We performed simulations choosing $\rho_i = d_e$ and $3d_e$, which correspond to the same values adopted in [3] for ρ_s. This choice gives the same linear growth rate for the two cases (see Section 1).

In Fig. 1, we draw the contour plots of ψ, φ, *J*, *U*, and *F* at a time such that the size of the magnetic island width has reached half the size of the box for two simulations characterized by the same value $d_e = 0.08L_x$. The plots in the first row are characterized by $\rho_i = 3d_e$ and $\rho_s = 0$. The plots in the second row are characterized by $\rho_i = 0$ and $\rho_s = 3d_e$. In Fig. 2, the profiles of δψ, φ, *J*, and *U* at different values of the *y* coordinate for the same simulations are drawn.

One important finding is that the nonlinear structure of φ is different for the two cases. In particular, when we consider the ion Larmor radius effects with $\rho_i > d_e$, we see that the contour plot of φ is similar to that of *U*. In the limit of a large ion Larmor radius, the density variation (i.e., the *U* field) is concentrated on a scale

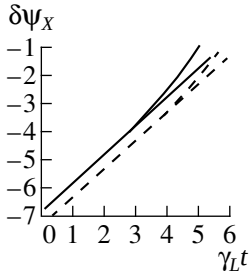

Fig. 3. Time evolution of the reconnected flux $\delta\psi_X$. The straight lines correspond to the linear growth rate extrapolated to nonlinear times. The solid lines correspond to the case $\rho_i = 3d_e$ and $\rho_s = 0$; the dashed lines correspond to the case $\rho_i = 0$ and $\rho_s = d_e$.

length much smaller than ρ_i. Thus, in this region, equation (5) gives $U \sim -\varphi/\rho_i^2$. Consequently, the contour lines of U tend to coincide with those of φ. In this limit, the advection term in (2) becomes negligibly small and equation (2) reduces simply to $\partial\varphi/\partial t = -\rho_i^2 [J, \psi]$. Also, the macroscopic flow cells are more localized in the region around the X-point. This can account for the stronger localization of the current density sheets on the separatrix of the magnetic flux. A similar result with both ρ_s and small ρ_i effects has been presented in [23] in the case when the magnetic configuration is stable and field line reconnection is forced from the boundaries. This feature is clearly evident in Fig. 2, where the profiles of the current density for $y = \pi/4$ are drawn. We see that the current density profile exhibits two peaks that merge into a single peak at $y = 0$. The distance between these two peaks increases with the distance from the X-point ($x = 0, y = 0$), which is consistent with the cross structure in Fig. 1. This distance increases in time with the same rate as the magnetic island width.

We also note the different behavior of the generalized flux F. As can be seen from Fig. 1, the topology is different in the two cases. In the former case of $\rho_i = 3d_e$ and $\rho_s = 0$, in the absence of dissipation, F is a Lagrangian invariant. However, due to finite viscosity, the F contour lines reconnect, following the behavior of the magnetic flux, i.e., with an X-point in the origin. In contrast, in the case $\rho_i = 0$ and $\rho_s = d_e$, F reconnects due to the combined effect of the electron inertia and the sound Larmor radius even in the absence of dissipation, developing the typical cross structure with an O-point in the origin [2], while the Lagrangian properties of the model are transferred to the $G_\pm$ fields, which conserve their topology. As a test of the small dissipative effects of the viscosity coefficients we used, we checked the conservation of the energy integral, given by (10). This integral is seen to vary by about 1.2% by the time the island has reached an amplitude comparable with the slab width. However, a more systematic study, which will be presented elsewhere, is required in order to establish the dependence on the dissipation parameters with certainty.

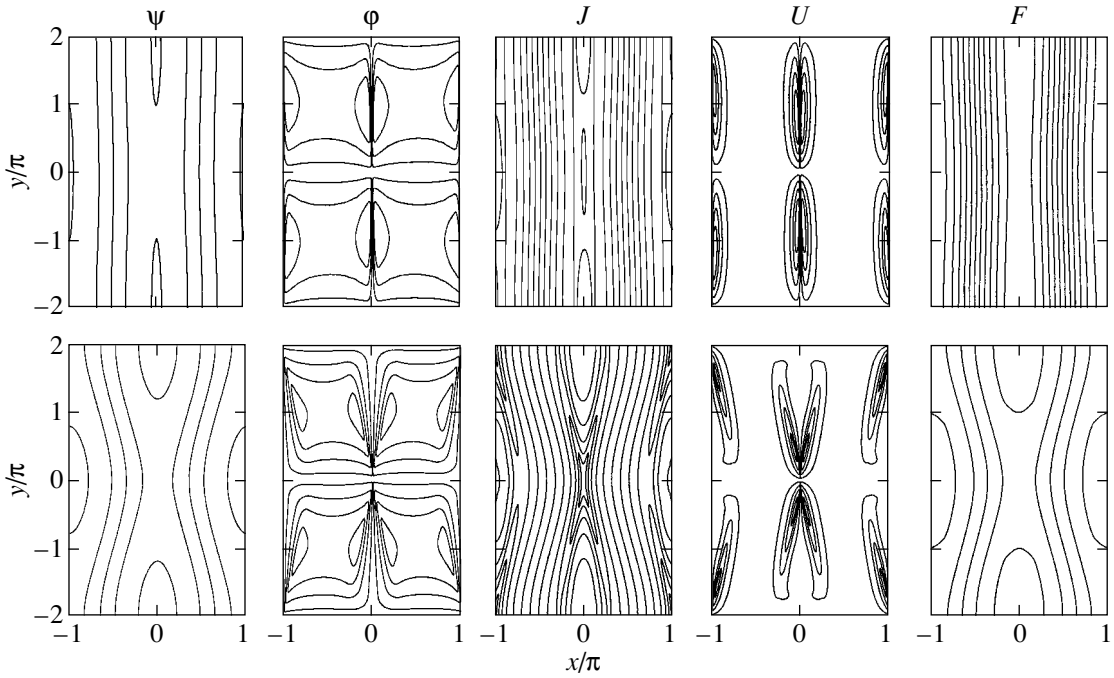

Fig. 4. Contour plots of the fields ψ, φ, J, U, and F at different times for a simulation with $d_e = 0.08$, $\rho_i = d_e$, and $\rho_s = 0$. The first row corresponds to a time in the linear phase such that $w = d_e$; the second row corresponds to a time in the nonlinear phase such that $w = 5.6d_e$. The x and y coordinates are normalized on the scale length L_x.

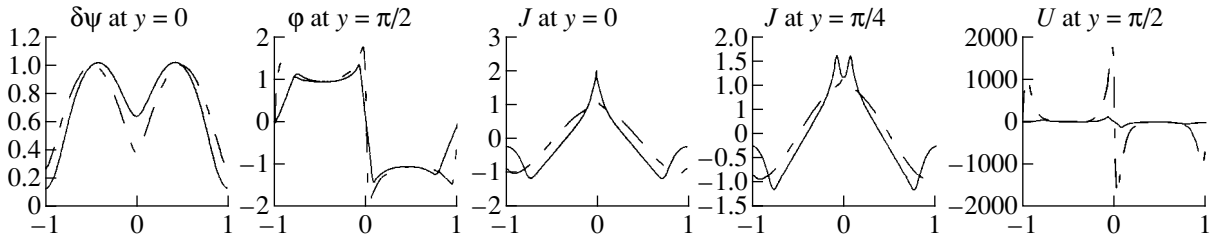

Fig. 5. Profiles of the fields δψ, φ, *J*, and *U* as functions of x/L_x for the simulation of Fig. 4 at different times. The solid lines correspond to a time such that $w = 5d_e$; the dashed lines correspond to a time such that $w = d_e$.

In Fig. 3, the time evolution of reconnected flux, as measured by $\delta\psi_X \equiv \psi(0, 0; t) - \psi_{eq}(0)$ (the magnetic flux function at the *X*-point, $x = y = 0$), is shown for the two simulations discussed above. For each curve, the corresponding linear fit is also drawn, as obtained from the data of the simulations. We see that the fitted curves are parallel, as expected from linear theory. Moreover the nonlinear phase exhibits a faster than exponential behavior in both cases.

In Figs. 4 and 5, the results of a simulation with $\rho_i = d_e$ are shown. In particular, in Fig. 4, the contour plots of ψ, φ, *J*, and *U* are shown for two different times: the first row corresponds to a time at the beginning of the nonlinear phase, in which the magnetic island *w* has reached a value of the order of d_e; the second row corresponds to a time in the full nonlinear phase, in which the magnetic island is $w = 5.6d_e$. In Fig. 5, the profiles at the same times are shown. In this case of a small Larmor radius, the contour plot of the stream function is similar to that obtained in the cold ion limit [3] with a smooth variation on the typical scale length $d_e \sim \rho_i$. When the nonlinear phase is fully entered, the difference between the two regimes becomes evident. The localization of the stream function around the *X*-point drives the splitting of the current density layer into two layers aligned whit the separatrix of the magnetic flux. Furthermore, the two vorticity layers tend to diverge from each other, reproducing the typical cross structure associated with ρ_s.

5. CONCLUSIONS

In this paper, we have analyzed the effect of ion temperature on nonlinear collisionless reconnection by including ion Larmor radius effects to all orders by means of a Padé approximation. Diamagnetic effects are not as of yet considered. Part of the motivation for this work was the testing of the applicability of the well-known cold-ion model in nonlinear regimes. In this model, which is frequently adopted for the sake of its algebraic simplicity in the linear analysis of small-scale instabilities and boundary layer dynamics, finite temperature effects in the direction perpendicular to the magnetic field lines are retained only through the electron contribution by taking the formal limit $T_e/T_i \longrightarrow \infty$. This model is known to mimic relatively well the linear response of a number of instabilities by introducing a hybrid Larmor radius (the so-called sound Larmor radius), which can represent some of the real ion Larmor radius effects. Numerical factors of order unity are missed, but the overall picture is in general well reproduced by the cold ion model. For example, in the case of magnetic field line reconnection, the growth rate turns out to be wrong by a factor of approximately two and the current channel is almost unaffected, but the velocity pattern inside the reconnection region is known to be different as the $E \times B$ ion motion is impeded.

We find that most of this picture remains valid nonlinearly. Our comparison shows that, in the two cases examined, the roles of the ion Larmor radius and the sound Larmor radius are somewhat interchangeable. In both cases, the growth in the early nonlinear phase is superexponential and is closely related to the value of linear growth rate, for which the "equivalence" of the two descriptions is known to hold. The difference between the velocity patterns persists in the early nonlinear regime and actually becomes more extreme. In the 2D doubly periodic case examined in this paper, the velocity pattern remains global in the sound Larmor radius case and becomes much more local ("microscopic" instead of macroscopic) in the ion Larmor radius case.

For the doubly periodic configuration adopted in this paper, it is not physically sensible to follow the reconnection process when the size of the magnetic island becomes of the order of the scale length of the gradient of the equilibrium current density, since the current and vorticity layers from different periodicity cells start to interact.

ACKNOWLEDGMENTS

This work was supported in part by the Italian National Research Council (CNR).

REFERENCES

1. M. Ottaviani and F. Porcelli, Phys. Rev. Lett. **71**, 3802 (1993).

2. E. Cafaro, D. Grasso, F. Pegoraro, *et al.*, Phys. Rev. Lett. **80**, 4430 (1998).
3. D. Grasso, F. Pegoraro, F. Porcelli, and F. Califano, Plasma Phys. Controlled Fusion **41**, 1497 (1999).
4. J. Rem and T. J. Schep, Plasma Phys. Controlled Fusion **40**, 138 (1998).
5. G. Valori, H. J. de Blank, J. Rem, and T. J. Schep, in *Proceedings of Joint Varenna–Lausanne International Workshop on Theory of Fusion Plasmas, Varenna, 1998* (Compositori, Bologna, 1999), p. 555.
6. G. Valori, D. Grasso, and H. J. de Blank, Phys. Plasmas **7**, 178 (2000).
7. D. Grasso, F. Pegoraro, F. Porcelli, and F. Califano, in *Proceedings of 26th European Conference on Controlled Fusion and Plasma Physics, Maastricht, 1999*, paper P3. 061.
8. D. Biskamp, E. Schwarz, and J. F. Drake, Phys. Plasmas **4**, 1002 (1997).
9. R. G. Kleva, J. Drake, and F. Waelbroeck, Phys. Plasmas **2**, 23 (1995).
10. L. Zakharov and B. Rogers, Phys. Fluids B **4**, 3285 (1992).
11. B. Coppi, Phys. Lett. **11**, 226 (1964).
12. V. M. Vasyliunas, Rev. Geophys. Space Phys. **13**, 303 (1975).
13. J. Wesson, Nucl. Fusion **30**, 2545 (1990).
14. T. Schep, F. Pegoraro, and B. Kuvshinov, Phys. Plasmas **1**, 2843 (1994).
15. F. Pegoraro, B. N. Kuvshinov, M. Romanelli, and T. J. Schep, in *Small-Scale Structure in Three-Dimensional Hydro- and Magnetohydrodynamic Turbulence*, Ed. by M. Meneguzzi, A. Pouquet, and P. L. Sulem (Springer-Verlag, 1995), p. 295 [Lecture Notes Phys. **462**, 295 (1995)].
16. B. N. Kuvshinov, F. Pegoraro, and T. Schep, Phys. Lett. A **191**, 296 (1994).
17. P. J. Morrison and R. D. Hazeltine, Phys. Fluids **27**, 886 (1984).
18. F. Pegoraro and T. Schep, Plasma Phys. Controlled Fusion **28**, 647 (1986).
19. F. Pegoraro, F. Porcelli, and T. J. Schep, Phys. Fluids B **1**, 364 (1989).
20. F. Porcelli, Phys. Rev. Lett. **66**, 425 (1991).
21. F. Porcelli, in *Proceedings of Joint Varenna–Lausanne Workshop on Theory of Fusion Plasmas, Varenna, 1992* (Società Italiana di Fisica, Bologna, 1992), p. 161.
22. B. N. Kuvshinov, V. P. Lakhin, F. Pegoraro, and T. J. Schep, J. Plasma Phys. **59**, 727 (1998).
23. G. Valori, H. J. de Blank, J. Rem, and T. J. Schep, in *Proceedings of 26th EPS Conference on Controlled Fusion and Plasma Physics, Maastricht, 1999*, paper P2.057.

Plasma Physics Reports, Vol. 26, No. 6, 2000, pp. 519–528. Translated from Fizika Plazmy, Vol. 26, No. 6, 2000, pp. 556–565.

PLASMA KINETICS

Multiparticle Nature of Collisions in Plasma and a Unique Feature of Coulomb Interaction

S. N. Gordienko

Landau Institute for Theoretical Physics, Russian Academy of Sciences, Russian Research Centre Kurchatov Institute, pl. Kurchatova 1, Moscow, 123182 Russia

Received May 20, 1999; in final form, August 12, 1999

Abstract—It is shown that the lower limit in the Coulomb logarithm is governed by the collective behavior of a plasma rather than by binary collisions with small impact parameters. For this reason, under the assumption that the particle-to-particle momentum transfer is governed mainly by binary collision, the numerical coefficient in the second moment of the momentum transferred turns out to be overestimated by a factor of two. In other words, the multiparticle character of the lower limit in the Coulomb logarithm governs not only the logarithm itself but also the numerical coefficient in front of it. Correctly incorporating the fluctuation electric fields on spatial scales shorter than or close to the Debye radius (the multiparticle nature of collisions in a plasma) provides a new insight into the physics of Coulomb collisions and leads to the appearance of a new characteristic spatial scale $(r_D r_{\min})^{1/2}$ in plasma theory. Hence, an almost ideal plasma possesses a unique feature: the existence of a spatial scale that is much shorter than the mean distance between the particles and has no analogues in the systems of particles in which the interaction potential is not of Coulomb origin. The problem is considered in the limit of infinitely large values of the Coulomb logarithm. © *2000 MAIK "Nauka/Interperiodica".*

1. INTRODUCTION

The problems of the penetration of charged particles through matter and the related particle energy losses arose at the same time as the first elaborations of the present concepts of the structure of matter (see, e.g., [1]). Most of the methods for investigating atomic nuclei and the interpretation of the majority of experimental data from measurements with cosmic-ray particles are to a greater or lesser extent based on the conclusions of the theory of the interaction between charged particles and matter [1]. Although the entire range of problems related to the penetration of a charged particle through matter and the methods for solving them cannot be reviewed even briefly, we are quite sure that one of the key problems here is the study of the laws describing particle scattering in Coulomb fields as well as the role of screening in scattering processes. However, numerous attempts to analyze screening-related problems and the question of whether the scattering in a real electric field can be described as a sequence of binary collision events were made under the implicit assumption that the small-scale fluctuation electric fields in media play a very minor role. Here, we examine as an example the interaction of a charged particle with a plasma in order to show that this assumption is incorrect: taking into account small-scale electric fields not only changes numerical coefficients in some expressions but also provides a fundamentally new insight into the physics of scattering processes in systems of Coulomb particles. A systematic analysis of the fluctuation electric fields in a plasma shows that Coulomb interaction in systems consisting of many particles is characterized by a new spatial scale that does not coincide with the Debye radius and has no analogues in systems with different interaction potentials. It is this nontrivial additional spatial scale that distinguishes the Coulomb potential from other interaction potentials.

2. SCATTERING BY FLUCTUATION ELECTRIC FIELDS IN A PLASMA

The electric field of a test particle moving in a plasma affects the other plasma particles, so that their velocities change and their trajectories become perturbed. In other words, the actual electric field can be regarded as a superposition of the fluctuation electric field (which is related to the electric field of plasma electrons and ions whose motion is not perturbed by the electric field of a test particle) and the polarization electric field (which results from the polarization of the plasma by a test particle, i.e., from the perturbation created by the test particle in the motion of other plasma particles). We analyze how the momentum of a test particle changes solely under the action of the fluctuation electric field. The range of validity of this analysis will be clarified in what follows (see also [2–4]).

We consider the statistical properties of the change in the momentum of a test particle with charge Z_0, which moves with the velocity v in a plasma and interacts with the other plasma particles over the time interval τ. We treat the problem in a formulation similar to

1063-780X/00/2606-0519$20.00

the model developed by Kogan [5]. We are interested in the time scales τ on which the velocities of the test particle and other plasma particles change only slightly, so that the particle motion can be regarded as being straight-line and uniform. According to Newton's second law, the change in the momentum of a test particle over the time τ is

$$\Delta\mathbf{p}_\tau = Z_0 e \int_t^{t+\tau} \mathbf{E}(t')dt', \tag{1}$$

where $\mathbf{E}(t')$ is the electric field created by the plasma particles at the point at which the test particle occurs at the time t'. Since we are interested in time scales on which the particle motion can be assumed to be straight-line and uniform, we can write

$$\begin{aligned}\mathbf{E}(t') = &-\sum e\frac{\mathbf{r}+\mathbf{v}(t'-t)-\mathbf{r}_i-\mathbf{v}_i(t'-t)}{\left|\mathbf{r}+\mathbf{v}(t'-t)-\mathbf{r}_i-\mathbf{v}_i(t'-t)\right|^3}\\ &+\sum Ze\frac{\mathbf{r}+\mathbf{v}(t'-t)-\mathbf{R}_i-\mathbf{V}_i(t'-t)}{\left|\mathbf{r}+\mathbf{v}(t'-t)-\mathbf{R}_i-\mathbf{V}_i(t'-t)\right|^3},\end{aligned} \tag{2}$$

where summation is implied over all of the plasma electrons (in the first sum) and ions (in the second sum); $\mathbf{r}$, $\mathbf{r}_i$, and $\mathbf{R}_i$ are, respectively, the position vectors of the test particle, the ith electron, and the ith ion at the time t; and $\mathbf{v}$, $\mathbf{v}_i$, and $\mathbf{V}_i$ are, respectively, their velocities at the time t.

For the characteristic function (the Fourier transformed distribution function) corresponding to the random quantity $\Delta\mathbf{p}_\tau$, we can write by definition

$$p(\mathbf{u}) = \langle \exp(i(\mathbf{u}, \Delta\mathbf{p}_\tau))\rangle, \tag{3}$$

where the angular brackets stand for ensemble averaging. The scalar and vector products of vectors **a** and **b** will be denoted by (**a**, **b**) and [**a**, **b**], respectively.

Assuming that the plasma is in thermal equilibrium and neglecting correlations among the plasma particles (i.e., keeping only zero-order terms in the parameter $e^2n^{1/3}/T$ in the statistical weighting factor), we can rewrite (3) as

$$\begin{aligned}p(\mathbf{u}) = &\left(\frac{1}{V}\right)^{N_e}\int\ldots\int\left\langle \exp\left[i\left(\mathbf{u}, \int_t^{t+\tau}\sum Z_0e^2\frac{\mathbf{r}+\mathbf{v}(t'-t)-\mathbf{r}_i-\mathbf{v}_i(t'-t)}{\left|\mathbf{r}+\mathbf{v}(t'-t)-\mathbf{r}_i-\mathbf{v}_i(t'-t)\right|^3}dt'\right)\right]\right\rangle_m d\mathbf{r}_1\ldots d\mathbf{r}_{N_e}\\ &\times\left(\frac{1}{V}\right)^{N_i}\int\ldots\int\left\langle \exp\left[i\left(\mathbf{u}, \int_t^{t+\tau}\sum Z_0Ze^2\frac{\mathbf{r}+\mathbf{v}(t'-t)-\mathbf{R}_i-\mathbf{V}_i(t'-t)}{\left|\mathbf{r}+\mathbf{v}(t'-t)-\mathbf{R}_i-\mathbf{V}_i(t'-t)\right|^3}dt'\right)\right]\right\rangle_m d\mathbf{R}_1\ldots d\mathbf{R}_{N_i},\end{aligned} \tag{4}$$

where the subscript m indicates averaging over a Maxwellian distribution; V is the plasma volume; and N_e and N_i are the number of electrons and ions, respectively.

To evaluate the characteristic function in explicit form, we introduce the quantities

$$U_e = \int\left\{\left\langle \exp\left[i\left(\mathbf{u}, \int_t^{t+\tau} Z_0e^2\frac{\mathbf{r}+\mathbf{v}(t'-t)-\mathbf{v}_i(t'-t)}{\left|\mathbf{r}+\mathbf{v}(t'-t)-\mathbf{v}_i(t'-t)\right|^3}dt'\right)\right]\right\rangle_m - 1\right\}d\mathbf{r} \tag{5}$$

(with averaging over a Maxwellian distribution over the velocities $\mathbf{v}_i$ of the plasma electrons) and

$$U_i = \int\left\{\left\langle \exp\left[-i\left(\mathbf{u}, \int_t^{t+\tau} Z_0Ze^2\frac{\mathbf{r}+\mathbf{v}(t'-t)-\mathbf{V}_i(t'-t)}{\left|\mathbf{r}+\mathbf{v}(t'-t)-\mathbf{V}_i(t'-t)\right|^3}dt'\right)\right]\right\rangle_m - 1\right\}d\mathbf{r} \tag{6}$$

(with averaging over a Maxwellian distribution over the velocities $\mathbf{V}_i$ of the plasma ions).

With the quantities U_e and U_i, the characteristic function $p(\mathbf{u})$ becomes

$$p(\mathbf{u}) = \left(1+\frac{U_e}{V}\right)^{N_e}\left(1+\frac{U_i}{V}\right)^{N_i},$$

and, in the limit $V \longrightarrow +\infty$ such that $N_e/V = n$ and $N_i/V = n/Z$, it passes over to

$$p(\mathbf{u}) = \exp(nU_e)\exp(nU_i/Z). \tag{7}$$

To examine the characteristic function (7), we consider the deceleration of a test particle moving with the velocity v and analyze the distribution function $f(\Delta\mathbf{p}_\tau)$

of the random quantity $\Delta\mathbf{p}_\tau$ on the time scales τ satisfying the inequalities

$$B_e = n(v^*\tau)^3 \gg 1 \quad \text{and} \quad B_i = n(V^*\tau)^3 \gg Z,$$

where $v^* = \max(v, v_T)$ and $V^* = \max(v, V_T)$. Switching to the variables $\mathbf{r}' = \mathbf{r}/v^*\tau$, we can readily see that the quantities B_e and B_i are large parameters in theory, so that they can be used to construct an asymptotic expansion of the distribution function. Since the real parts of the exponential functions in (7) are nonpositive and the parameters B_e and B_i are large, the main contribution to the distribution function

$$f(\Delta\mathbf{p}_\tau) = \int \exp[-i(\mathbf{u}, \Delta\mathbf{p}_\tau)]p(\mathbf{u})\frac{d\mathbf{u}}{(2\pi)^3} \tag{8}$$

comes from the vicinity of the point in the $\mathbf{u}$-space at which the real part of the exponential function in (7) is maximum. The contribution from the exterior of the vicinity of this point in the $\mathbf{u}$-space is exponentially small, because B_i and B_e are large. It is easy to see that the real parts of the arguments of the exponential functions in (7) are nonpositive and that the distribution function should be found by analyzing the functions U_e and U_i in the vicinity of the point $\mathbf{u} = 0$. We perform the necessary manipulations and, to the leading order in the large quantity $\ln(1/|\mathbf{u}|)$, obtain (see Appendix 1)

$$U_e = \left\langle -\frac{2\pi Z_0^2 e^4 \tau}{|\mathbf{x}|^3}(\mathbf{u}, \mathbf{x})^2 - \frac{\pi Z_0^2 e^4 \tau}{|\mathbf{x}|^3}[\mathbf{u}, \mathbf{x}]^2 \ln\left(\frac{|\mathbf{x}|^6\tau^2}{e^4 Z_0^2 [\mathbf{u}, \mathbf{x}]^2}\right)\right\rangle_m, \tag{9}$$

$$U_i = \left\langle -\frac{2\pi Z_0^2 Z^2 e^4 \tau}{|\mathbf{X}|^3}(\mathbf{u}, \mathbf{X})^2 - \frac{\pi Z_0^2 Z^2 e^4 \tau}{|\mathbf{X}|^3}[\mathbf{u}, \mathbf{X}]^2 \ln\left(\frac{|\mathbf{X}|^6\tau^2}{Z^2 Z_0^2 e^4 [\mathbf{u}, \mathbf{X}]^2}\right)\right\rangle_m, \tag{10}$$

where $\mathbf{x} = \mathbf{v} - \mathbf{v}_i$ and $\mathbf{X} = \mathbf{v} - \mathbf{V}_i$. Averaging over Maxwellian velocity distributions (the angular brackets) concerns only $\mathbf{x}$ and $\mathbf{X}$ and does not apply to the functional dependence on $\mathbf{u}$ in which we are interested here. In the explicit form, this averaging results in the appearance of an error function in (9) and (10).

Note that, by virtue of the logarithmic singularity at $\mathbf{u} = 0$, the functions U_e and U_i have a finite number of continuous derivatives. Consequently, for a significant amount of momentum transfer, the distribution function decreases as a power function or slower, so that only the lowest moments of the momentum transferred converge. Below, we will show that even the second moment diverges.

The higher moments turn out to be diverging, because the particle trajectories were assumed to be straight in solving for the momentum transferred. Consequently, expression (7) cannot be applied to correctly analyze large momentum transfer between the particles that pass so close to one another that their trajectories become curved. In this case, expression (7) greatly overestimates (and, consequently, renders physically meaningless) the momentum transferred between the particles. However, such an unrealistically large momentum transfer described by (7) can be avoided by evaluating the distribution functions with the help of (9) and (10) in the limit of infinitely large values of the Coulomb logarithm. As an example, we consider an electron moving with the thermal velocity in a plasma. Over the mean free path λ_{st}, the electron will experience a large momentum transfer with each of the $r_{\min}^2 \lambda_{st} n \sim 1/\Lambda$ plasma particles that are at distances shorter than $r_{\min} = e^2/T$ from it. Hence, expression (7), according to which the momentum transfer is physically meaningless because of the incorrect description of the particles that pass close to each other, should be treated with the additional small parameter $1/\Lambda$. Consequently, in order to overcome such fictitious momentum transfers, the calculations should be carried out to the leading order in $1/\Lambda$ (in the limit $\Lambda = +\infty$, there are no particles over distances shorter than $r_{\min}$ from the test particle during its mean free time, which thus turns out to be short enough for the impact parameters associated with unrealistically great momentum transfers not to come into play). It is easy to see that, in this way, the functions U_e and U_i in expression (7) can be replaced with the functions (see Appendix 2)

$$U_e^* = \left\langle -\frac{2\pi Z_0^2 e^4 \tau}{|\mathbf{x}|^3}(\mathbf{u}, \mathbf{x})^2 - \frac{\pi Z_0^2 e^4 \tau}{|\mathbf{x}|^3}[\mathbf{u}, \mathbf{x}]^2 \ln\left(\frac{|\mathbf{x}|^4\tau^2}{e^4 Z_0^2}\xi_e\right)\right\rangle_m, \tag{11}$$

$$U_i^* = \left\langle -\frac{2\pi Z_0^2 Z^2 e^4 \tau}{|\mathbf{X}|^3}(\mathbf{u}, \mathbf{X})^2 - \frac{\pi Z_0^2 Z^2 e^4 \tau}{|\mathbf{X}|^3}[\mathbf{u}, \mathbf{X}]^2 \ln\left(\frac{|\mathbf{X}|^4\tau^2}{Z^2 Z_0^2 e^4}\xi_i\right)\right\rangle_m, \tag{12}$$

where $\xi_e = \min[A_e \text{ and } A_e^2/(\Delta\mathbf{p}_\tau)^2]$, $\xi_i = \min[A_i, A_i^2/(\Delta\mathbf{p}_\tau)^2]$ with $A_e = \pi Z_0^2 e^4\tau/|\mathbf{x}|$ and $A_i = \pi Z_0^2 Z^2 e^4\tau/|\mathbf{X}|$.

We emphasize that, in this paper, the problem is considered in the limit of infinitely large values of the Coulomb logarithm. It is this case in which the effects in question are most pronounced. Note that, in Appendix 2, we present the expressions that allow one to analyze the case of finite values of the Coulomb logarithm

and thus clarify the physical meaning of the limit $\Lambda = +\infty$.

A distribution function that is consistent with (11) and (12) and is very similar in structure to the Gaussian function (i.e., a Gaussian function with a deformed tail) allows us to evaluate the second moment of the momentum transferred by determining the trace of a certain matrix and to write

$$\begin{aligned}\langle(\Delta\mathbf{p}_\tau)^2\rangle &= 4n\pi Z_0^2 e^4 \tau\left\langle\frac{1}{|\mathbf{x}|}\right\rangle_m \ln[n(V^*\tau)^3] \\ &+ 4n\pi Z Z_0^2 e^4 \tau\left\langle\frac{1}{|\mathbf{X}|}\right\rangle_m \ln[n(V^*\tau)^3/Z].\end{aligned} \tag{13}$$

3. SOLVING FOR THE SECOND MOMENT OF THE MOMENTUM TRANSFERRED IN THE APPROXIMATION OF BINARY COLLISIONS

In order to give a better insight into the qualitatively new physical meaning of expression (13), we evaluate the second moment under the assumption that the momentum is transferred via binary collisions with small impact parameters. Under the above verisimilar assumption, the second moment was calculated by Kogan [5]. To solve for the second moment, we must find the second derivatives of the characteristic function at $\mathbf{u} = 0$,

$$\langle(\Delta\mathbf{p}_\tau)^2\rangle = \left.\frac{\partial^2 p(\mathbf{u})}{\partial\mathbf{u}\partial\mathbf{u}}\right|_{\mathbf{u}=0}. \tag{14}$$

Substituting (7) into (14) yields (see Appendix 3)

$$\begin{aligned}\langle(\Delta\mathbf{p}_\tau)^2\rangle &= 8\pi Z_0^2 e^4 n\tau\left\langle\frac{1}{|\mathbf{x}|}\int_1^{+\infty}\frac{d\mu}{\mu^2-1}\right\rangle_m \\ &+ 8\pi Z_0^2 Z e^4 n\tau\left\langle\frac{1}{|\mathbf{X}|}\int_1^{+\infty}\frac{d\mu}{\mu^2-1}\right\rangle_m.\end{aligned} \tag{15}$$

At $\mu = 1$, the integrals in (15) diverge logarithmically. Consequently, under the above assumption that the momentum transferred via binary collisions with small impact parameters is maximum, the lower limit $\mu = 1$ of integration in (15) should be replaced by $\mu_1 = 1 + (r_{\min}^{(e)}/|\mathbf{x}|\tau)^2$ with $r_{\min}^{(e)} = Z_0 e^2/\min[MV^{*2}, m_e V^{*2}]$ in the first term and by $\mu_2 = 1 + (r_{\min}^{(i)}/|\mathbf{X}|\tau)^2$ with $r_{\min}^{(i)} = Z_0 Z e^2/\min[MV^{*2}, m_i V^{*2}]$ in the second term, because it is these impact parameters for which the trajectories of the colliding particles become significantly curved. With the new lower limits of integration, we obtain with logarithmic accuracy

$$\begin{aligned}\langle(\Delta\mathbf{p}_\tau)^2\rangle_P &= 8\pi Z_0^2 e^4 n\tau\left\langle\frac{1}{|\mathbf{x}|}\right\rangle_m \ln\left(\frac{V^*\tau}{r_{\min}^{(e)}}\right) \\ &+ 8\pi Z Z_0^2 e^4 n\left\langle\frac{1}{|\mathbf{X}|}\right\rangle_m \ln\left(\frac{V^*\tau}{r_{\min}^{(i)}}\right),\end{aligned} \tag{16}$$

where the subscript P indicates that a quantity is calculated in the approximation of binary collisions. Expression (16) was first derived by Kogan [5] using a method that differs from that described above only in the calculation technique. We emphasize that the arguments of the logarithmic functions in (13) and (16) are radically different: the arguments of the logarithmic functions in (13) depend on the plasma density, whereas those in (16) are density-independent.

Notably, it is the assumption about the substantial deformation of the particle trajectories in the course of momentum transfer via head-on binary collisions that changes the structure of the Coulomb logarithm and results in an erroneous coefficient in front of it: according to (13) and (16), for $\tau \sim 1/\omega_{pe}$, the erroneous coefficient differs from the correct one by a factor of two. Consequently, the trajectory of a particle becomes significantly curved (due to its interaction with the collective plasma electric fields) before the particle experiences a head-on collision event, which is accompanied by significant momentum transfer. Hence, we have shown that both the upper and lower limits in the Coulomb logarithm are governed by the scattering on collective plasma fields rather than by binary collisions.

4. THE ROLE OF DEBYE SCREENING IN A PLASMA

Now, we present the expression for the second moment with allowance for the plasma permittivity (the Debye screening). For simplicity, we assume that the velocity of the test particle is much higher than the thermal velocities of both ions and electrons. In this case, over times τ during which the test particle passes a distance shorter than the Debye radius, the Debye screening does not affect the test particle deceleration. For times during which the test particle passes a distance longer than the Debye radius, we have (see Appendix 4)

$$\begin{aligned}\langle(\Delta\mathbf{p}_\tau)^2\rangle &= 4n\pi Z_0^2 e^4 \tau\left\langle\frac{1}{|\mathbf{x}|}\right\rangle_m \ln(nr_D^2 V\tau) \\ &+ 4n\pi Z Z_0^2 e^4 \tau\left\langle\frac{1}{|\mathbf{X}|}\right\rangle_m \ln(nr_D^2 V\tau/Z)\end{aligned} \tag{17}$$

and, accordingly,

$$\langle(\Delta\mathbf{p}_\tau)^2\rangle_P = 8\pi Z_0^2 e^4 n\tau\left\langle\frac{1}{|\mathbf{x}|}\right\rangle_m \ln\left(\frac{r_D}{r_{\min}^{(e)}}\right) + 8\pi Z Z_0^2 e^4 n\tau\left\langle\frac{1}{|\mathbf{X}|}\right\rangle_m \ln\left(\frac{r_D}{r_{\min}^{(i)}}\right), \quad (18)$$

where r_D is the Debye radius. In this case, the arguments of the logarithmic functions radically differ from each other. Note that, for the time τ on the order of the time during which the test particle passes the distance equal to the Debye radius, the difference between the arguments of the logarithmic functions are so different that the numerical coefficients in front of the logarithmic functions differ by a factor of two.

Of course, a correct (in the limit of infinitely large values of the Coulomb logarithm) expression for the second moment transferred can be derived from (18) by appropriately choosing the lower limits of the diverging integrals in the range of short spatial scales. Comparing (17) with (18) and (13) with (15), we find that, for τ on the order of the time during which the test particle passes the distance equal to the Debye radius, the integrals should be truncated at $\lambda_e = \sqrt{1/nr_D}$. Note that the spatial scale λ_e is shorter than the mean interparticle distance by a factor of approximately $N_D^{1/6}$ and is longer than $r_{\min}$ by a factor of $N_D^{1/2}$, where $N_D = nr_D^3$ is the number of particles within the Debye sphere.

5. MULTIPARTICLE NATURE OF COLLISIONS IN A PLASMA AND A FEATURE OF THE COULOMB INTERACTION

Expression (18) is based on the approximation of binary collisions [3]. The approach to describing the interaction between plasma particles via binary collisions is used to derive the Boltzmann equation with a short-range interaction potential and implies that the particles are statistically independent and that it is possible to single out the time interval Δt over which a test particle experiences no more than one collision event and which, on the other hand, is long in comparison with the duration τ_{int} of a collision event. In a plasma, however, the duration τ_{int} depends on the impact parameter r as $\tau_{\text{int}} \sim r/v^*$. For example, in the course of one collision event between two particles with the impact parameter $r \sim r_D$, the particles whose impact parameters are smaller than the mean interparticle distance experience $N_D^{2/3}$ collision events. Consequently, the applicability conditions for the approximation of binary collisions fail to hold. (In Appendix 5, this topic is analyzed in a more formal way.) In other words, collision events with large impact parameters have enough time to substantially change the momentum of a test particle before the collision events with small impact parameters, accompanied by large momentum transfers, come into play. It is this circumstance that is responsible for the appearance of a new characteristic spatial scale λ_e. The new spatial scale has a clear physical meaning: for the interaction potentials $U(r) \sim 1/r^k$ with $k > 1$, the momentum transfer is governed by head-on collisions (i.e., collisions between the particles whose impact parameters are small), and, for the potentials $U(r) \sim 1/r^k$ with $k < 1$, it is governed by long-range collisions (i.e., collisions between the particles whose impact parameters are large). The intermediate case $k = 1$ possesses unique properties and should be investigated separately.

It is also of interest to note that our approach to analyzing low interaction potentials that have no singularities over the entire plasma volume and that come into play on the finite radial scale r_0 or shorter actually does not result in a characteristic spatial scale of about $\sqrt{1/nr_0}$, although such a spatial scale does not contradict the dimensionality considerations. This circumstance provides evidence that the new spatial scale, which appears in the problem of Coulomb interaction and can formally be supported by "naive" interpretations, has a deep dynamical meaning. In order to better understand the role of the new scale in the physics of Coulomb interaction, we can rewrite λ_e in the form $\lambda_e = (r_D r_{\min})^{1/2}$ [the clear physical interpretation of the scale $(r_D r_{\min})^{1/2}$ as has been associated with the "statistical spreading" of particle trajectories in a plasma is discussed in Appendix 4].

6. CONCLUSION

We have shown that the profound difference between the physics of systems with the Coulomb potential of interaction among the particles and systems with other interaction potentials consists in the presence of a nontrivial characteristic short spatial scale in former systems. Accounting for the multiparticle nature of particle scattering in plasmas improves the formulas containing the Coulomb logarithm (e.g., the expression for the polarization losses in a plasma) through the refinement of the numerical coefficients in front of it [4]. However, this problem is closely associated with the question of whether the Born and quasiclassical approximations can be applied to describe an almost ideal nondegenerate plasma and requires separate investigation. We emphasize that taking into account the new short spatial scale that results from the multiparticle character of the lower limit in the Coulomb logarithm should inevitably modify the applicability conditions for these approximations [3]. In this sense, the problem we have analyzed serves only to illustrate the fundamental role of the small-scale fluctuation electric fields, so that each approach that neglects fluctuation electric fields and/or describes the interaction between particles in terms of binary collisions [2, 3] requires strong justification for its use.

We emphasize that the Coulomb logarithm enters the expressions for the transport coefficients in a thermodynamically equilibrium plasma that are derived from the kinetic equation with the Landau collision integral. This raises the question of whether the transport coefficients with the Coulomb logarithm lowered by a factor of approximately two will reduce accordingly. To answer this question, note that the kinetic equation with the Landau collision integral was derived in the approximation in which plasma fluctuations are neglected, so that the related Coulomb logarithm is consistent with this approximation. For this reason, the transport coefficients can be evaluated correctly only with allowance for the contribution to the Coulomb logarithm from the fluctuations, which, in turn, should be examined systematically, taking into account their contribution to the kinetic coefficients. However, this problem, which is of crucial importance and was partially analyzed in our earlier papers, is beyond the scope of this study. To avoid misunderstanding, we emphasize again that, in this paper, the problem is considered in the limit of infinitely large values of the Coulomb logarithm.

ACKNOWLEDGMENTS

I am grateful to S.I. Anisimov and É.I. Yurchenko for discussing the method and the results obtained; to V.D. Shafranov, who gave insights into the physical meaning of the results obtained, suggested the idea of this study, and proposed the structure of the paper; to V.P. Pastukhov, who outlined the picture of the statistical spreading of particle trajectories; and, especially, to V.I. Kogan, because this work has benefited from many useful discussions with him and from his deep understanding of the physical meaning of the Coulomb logarithm. This work was supported in part by the Russian Foundation for Basic Research, project no. 96-15-96448 (under the program "Leading Scientific Schools").

APPENDIX 1

First, we evaluate the vector defined in integral form:

$$\mathbf{I} = \int_0^\tau \frac{\mathbf{r}+\mathbf{v}t}{|\mathbf{r}+\mathbf{v}t|^3}dt = -\frac{\partial}{\partial \mathbf{r}}\int_0^\tau \frac{dt}{|\mathbf{r}+\mathbf{v}t|},$$
$$I_0 = \int_0^\tau \frac{dt}{|\mathbf{r}+\mathbf{v}t|}. \quad \text{(A1.1)}$$

We introduce a coordinate system in which the z-axis is aligned with the vector $\mathbf{v}$. In these coordinates, we have

$$I_0 = \frac{1}{v}\ln\left[\frac{z+v\tau+\sqrt{(z+v\tau)^2+x^2+y^2}}{z+\sqrt{z^2+x^2+y^2}}\right], \quad \text{(A1.2)}$$

where $\mathbf{r} = x\mathbf{i} + y\mathbf{j} + z\mathbf{k}$.

For further analysis, it is convenient to transform (A1.2) to elliptic coordinates. Let the origin of the elliptic coordinates be located at the point A, and let B be the point with the coordinates $(0, 0, -v\tau)$. We denote by r_a and r_b the distances from the point with the position vector $\mathbf{r}$ to the points A and B, respectively. We define the elliptic coordinates as

$$\mu = \frac{r_a + r_b}{v\tau}, \quad \nu = \frac{r_a - r_b}{v\tau}, \quad \text{(A1.3)}$$

the third coordinate being the angle ϕ of rotation of a triangle with vertices at the points A and B and at the point with the position vector $\mathbf{r}$ around the z-axis.

In elliptic coordinates, the quantity I_0 has a very simple form,

$$I_0 = \frac{1}{v}\ln\left(\frac{\mu+1}{\mu-1}\right). \quad \text{(A1.4)}$$

We introduce the following function, which is linear in $\mathbf{u}$ and $\mathbf{r}$:

$$F(\mathbf{r}) = (\mathbf{u}, \mathbf{r}) = \frac{u_z}{2}v\tau(1+\mu\nu)$$
$$+\left[\frac{u_x}{2}v\tau\cos\phi + \frac{u_y}{2}v\tau\sin\phi\right][(\mu^2-1)(1-\nu^2)]^{1/2}. \quad \text{(A1.5)}$$

According to (A1.1) and (A1.5), we can write

$$(\mathbf{u}, \mathbf{I}) = -\left(\frac{\partial F(\mathbf{r})}{\partial \mathbf{r}}, \frac{\partial I_0(\mathbf{r})}{\partial \mathbf{r}}\right). \quad \text{(A1.6)}$$

In elliptic coordinates, by virtue of $\partial I_0/\partial\nu = \partial I_0/\partial\phi = 0$, (A1.6) reduces to

$$-(\mathbf{u}, \mathbf{I}) = \frac{4}{(v\tau)^2}\frac{\mu^2-1}{\mu^2-\nu^2}\frac{\partial F}{\partial\mu}\frac{\partial I_0}{\partial\mu} + \frac{4}{(v\tau)^2}\frac{\mu^2-1}{\mu^2-\nu^2}\frac{\partial F}{\partial\nu}\frac{\partial I_0}{\partial\nu}$$
$$+\frac{4}{(v\tau)^2}\frac{1}{(\mu^2-1)(1-\nu^2)}\frac{\partial F}{\partial\phi}\frac{\partial I_0}{\partial\phi} \quad \text{(A1.7)}$$
$$= \frac{4}{(v\tau)^2}\frac{\mu^2-1}{\mu^2-\nu^2}\frac{\partial F}{\partial\mu}\frac{\partial I_0}{\partial\mu}.$$

Inserting (A1.5) into (A1.7) yields

$$-(\mathbf{u}, \mathbf{I}) = \frac{4}{v^2\tau}\frac{\mu^2-1}{\mu^2-\nu^2}$$
$$\times\left[u_z\nu + \mu(u_x\cos\phi + u_y\sin\phi)\left(\frac{1-\nu^2}{\mu^2-1}\right)^{1/2}\right]. \quad \text{(A1.8)}$$

We now need to investigate the properties of the integral

$$U = \int[\exp(iZ_0e^2(\mathbf{u}, \mathbf{I})) - 1]d^3\mathbf{r} \quad \text{(A1.9)}$$

in the limit of small **u** values. In elliptic coordinates, the integral in (A1.9) has the form

$$U = \frac{(V\tau)^3}{8}\int_1^{+\infty} d\mu \int_{-1}^{1} d\nu(\mu^2-\nu^2) \times \int_0^{2\pi}[\exp(iZ_0e^2(\mathbf{u},\mathbf{I}))-1]d\phi$$

so that we have

$$\mathrm{Im}\,U = \frac{(V\tau)^3}{8}\int_1^{+\infty} d\mu \int_{-1}^{1} d\nu(\mu^2-\nu^2) \times \int_0^{2\pi}\sin(Z_0e^2(\mathbf{u},\mathbf{I}))d\phi, \quad \text{(A1.10)}$$

which gives $\mathrm{Im}\,U = 0$. This equality can be verified in a straightforward way. We rewrite the integral in (A1.10) as

$$\mathrm{Im}\,U = \frac{(V\tau)^3}{8}\int_1^{+\infty} d\mu \lim_{\epsilon\to+0}\int_{-1+\epsilon}^{1-\epsilon} d\nu(\mu^2-\nu^2) \times \int_0^{2\pi}\sin(Z_0e^2(\mathbf{u},\mathbf{I}))d\phi \quad \text{(A1.11)}$$

and expand the sine function in powers of its argument to obtain that all of the expansion coefficients vanish:

$$\lim_{\epsilon\to+0}\int_{-1+\epsilon}^{1-\epsilon} d\nu(\mu^2-\nu^2)\int_0^{2\pi}\frac{(-1)^n}{(2n+1)!}\left(\frac{4}{V^2\tau}\right)^{2n+1}\frac{1}{\mu^2-\nu^2} \times\left[u_z\nu+\mu(u_x\cos\phi+u_y\sin\phi)\left(\frac{1-\nu^2}{\mu^2-1}\right)^{1/2}\right]^{2n+1}d\phi = 0,$$

where n is an arbitrary nonnegative integer. Consequently, we can rewrite (A1.9) as

$$U = \frac{(V\tau)^3}{8}\int_1^{+\infty} d\mu \int_{-1}^{1} d\nu(\mu^2-\nu^2) \times \int_0^{2\pi}[\cos(Z_0e^2(\mathbf{u},\mathbf{I}))-1]d\phi. \quad \text{(A1.12)}$$

We consider the limit of small $|\mathbf{u}|$ values. As will be shown below, the main contribution to the integral in (A1.12) comes from the spatial region where the argument of the cosine function is small [the contribution of the region where the argument is larger than or close to unity turns out to be small because the quantity $\ln(1/|\mathbf{u}|)$ is large]. As a result, we obtain

$$U = -\frac{(V\tau)^3}{16}\int_G(\mu^2-\nu^2)Z_0^2e^4(\mathbf{u},\mathbf{I})^2 d\mu d\nu d\phi, \quad \text{(A1.13)}$$

where the domain of integration G is limited by the inequality

$$Z_0e^2|(\mathbf{u},\mathbf{I})| < 1. \quad \text{(A1.14)}$$

We need to evaluate the quantity U with logarithmic accuracy in terms of the parameter $\ln(1/|\mathbf{u}|)$. Using (A1.8), (A1.13), and (A1.14), we obtain to the lowest order in u_x, u_y, and u_z

$$U = -\frac{2\pi Z_0^2e^4\tau}{V}u_z^2\int_1^{+\infty} d\mu\int_{-1}^{1}\frac{\nu^2 d\nu}{\mu^2-\nu^2} - \frac{\pi Z_0^2e^4\tau}{V}(u_x^2+u_y^2)\int_{\mu_0(\mathbf{u})}^{+\infty} d\mu\int_{-1}^{1}\frac{\mu^2(1-\nu^2)}{(\mu^2-1)(\mu^2-\nu^2)}d\nu, \quad \text{(A1.15)}$$

where $\mu_0^2(\mathbf{u}) - 1 = Z_0^2e^4(u_x^2+u_y^2)/V^4\tau^2$. It is an easy matter to take the integrals in (A1.15), so that, with the desired accuracy, we finally arrive at

$$U = -\frac{2\pi Z_0^2e^4\tau}{V}u_z^2 - \frac{\pi Z_0^2e^4\tau}{V}(u_x^2+u_y^2)\ln\left[\frac{V^4\tau^2}{Z_0^2e^4(u_x^2+u_y^2)}\right]. \quad \text{(A1.16)}$$

APPENDIX 2

In order to make the analysis more clear and compact, we illustrate how the Coulomb logarithm can be used as a large parameter, taking as an example the integral of a function of one variable. We consider the function $f(p)$ defined in terms of the Gaussian integral,

$$f(p) = \int_{-\infty}^{+\infty}\exp(ipu-u^2)du = 2\mathrm{Re}\int_0^{+\infty}\exp(ipu-u^2)du. \quad \text{(A2.1)}$$

Of course, the integral in (A2.1) is easy to take and the final result is well known. However, in order to clarify the general approach to the problem, it is of interest to consider the method for evaluating this integral. Let $p > 0$. Note that the derivative of the argument of the exponential function in (A2.1) vanishes at the point $u(p) = ip/2$, which lies in the upper half-plane. We convert from an integration over the positive real semiaxis to an integration over a new contour composed of a segment between the points 0 and $u(p)$ at the imaginary axis and a horizontal ray between the point $u(p)$ and the infinitely remote point $u(p) + \infty$. Since, for large values of p, the integrand in (A2.1) is exponentially small along the ray between the point $u(p)$ and the infinitely remote point u $u(p) + \infty$, the ray makes an exponentially small contribution to the integral. Over the segment

between the points 0 and $u(p)$, the integrand is not exponentially small, so that the contribution to the integral from the segment also is not exponentially small. However, this contribution is purely imaginary and does not affect the real part of the function $f(p)$ in (A2.1).

This example allows us to understand why, in the range of large p values, the integrals of the form (A2.1) are very sensitive even to slight changes in the argument of the exponential function: the contribution of the integral over the segment at the imaginary axis, which may contain a nonzero real part, can be much larger than the contribution of the horizontal ray.

We consider a function having a logarithmic singularity at the origin of the coordinates in the complex plane; i.e., we analyze the function $f^*(p)$ defined by

$$\begin{aligned} f^*(p) &= \int_{-R/2}^{R/2} \exp[ipu - u^2\ln(R^2/u^2)]du \\ &= 2\,\mathrm{Re}\int_0^{R/2} \exp[ipu - u^2\ln(R^2/u^2)]du, \end{aligned} \tag{A2.2}$$

where $p \gg 1$ and $R \longrightarrow +\infty$. We choose the integration contour to be composed of a segment between the points 0 and $u^*(p) = ip/2\ln(R^2/p^2)$ at the imaginary axis, a horizontal segment between the points $u^*(p)$ and $u^*(p) + R/2$, and a segment between the points $u^*(p) + R/2$ and $R/2$. For large p values, only the contribution from the segment at the imaginary axis is not exponentially small, so that it is sufficient to consider the quantity

$$\begin{aligned} \Delta &= \mathrm{Re}\, i\int_0^{p/2\ln(R^2/p^2)} \exp[-pu + u^2\ln(R^2/u^2) + \pi i u^2]du. \end{aligned} \tag{A2.3}$$

Note that the last term in the integrand in (A2.3) results from a logarithmic singularity in the argument of the exponential function in (A2.2). If this term were absent, then Δ would vanish. To exploit the large value of the logarithm $\ln(R^2/p^2)$, we introduce a new variable z such that $u = zp/\ln(R^2/p^2)$. In the argument of the exponential function in (A2.3), we retain the leading-order terms in $\ln(R^2/p^2)$ and keep the imaginary term, which appears due to the logarithmic singularity. As a result, in the limit $\ln(R^2/p^2) \longrightarrow +\infty$, we obtain

$$\begin{aligned} \Delta = \mathrm{Re}\, i\int_0^{1/2} \exp\Bigg[&-\frac{p^2}{\ln(R^2/p^2)}z + \frac{p^2}{\ln(R^2/p^2)}z^2 \\ &+ \pi i\frac{p^2}{\ln(R^2/p^2)^2}z^2\Bigg]dz. \end{aligned} \tag{A2.4}$$

Expression (A2.4) incorporates a logarithmic singularity in the limit of infinitely large values of the Coulomb logarithm. It is easily seen from (A2.2) and (A2.4) that the function $f^*(p)$ is Gaussian at $p^2 < p_0^2 = 2\ln(R^2)\ln(\ln(R^2))$ and decreases as $1/p^3$ at $p^2 > p_0^2$.

Now, we can examine the distribution function

$$\begin{aligned} f_0(\mathbf{p}) &= \int \exp\Bigg(i(\mathbf{u}, \mathbf{p}) - \frac{\pi n Z_0^2 e^4}{v} \\ &\times \mathbf{u}^2\ln\left(\frac{v^4\tau}{Z_0^2 e^4 \mathbf{u}^2}\right)\Bigg)\frac{\mathrm{d}\mathbf{u}}{(2\pi)^2}, \end{aligned} \tag{A2.5}$$

where $\mathbf{u} = (u_x, u_y)$ and $\mathbf{p}$ is the two-dimensional vector whose distribution we study here. The relation between the distribution function (A2.5) and expression (A1.16) is obvious. Our purpose is to study the "tail" of distribution (A2.5) at $p \longrightarrow \infty$. Since the function $f_0(p)$ depends only on the absolute value of the vector p, we can assume without loss of generality that this vector is directed along the x-axis. We introduce the new integration variable $\boldsymbol{\xi} = p\mathbf{u}$ to obtain

$$\begin{aligned} f_0 &= \frac{1}{p^2}\int \exp\Bigg(i\xi_x - \frac{\pi n Z_0^2 e^4}{v p^2}(\xi_x^2 + \xi_y^2) \\ &\times \ln\left(\frac{v^4\tau}{Z_0^2 e^4(\xi_x^2 + \xi_y^2)}\right)\Bigg)\frac{d\xi_x\xi_y}{(2\pi)^2}. \end{aligned} \tag{A2.6}$$

To study the asymptotic behavior of the function f_0 at $p \longrightarrow \infty$ accurate to the terms decreasing as $1/p^4$ or more rapidly, it is sufficient to rewrite the integrand of expression (A2.6) in the form

$$\begin{aligned} &\exp\left(i\xi_x - \frac{\pi n Z_0^2 e^4\tau}{v p^2}(\xi_x^2 + \xi_y^2)\ln\left(\frac{v^4\tau^2 p^2}{Z_0^2 e^4}\right)\right) \\ &\times\left[1 + \frac{\pi n Z_0^2 e^4\tau}{v p^2}(\xi_x^2 + \xi_y^2)\ln(\xi_x^2 + \xi_y^2) + \ldots\right]. \end{aligned} \tag{A2.7}$$

It is easily seen that the principal power-law part of the function f_0 at $p \longrightarrow \infty$ is

$$\begin{aligned} f_0 &= a\int \exp(i\xi_x - b(\xi_x^2 + \xi_y^2)) \\ &\times(\xi_x^2 + \xi_y^2)\ln(\xi_x^2 + \xi_y^2)d\xi_x d\xi_y, \end{aligned} \tag{A2.8}$$

where $a = (ne^4 Z_0^2\tau)/(4\pi v p^4)$ and $b = (\pi ne^4 Z_0^2\tau\ln(v^4p^2\tau^2/Z_0^2 e^4))/(vp^4)$. Integrating (A2.8) by parts over the variable ξ_x, to first order in p, we obtain

$$f_0 = a\int \exp(i\xi_x - b(\xi_x^2 + \xi_y^2))\frac{4i\xi_x + 4\xi_x^2}{\xi_x^2 + \xi_y^2}d\xi_x d\xi_y. \tag{A2.9}$$

The integral in (A2.9) is easy to calculate. First, we integrate over ξ_x by shifting the path of integration to the complex plane. The expression obtained is elementarily integrable over ξ_y. As a result, we obtain

$$f_0(p) = \frac{4\pi n Z_0^2 e^4 \tau}{v p^4}. \quad \text{(A2.10)}$$

It is easy to verify that expression (A2.10) describes the distribution function at $p^2 > p_0^2 \ln(\Lambda/4)$, where Λ is the root of the equation $\Lambda = \ln(2\pi\Lambda n(v\tau)^3)$. At smaller values of p, the distribution function is Gaussian,

$$f_0 = \frac{1}{4\pi p_0^2} \exp\left(-\frac{p^2}{2p_0^2}\right). \quad \text{(A2.11)}$$

The distribution function (A2.10) describes the scattering of only $1/(\Lambda\ln(\Lambda/4))$ fraction of all the particles; however, in the general case, the second moment of the momentum transferred related to these particles turns out to be significant. Therefore, the passage to the limit $\Lambda \longrightarrow \infty$ is rather nontrivial. In this paper, we do not consider this problem in more detail, because here we are interested just in the limiting case $\Lambda = +\infty$. The question of what real situation this limit corresponds to deserves a separate study.

APPENDIX 3

To find the second moment of the momentum transferred, we must evaluate the integral

$$I_1 = \int (\mathbf{I}, \mathbf{I}) d^3\mathbf{r}. \quad \text{(A3.1)}$$

Using (A1.1) and (A1.4), we obtain

$$I_1 = \frac{v\tau}{2} \int_1^{+\infty} d\mu(\mu^2 - 1) \int_{-1}^{1} d\nu \int_0^{2\pi} \left(\frac{\partial I_0}{\partial \mu}\right)^2 d\phi = \frac{8\pi\tau}{v} \int_1^{+\infty} \frac{d\mu}{\mu^2 - 1}. \quad \text{(A3.2)}$$

APPENDIX 4

Here, we consider how the finite plasma permittivity (i.e., the Debye screening of the Coulomb potential of the interaction between plasma particles) can be incorporated into our approach. Note that the screening of the Coulomb interaction potential should be described with allowance for correlation between the plasma particles. On the other hand, the expressions for the characteristic functions involved in our analysis were derived without allowance for correlation between the plasma particles. This brings about the question of whether it is possible in principle to refine the characteristic functions so as to take into account the Debye screening. Note that, in the limit of an arbitrarily large number of particles within the Debye sphere, the motion of each plasma particle can be regarded as being statistically independent of the other particles. However, the finite Coulomb interaction potential perturbs the trajectories of the particles, thereby giving rise to correlation between them. It is the slight deformations of the particle trajectories that are responsible for the screening of the Coulomb potential.

To make simple estimates, we consider a test electron moving with a nearly thermal velocity in a plasma and interacting with another thermal electron (or ion) whose impact parameter is equal to R. After the collision event, the trajectory of the test electron is displaced by a distance of about δx. In other words, the collision event causes the point at which the trajectory of the test electron leaves the sphere of radius, e.g., $2R$, with the center at the point at which the particle scattering occurs to displace by the distance

$$\delta x \sim \frac{e^2}{mR^2}\left(\frac{R}{v_T}\right)^2 \sim \frac{e^2}{T}, \quad \text{(A4.1)}$$

where v_T is the electron thermal velocity. However, the Debye sphere contains about $N_D = n r_D^3$ particles, which perturb the trajectory of a test electron in a statistically independent manner. Consequently, the deviation Δx of the trajectory of the test electron that has traversed the Debye sphere from the unperturbed trajectory can be estimated as

$$(\Delta x)^2 \sim (\delta x)^2 N_D = r_D r_{\min}. \quad \text{(A4.2)}$$

This indicates that Coulomb interaction among plasma particles and the related correlations force the particles to make random excursions away from their unperturbed trajectories on a spatial scale of about $(r_D r_{\min})^{1/2}$. In other words, the plasma particles are statistically "smeared" around their unperturbed trajectories, while the "smeared" trajectories remain statistically independent. This analysis results in the appearance of the characteristic spatial scale $(r_D r_{\min})^{1/2}$, which makes it possible to distinguish between the phenomena for which the notion of Debye screening is consistent with the approach to treating the plasma particles in a statistically independent fashion.

The above analysis provides a way to incorporate the Debye screening into the approach developed. We can readily see that, to account for the Debye screening on time scales τ such that $\tau_{\min}[v^*, V^*] \gg r_D$, it is sufficient to carry out the manipulations from Appendix 1 with another expression for I_0. Specifically, in the calculations to logarithmic accuracy with allowance for Debye screening, we may set

$$I_0 = \frac{1}{v} \ln \frac{r_D^2}{x^2 + y^2}, \quad \text{for} \quad x^2 + y^2 < r_D^2, \quad -v\tau < z < 0, \quad \text{(A4.3)}$$

and $I_0 = 0$ at any point (x, y, z) outside the cylinder ($x^2 + y^2 < r_D^2$, $-v\tau < z < 0$), in which case the calculations are simpler to perform in cylindrical coordinates.

APPENDIX 5

Since any gas medium consisting of interacting particles can be characterized by a certain evolving spatial distribution of the interaction potential, we can construct the dimensionless parameter

$$\Theta = \frac{1}{\Pi_{ch}}\frac{p_{ch}^2}{2m}, \tag{A5.1}$$

where p_{ch} is the characteristic change in the momentum of a particle on a characteristic time scale and Π_{ch} is the characteristic potential difference between the points at the beginning and end of the characteristic time interval. Note that such gases can be described by the theory of binary collisions, because the parameter Θ is large. In fact, the theory of binary collisions assumes that a collision event either has not yet occur or has already come to an end; i.e., we always have $\Pi_{ch} = 0$ and, accordingly, $\Theta = +\infty$. For a gas with a short-range interaction potential, as the characteristic time scale, one must adopt the mean free time, in which case $\Theta \longrightarrow +\infty$. The situation with a plasma is radically different: the characteristic time scale should be set to be $1/\omega_{pe}$, so that, for an electron moving with a nearly thermal velocity, we obtain the estimates

$$\Pi_{ch}^2 \sim \int_0^{r_D} \frac{e^4}{r^2} n r^2 dr = e^4 n r_D, \tag{A5.2}$$

which yields

$$\frac{p_{ch}^2}{2m} \sim \frac{T}{N_D}, \tag{A5.3}$$

$$\Theta \sim 1/N_D^{3/4}, \tag{A5.4}$$

where $N_D = n r_D^3$ is the number of particles inside the Debye sphere.

On the other hand, the theory of binary collisions between plasma particles does not take into account the potential energy distribution in a plasma and, consequently, implicitly assumes redefinition of the particle momentum in formulas: the momentum transferred to a particle always means the change in the momentum of a particle due to the collision events that have already come to an end. From the standpoint of the long-range nature of the Coulomb potential, the momentum transferred between two particles in a collision event is a poorly defined mathematical quantity, which may differ substantially from the momentum really transferred. The simplest way to see that is to analyze the squared moment of the change in the z-component of the momentum of a test particle using formula (A1.16) and the methods of the theory of binary collisions [3]. These two approaches give results that differ by a factor of approximately N_D (to avoid misunderstanding, we emphasize that the second moment of the longitudinal momentum transferred is a small quantity in comparison with the second moment of the transverse momentum transferred; this indicates that such a large difference causes no dramatic consequences, because this is merely the difference in a small correction to the leading-order term in the kinetic equation [3]: the correction always remains small, no matter how much the values obtained with the above approaches differ from one another).

REFERENCES

1. N. Bohr, K. Dan. Vidensk. Selsk. Mat. Fys. Medd. **8**, 18 (1948) [*The Penetration of Atomic Particles through Matter* (Inostrannaya Literatura, Moscow, 1950)].
2. B. A. Trubnikov, in *Reviews of Plasma Physics*, Ed. by M. A. Leontovich (Gosatomizdat, Moscow, 1961; Consultants Bureau, New York, 1963), Vol. 1.
3. D. V. Sivukhin and M. A. Leontovich, in *Reviews of Plasma Physics*, Ed. by M. A. Leontovich (Gosatomizdat, Moscow, 1964; Consultants Bureau, New York, 1968), Vol. 4.
4. V. D. Shafranov, in *Reviews of Plasma Physics*, Ed. by M. A. Leontovich (Gosatomizdat, Moscow, 1963; Consultants Bureau, New York, 1967), Vol. 3.
5. V. I. Kogan, Dokl. Akad. Nauk SSSR **135**, 1374 (1960) [Sov. Phys. Dokl. **5**, 1316 (1960)].

Translated by G. V. Shepekina

Plasma Physics Reports, Vol. 26, No. 6, 2000, pp. 529–538. Translated from Fizika Plazmy, Vol. 26, No. 6, 2000, pp. 566–576.

MAGNETIC HYDRODYNAMICS

Adiabatic Separation of Motions and Reduced MHD Equations

V. P. Pastukhov

Russian Research Centre Kurchatov Institute, pl. Kurchatova 1, Moscow, 123182 Russia

Received November 15, 1999

Abstract—A variational method for separating fast and slow motions in quasi-Lagrangian continuous media is proposed, which makes it possible to discard fast stable collective degrees of freedom and to derive simpler (reduced) nonlinear equations describing the adiabatic dynamics of quasi-Lagrangian systems. The method is applied to derive an improved version of the reduced Kadomtsev–Pogutse–Strauss MHD equations that describe the dynamics of a tokamak plasma with steady-state sheared flows, as well as adiabatic equations for two-dimensional modeling of MHD plasma convection near the threshold for flute instability in systems like compact tori. © *2000 MAIK "Nauka/Interperiodica".*

1. INTRODUCTION

The well-known method of the adiabatic separation of weakly coupled fast and slow motions is widely used in classical mechanics. The method is based on revealing rapidly oscillating stable degrees of freedom in the dynamic system under analysis. The characteristic oscillation period T_f of the fast motion should satisfy the condition $T_f/\tau_s \sim \varepsilon \ll 1$, where τ_s is the characteristic time of slow motions. Further analysis of the fast degree of freedom involves the construction of an adiabatic invariant, i.e., an approximate integral of motion, which remains unchanged during a slow evolution (on a time scale of about τ_s) of the system. This slow evolution can be described by adiabatic (reduced) equations of motion that are derived from the complete set of basic equations under the assumption that the adiabatic invariant is an exact integral of motion of the system. An obvious advantage of the adiabatic description of the system dynamics is that it becomes possible to reduce the number of independent degrees of freedom and to exclude the short time scales from consideration (the latter circumstance is especially important for developing computer codes). As a rule, allowing for an additional integral of motion (adiabatic invariant) also makes it possible to reveal important qualitative features of the system dynamics that are hidden attributes of the complete set of basic equations. As an example illustrating the advantages of adiabatic equations in plasma physics studies, we can mention drift equations describing particle motion in a strong magnetic field.

Many of the mathematical methods that were originally developed in classical mechanics for systems with a finite number of degrees of freedom (in particular, Lagrangian and Hamiltonian formalisms) have been successfully applied to continuous media, which are described by various quasi-hydrodynamic models (see, e.g., reviews [1, 2]). Thus, it seems worthwhile to apply the method of adiabatic separation of fast and slow motions to a description of continuous media. However, the implementation of this approach runs into serious difficulties that stem primarily from the fact that continuous systems are characterized by a continual or denumerable set of the degrees of freedom, so that we can only speak of the adiabatic separation of infinite subsets (or classes) of the degrees of freedom characterized by different time scales (rather than individual degrees of freedom).

The first problem is to prove that there is no resonant interaction between the motions associated with the degrees of freedom that are to be separated. A rigorous mathematical treatment of this problem is very complicated even when the number of degrees of freedom is finite (see, e.g., review [3]). However, discarding a rigorous proof, we can formulate this problem in a slightly different manner, i.e., as the problem of the stability of fast motion in the presence of a prescribed slow motion. In this case, based on the preliminary analysis and *a priori* data, we can, first, separate the motions in a desired fashion, assuming that the fast motion is stable and, then, establish whether the fast motion is stable in the presence of the most interesting and important modes of the slow motion.

The second difficulty is associated with the development of an adequate procedure for separating fast and slow motions, because, in the case of continuous media, this procedure is rather nontrivial and is *a priori* unclear. Solving this problem is the main objective of our paper.

The third problem—the construction of adiabatic invariants for continuous media—seems to be the most complicated, because the desired invariants should reflect the conservation of the phase volume of a subset of fast motions, which is characterized, as a rule, by an infinite number of coupled collective oscillatory degrees of freedom. To the best of my knowledge, an adequate mathematical formalism for treating this problem is lacking. However, we can easily overcome this difficulty for many specific dynamic problems for

1063-780X/00/2606-0529$20.00

continuous media. The reason is that, to the lowest order, the adiabatic invariant under discussion, regardless of the details of its structure, is proportional to a weighted sum of the squared amplitudes of fast oscillations. In other words, for this order, the adiabatic invariant is positively definite. If no fast oscillations are excited in the initial state (i.e., the invariant is initially equal to zero), then the conservation of the invariant guarantees that no fast motions will be driven during an arbitrary adiabatic evolution of a slow dynamic subsystem.

Adiabatic equations with a zero adiabatic invariant for fast degrees of freedom are applicable to a wide variety of dynamic problems for continuous media, in particular, the problems of stability and nonlinear convection, formation of vortex structures, etc. A classical example of the above set of adiabatic equations is the equations of incompressible fluid that are derived by eliminating fast stable acoustic oscillations from the complete set of hydrodynamic equations.

Magnetically confined high-temperature plasmas are often investigated by means of reduced MHD equations, which were first derived by Kadomtsev and Pogutse [4, 5] for describing plasma dynamics in tokamaks and were further developed in a number of papers [6–9] (mostly by Strauss) with allowance for a low (but finite) plasma pressure and longitudinal ion acoustic oscillations. The key idea underlying the Kadomtsev–Pogutse–Strauss (KPS) equations is to exclude fast stable magnetosonic (compressional Alfvén) waves from the complete set of MHD equations and to consider slower degrees of freedom associated with shear Alfvén and longitudinal acoustic motions. In terms of the way in which the KPS equations were constructed, they seem to belong to the above class of adiabatic equations; however, the procedure used to separate fast and slow motions in deriving these equations was not quite accurate. For example, because of the assumed structure of the velocity field of slow motions, the force terms in the basic equations of motion vanish only through the leading order in ϵ, while a correct reduction procedure should drive the force terms to zero through both the leading and first orders. That the reduced equations derived in [4–9] are incorrect is evidenced even more clearly by the fact that they admit no solutions describing plasma flows in steady states consistent with the basic MHD equations, because an incorrect reduction procedure violates their symmetry properties. The modified versions of reduced equations that were proposed in more recent papers [10, 11] to describe the dynamics of plasmas with steady-state, magnetic field–aligned flows have the same drawbacks: in particular, they admit no solutions describing general steady-state plasma flows. In this connection, it is desirable to derive an improved (completely adiabatic) version of MHD equations that is free of these drawbacks.

The above examples do not exhaust the problem of derivation of the adiabatic equations of motion for continuous media. An infinite number of degrees of freedom and a large number of possible adiabaticity parameters ϵ stemming from the wide variety of specific problems necessitate the development of a fairly general regular method of deriving adiabatic equations for a large class of physical problems. This is the subject of our paper. In Section 2, we describe the ideas underlying the variational method for separating fast and slow motions and deriving adiabatic equations for continuous media. In Section 3, we apply this method to derive an improved version of the KPS equations that is free of the aforementioned drawbacks. In Section 4, we derive adiabatic equations for modeling two-dimensional MHD plasma convection near the threshold for flute instability in systems of the compact torus type. In Section 5, we briefly summarize the results obtained.

2. BASIC PRINCIPLES OF THE VARIATIONAL METHOD FOR SEPARATING FAST AND SLOW MOTIONS

The method proposed here for adiabatic separation of fast and slow motions is applicable, strictly speaking, to Lagrangian systems, i.e., those systems in which the equations of motion can be derived from the principle of least action (Hamilton's principle) (see, e.g., [12]). Typical examples of Lagrangian systems are those described in terms of traditional magnetohydrodynamics, Chew–Goldberger–Low collisionless anisotropic magnetohydrodynamics, Hall magnetohydrodynamics, and other ideal hydrodynamic models. However, this method can also be applied to weakly nonideal (quasi-Lagrangian) models, which can be reduced to Lagrangian models by neglecting weak dissipation.

We assume that the equations of motion for a system can be derived from Hamilton's variational principle

$$\delta\int_{t_1}^{t_2} dt \int_{\Gamma} L d^3\mathbf{r} = 0 \qquad (1)$$

with the Lagrangian density $L(\{\alpha^i\}, \{\partial_t\alpha^i\}, \{\nabla\alpha^i\})$, which depends on the nondegenerate set of the generalized coordinates $\alpha^i(\mathbf{r}, t)$ ($i = 1, \ldots, n$) and their first space and time derivatives. If there is an infinitesimal transformation of the generalized coordinates, $\delta_s\alpha^i$, such that it does not change the Lagrangian of the system, then, according to Noether's theorem [12], the system possesses an implicit symmetry and, accordingly, the related additional integral of motion. In mathematics, the transformation $\delta_s\alpha^i$ that depends only on the generalized coordinates is known as point transformation, while, in hydrodynamic problems, it is referred to as relabeling transformation. In the latter case, in terms of classical mechanics, the transformation $\delta_s\alpha^i$ corresponds to the variation of a certain cyclic coordinate and the canonical momentum conjugate to this coordi-

nate is an integral of motion. An important consequence of momentum conservation is the existence of dynamic steady states of a system that possess relabeling symmetry. In continuous systems, these are states with steady n-dimensional flows, whose velocity fields are similar in structure to the transformation $\delta_s\alpha^i$. In particular, for toroidal MHD configurations with nested magnetic surfaces (tokamaks, stellarators, etc.), analogous symmetry transformations and similar structures of the related steady-state flows were obtained by Il'gisonis and Pastukhov [13].

Now, we assume that the system described by the equations derived from Hamilton's principle (1) possesses motions that occur on different time scales. This indicates that the Lagrangian of the system implicitly contains the parameter $\epsilon \ll 1$, which reflects the ratio of the characteristic times of fast and slow motions. As a rule, the manifestation of the parameter ϵ is that the expression for the perturbed potential energy contains terms of order unity and ϵ^2, which correspond to structurally different classes of motions. By analogy with the procedure of searching for a symmetry transformation, we are seeking an infinitesimal transformation $\delta_a\alpha^i$ that does not change the Lagrangian of the system through both the leading and first orders in ϵ. In other words, we are interested in the transformation satisfying the condition

$$\delta_a\int_\Gamma L(\{\alpha^i\}, \{\partial_t\alpha^i\}, \{\nabla\alpha^i\}, \epsilon)d^3\mathbf{r} = O(\epsilon^2). \quad (2)$$

If a transformation of this sort (which will be referred to as adiabatic transformation) does indeed exist, then it plays a role similar to that of the symmetry transformation for fast motion. In fact, the equations describing the dynamics of fast motion on time scales shorter than the characteristic time of slow motions can be derived from Hamilton's principle (1) by neglecting terms on the order of ϵ^2 in the variation of the Lagrangian.

If the functions $\delta_a\alpha^i$ satisfying condition (2) depend only on the generalized coordinates α^i and slow time, $\delta_a\alpha^i = f^i(\{\alpha^j\}, \epsilon t)$, then the functions $\delta_a\alpha^i$ play the role of relabeling transformation but only for fast motion. To continue drawing an analogy with symmetry transformations, we introduce an adiabatic field of the generalized velocities that has the same functional structure as the transformation $\delta_a\alpha^i$. For fast motions, the adiabatic velocity field plays the role of the above steady-state (neutral) flows. If no fast stable degrees of freedom (fast motions) are excited at the initial state (this corresponds to a zero adiabatic invariant, which was mentioned in the Introduction), then the system only evolves in the frame of the adiabatic velocity field, as is the case with conservation of the steady-state character of the flows in a stable system possessing the corresponding type of symmetry.

Since the transformation $\delta_a\alpha^i$ is a certain subset of the initial set of arbitrary variations of the generalized coordinates, the functions $\delta_a\alpha^i$ and, accordingly, the generalized velocities depend on a smaller number ($n_a < n$) of independent functions (adiabatic generalized coordinates) and can be obtained from a smaller number of equations, e.g., from n_a independent consequences of the basic set of the equations of motion. However, a more regular method, which is analogous to that of deriving the Lagrange equations from the variational principle (1), consists in driving to zero the coefficients in front of the independent variations of n_a adiabatic generalized coordinates in equation (1) taken with $\delta\alpha^i = \delta_a\alpha^i$. The equations constructed in this fashion, together with the adiabatic velocity field, constitute the desired set of adiabatic (reduced) equations describing the dynamics of slow motion when no fast stable motions are initially excited.

Hence, the procedure outlined above provides a regular method for both solving the problem of the adiabatic separation of fast and slow motions and deriving adiabatic equations that describe the dynamics of slow motion. Since the symmetry transformations $\delta_s\alpha^i$ of the basic equations are a subset of the set of the adiabatic transformations $\delta_a\alpha^i$, the way in which the latter are constructed implies that the adiabatic equations of motion possess all of the symmetry properties of the basic equations. In particular, the adiabatic equations admit such solutions describing plasma flows in steady states that are consistent with the basic equations of motion. We emphasize that, for the proposed procedure to be correct, it is necessary to satisfy all of the conditions formulated above.

The procedure for applying the method developed here to weakly nonideal systems consists of the following steps. First, it is necessary to neglect dissipation and to rewrite the basic set of equations in Lagrangian form. Second, in the resulting Lagrangian model, fast and slow motions should be separated adiabatically. If the fast degrees of freedom constitute a stable subsystem with positive energy, then the effect of dissipative processes on the fast subsystem shows up exclusively as a reduction in its energy, which does not change the condition for the conservation of the zero adiabatic invariant. And finally, the basic nonideal equations should be taken with the resulting adiabatic velocity field in order to obtain n_a independent consequences required to describe the slow nonlinear dynamics of the corresponding adiabatic coordinates.

3. IDEAL ADIABATIC MHD EQUATIONS FOR TOKAMAK-LIKE MAGNETIC CONFINEMENT SYSTEMS

To illustrate how the procedure outlined above should be applied, we will first derive adiabatic equations describing ideal MHD plasma dynamics in a tor-

oidal magnetic confinement system with nested magnetic surfaces and a low ratio of plasma to magnetic field pressure, $\beta \equiv 8\pi p/B^2 \ll 1$. To simplify the formulas, we restrict ourselves to considering steady-state axisymmetric (tokamak-like) systems, in which all of the physical parameters in a steady state are independent of the toroidal angle φ. In other words, we are going to derive a more accurate version of the reduced KPS equations [4–11]. Note that preliminary results of deriving such adiabatic equations were briefly described in my recent paper [14]. Here, we present the derivation in a general form, with allowance for a number of important aspects.

As was mentioned in the Introduction, plasma dynamics in a strong magnetic field ($\beta \ll 1$) is characterized by motions with relatively weak perturbations of the magnetic field. According to linear theory, the magnetic field energy is perturbed most strongly by magnetosonic oscillations with the characteristic frequency $\omega \sim C_A|\nabla_\perp|$ (where C_A is the Alfvén speed). On the other hand, the most interesting dynamic processes (in particular, those driven by MHD instabilities) are associated with perturbations that are very stretched out along the magnetic field ($|\nabla_\parallel| \ll |\nabla_\perp|$) and have characteristic frequencies typical of Alfvén waves, $\omega \sim C_A|\nabla_\parallel|$, or lower. Since, in such processes, fast stable magnetosonic degrees of freedom remain essentially unperturbed, we can exclude them from consideration with the help of the procedure proposed for the adiabatic separation of motions.

As in the KPS equations, we adopt the ratio of the poloidal to toroidal magnetic fields (or the inverse aspect ratio) $\epsilon = B_p/B_T \sim a/R$ (where a and R are the minor and major radii of the toroidal plasma column) as a small parameter of the adiabatic separation of motions. By analogy with the KPS equations, we also assume that the transverse and longitudinal gradients of the perturbed quantities satisfy the condition $|\nabla_\parallel| \le \epsilon|\nabla_\perp|$ and that $\beta \sim \epsilon^2 a|\nabla_\perp|$.

We consider the variation of the standard Lagrangian in the one-fluid MHD model [15]:

$$\delta\mathcal{L} = \int d\mathbf{r}^3\left(\rho\mathbf{V}\cdot\delta\mathbf{V} + \frac{V^2}{2}\delta\rho - \frac{\delta p}{\gamma-1} - \mathbf{B}\cdot\delta\mathbf{B}\right). \quad (3)$$

Here and below, the coefficient $1/4\pi$ is incorporated into the normalized field $\mathbf{B}$. In (3), the variations of the physical quantities are not completely independent, because they should satisfy the frozen-in equation, continuity equation, and adiabatic equation:

$$\partial_t\mathbf{B} = \mathrm{curl}[\mathbf{V}\times\mathbf{B}], \quad (4)$$

$$\partial_t\rho + \mathrm{div}\,\rho\mathbf{V} = 0, \quad (5)$$

$$\partial_t s + \mathbf{V}\cdot\nabla s = 0, \quad (6)$$

where $s = p/\rho^\gamma$ is the entropy function. Equations (4)–(6) are local conservation laws in the sense that the corresponding Lie derivatives vanish. The scalar functions satisfying equation (5) are often called local Eulerian invariants (LEI), and the functions satisfying equation (6) are referred to as local Lagrangian invariants (LLI). According to [15], equations (4)–(6) can generally be integrated by introducing three independent LLI α^i, which play the role of generalized coordinates with a nondegenerate Jacobian $J = \nabla\alpha^1\cdot[\nabla\alpha^2\times\nabla\alpha^3] \neq 0$. In this case, J (similarly to ρ) satisfies equation (5).

In this paper, we are considering magnetic systems with an omnigenous topology of the toroidal magnetic surfaces. Following paper [13], which presents the most detailed analysis of the dynamics of such confinement systems, we choose the poloidal magnetic flux ψ and the angle variables θ and ζ as the Lagrangian coordinates. In the initial steady state, the latter are the poloidal and toroidal angles in the flux coordinate system with straightened magnetic field lines [16]. In these variables, the physical quantities $\mathbf{B}$, ρ, and s satisfying equations (4)–(6) are represented as

$$\begin{aligned}\mathbf{B} &= [\nabla\psi\times(q\nabla\theta - \nabla\zeta)],\\ \rho &= Jf(\psi,\theta,\zeta), \quad s = s(\psi),\end{aligned} \quad (7)$$

where $q(\psi)$ is the traditional safety factor, f is an arbitrary function of the Lagrangian coordinates, and $J = \nabla\psi\cdot[\nabla\theta\times\nabla\zeta]$. The coordinates just introduced generate the contravariant basis $\nabla\psi$, $\nabla\theta$, and $\nabla\zeta$ and the covariant one

$$\mathbf{e}_\psi = [\nabla\theta\times\nabla\zeta]/J, \quad \mathbf{e}_\theta = [\nabla\zeta\times\nabla\psi]/J,$$
$$\mathbf{e}_\zeta = [\nabla\psi\times\nabla\theta]/J,$$

in which the velocity has the form

$$\mathbf{V} = -\mathbf{e}_\psi\dot\psi - \mathbf{e}_\theta\dot\theta - \mathbf{e}_\zeta\dot\zeta, \quad (8)$$

where a superior dot denotes the partial derivative ∂_t. The above expressions allow us to explicitly express the Lagrangian of the system as a function of the independent Lagrangian coordinates and their first space and time derivatives, which is especially important in seeking both symmetry and adiabatic transformations with the help of the method described in the previous section.

In systems with axisymmetric steady states (such as tokamaks), all of the physical quantities in a steady state are independent of ζ. For such systems, the velocity of the neutral flows can be written as [13]

$$\begin{aligned}\mathbf{V}_0 &= \kappa(\psi)\frac{\mathbf{B}}{\rho} - \Phi_0'(\psi)\mathbf{e}_\zeta\\ &= \frac{\mathbf{B}}{qJ}\left(\kappa\frac{qJ}{\rho} - \Phi_0'\right) + \frac{1}{qJ}[\nabla\zeta\times\nabla\Phi_0],\end{aligned} \quad (9)$$

where $\kappa(\psi)$ and $\Phi_0(\psi)$ are arbitrary functions of ψ that specify the transverse profiles of the flows. The relationships $\mathrm{curl}[\mathbf{V}_0\times\mathbf{B}] = 0$, $\mathrm{div}\,\rho\mathbf{V}_0 = 0$, and $\mathbf{V}_0\cdot\nabla s = 0$

imply that the neutral flows do not change the real physical quantities $\mathbf{B}$, ρ, and p and the basis vectors $\nabla\psi$ and $\mathbf{e}_\zeta$ in both a steady state and in an arbitrary dynamic state. However, in the presence of neutral flows, the remaining basis vectors are time-dependent even in a steady state. Since this circumstance complicates further analysis, we switch to modified (pseudo-Lagrangian) flux coordinates satisfying the conditions

$$\dot{\psi} + \mathbf{v}\cdot\nabla\psi = 0, \quad \dot{\theta} + \mathbf{v}\cdot\nabla\theta = 0, \quad \dot{\zeta} + \mathbf{v}\cdot\nabla\zeta = 0, \tag{10}$$

where $\mathbf{v} = \mathbf{V} - \mathbf{V}_0$. This change makes it possible to eliminate the secular (in time) terms associated with neutral flows from the independent variables. In particular, in a steady state, the pseudo-Lagrangian function ζ coincides with the traditional toroidal angle φ. In the modified flux coordinates, expressions (7) and (9) remain unchanged, while $\mathbf{V}$ in (8) should be replaced by $\mathbf{v}$. Since $\nabla\zeta$ will play the role of the basis vector of the adiabatic transformation, it is important to note that the functions ζ and θ defined in such a manner satisfy the condition $|\nabla\zeta| \sim \epsilon|\nabla\theta|$.

With allowance for (7), the leading-order term in the variation of the Lagrangian (1) has the form

$$\mathbf{B}\cdot\delta\mathbf{B} = \frac{B^2}{q}(\mathbf{e}_\psi\cdot\nabla(q\delta\psi) + \mathbf{e}_\theta\cdot\nabla(q\delta\theta - \delta\zeta)) - J\mathbf{B}\cdot\mathbf{e}_\theta\left(\frac{q'}{q}\delta\psi + \frac{1}{qJ}(\mathbf{B}\cdot\nabla)(q\delta\theta - \delta\zeta)\right) - \mathbf{B}\cdot\mathbf{e}_\psi(\mathbf{B}\cdot\nabla\delta\psi). \tag{11}$$

We can readily see that, in (11), the first term is dominant. The adiabatic transformation of independent variables that drives the first term to zero is

$$\delta_a\psi = \frac{1}{q}\mathbf{e}_\theta\cdot\nabla\delta\alpha, \quad \delta_a\theta = -\frac{1}{q}\mathbf{e}_\psi\cdot\nabla\delta\alpha + \frac{\delta\zeta}{q}, \tag{12}$$

where $\delta\alpha$ and $\delta\zeta$ are arbitrary functions of the coordinates and time. By analogy with [13], this transformation can be written in terms of the infinitesimal displacement vector

$$\boldsymbol{\xi}_a = \frac{1}{qJ}[\nabla\zeta\times\nabla\delta\alpha] - \frac{1}{qJ}\mathbf{B}\delta\zeta. \tag{13}$$

A comparison with (9) clearly shows that, for $\delta\alpha = \Phi_0(\psi)\tau$ and $\delta\zeta = (\kappa qJ/\rho - \Phi_0')\tau$ (where τ is an arbitrarily small quantity having the dimensionality of time), transformation (13) passes over to the symmetry transformation. Under the adiabatic transformation (13), the remainder in expression (11) becomes

$$\mathbf{B}\cdot\delta_a\mathbf{B} = \mathbf{B}\cdot\left[\nabla\zeta\times\nabla\frac{\mathbf{B}\cdot\nabla\delta\alpha}{qJ}\right] \tag{14}$$

so that, for $|\nabla_\parallel\delta\alpha| \sim \epsilon|\nabla_\perp\delta\alpha|$, it is on the order of ϵ^2. With allowance for $\nabla_\perp qJ \sim \epsilon qJ/a$, we obtain the estimate $\mathrm{div}\,\boldsymbol{\xi}_a \sim \epsilon|\nabla_\perp\boldsymbol{\xi}_a|$, and, with allowance for the initial assumption about the β value, we find $\delta_a p \sim B^2\xi\beta/a \sim O(\epsilon^2)$. Under the traditional hydrodynamic assumption that, in order of magnitude, V does not exceed the speed of sound c_s, the term $V^2\delta_a\rho$ is of the same order. For an arbitrary (unreduced) motion, the term $\rho\mathbf{V}\cdot\delta\mathbf{v}$ is on the order of ϵ, because $\boldsymbol{\xi}$ depends on the fast time. In this case, we have $\delta\mathbf{v} \sim C_A|\nabla_\perp\xi|$. To make this term comparable in order of magnitude to the remaining reduced terms, we consider the following form of $\delta_a\mathbf{v}$, which can be obtained with allowance for the relationship $\delta\mathbf{v} = \dot{\boldsymbol{\xi}} + (\mathbf{v}\cdot\nabla)\boldsymbol{\xi} - (\boldsymbol{\xi}\cdot\nabla)\mathbf{v}$:

$$\delta_a\mathbf{v} = \frac{1}{qJ}[\nabla\zeta\times\nabla(\delta\dot{\alpha} + \mathbf{v}\cdot\nabla\delta\alpha)] - \frac{\mathbf{B}}{qJ}(\delta\dot{\zeta} + \mathbf{v}\cdot\nabla\delta\zeta). \tag{15}$$

For the quantity $\delta_a\mathbf{v}$ to be of the desired order, it is necessary to satisfy the conditions $\delta_a\dot{\alpha} + \mathbf{v}\cdot\nabla\delta_a\alpha \sim \epsilon C_A|\nabla_\perp\delta_a\alpha|$ and $\delta_a\dot{\zeta} + \mathbf{v}\cdot\nabla\delta_a\zeta \sim \epsilon C_A|\nabla_\perp\delta_a\zeta|$, which imply that the functions $\delta_a\alpha$ and $\delta_a\zeta$ depend only on the pseudo-Lagrangian coordinates and slow time; in other words, they play a role similar to that of the relabeling transformation for fast motion. By analogy with the neutral flows treated in [13], such infinitesimal adiabatic transformations refer to adiabatic flows of the form

$$\mathbf{v}_a = \frac{1}{qJ}[\nabla\zeta\times\nabla\phi] - \frac{\nu}{qJ}\mathbf{B}, \tag{16}$$

which do not excite fast degrees of freedom. In (16), ϕ and ν are arbitrary functions of the pseudo-Lagrangian coordinates and slow time.

Expression (16) specifies the general structure of the adiabatic velocity field $\mathbf{v}_a$. In the absence of fast motions, equations (10) yield $\nu = \dot{\zeta}$. With allowance for the definitions of the velocities $\mathbf{v}$ and $\mathbf{V}_0$ and of the cross-helicity $\chi = \mathbf{V}\cdot\mathbf{B}$, the general structure of the adiabatic velocity field can be represented as

$$\mathbf{V}_a = \frac{1}{B^2}\left[\mathbf{B}\times\left(\nabla\Phi - \nabla\zeta\frac{\mathbf{B}\cdot\nabla\Phi}{\eta}\right)\right] + \mathbf{B}\frac{\chi}{B^2}, \tag{17}$$

where $\eta = \mathbf{B}\cdot\nabla\zeta = qJ$, the quantity $\Phi = \phi + \Phi_0(\psi)$ has the meaning of the electric potential, and the relationship

$$\partial_t\mathbf{A} = -\nabla\zeta\frac{(\mathbf{B}\cdot\nabla\Phi)}{\eta}$$

determines adiabatic variations of the vector potential. Accordingly, the adiabatic frozen-in equation takes the form

$$\partial_t \mathbf{B} = \left[\nabla\zeta \times \nabla \frac{\mathbf{B}\cdot\nabla\Phi}{\eta}\right]. \quad (18)$$

As was mentioned in the previous section, the adiabatic equations of motion can be derived from Hamilton's principle (1). To do this, we substitute the adiabatic variations (3) of the Lagrangian into (1), perform straightforward integration by parts, and equate to zero the coefficients of the independent functions $\delta\alpha$ and $\delta\zeta$, which now can be regarded as arbitrary functions of $\mathbf{r}$ and t (here and below, we omit the subscript a). Forcing the coefficient of $\delta\zeta$ to zero and taking into account the pseudo-Lagrangian character of the functions ρ/η and $s = s(\psi)$, we arrive at the following differential conservation law for the cross-helicity:

$$\partial_t \chi + \mathrm{div}\left\{\mathbf{V}\chi - \mathbf{B}\left(\frac{V^2}{2} - \frac{\gamma}{\gamma-1}\frac{p}{\rho}\right)\right\} = 0, \quad (19)$$

which is also valid for the basic (unreduced) MHD equations and can be obtained by multiplying the complete equation of motion by $\mathbf{B}/\rho$. In particular, the conservation law (19) gives the first of the integral invariants (29) in [13]. Driving the coefficient of $\delta\alpha$ to zero, we arrive at the second dynamic equation of the adiabatic MHD model in the form of the conservation law for the generalized momentum P_α, which is canonically conjugate to the adiabatic coordinate α:

$$\partial_t P_\alpha + \mathrm{div}\left\{\mathbf{V}P_\alpha - \frac{\mathbf{B}}{\eta}\mathrm{div}[\mathbf{B}\times\nabla\zeta] - \frac{1}{\eta}[\nabla\zeta\times\nabla p] + \frac{\rho}{\eta}\left[\nabla\zeta\times\nabla\frac{V^2}{2}\right] - \frac{\rho}{\eta}[\mathbf{V}\times\nabla(\mathbf{V}_0\cdot\nabla\zeta)]\right\} = 0, \quad (20)$$

$$P_\alpha = \mathrm{div}(\rho[\mathbf{V}\times\nabla\zeta]/\eta).$$

This equation can also be derived directly from the unreduced vector equation of motion.

Equations (17)–(20), which are the basic equations of the adiabatic MHD model, should be supplemented with the equations for ζ and η in the form

$$\dot\zeta = \frac{[\mathbf{B}\times\nabla\zeta]}{B^2}\cdot\nabla\Phi - \chi\frac{\eta}{B^2} + \mathbf{V}_0\cdot\nabla\zeta, \quad \dot\eta = \mathbf{B}\cdot\nabla\dot\zeta, \quad (21)$$

following from (17) and (18); the equations for ψ and ρ,

$$\dot\psi + [\nabla\zeta\times\nabla\Phi]\cdot\nabla\psi/\eta = 0,$$
$$\dot\rho + [\nabla\zeta\times\nabla\Phi]\cdot\nabla\left(\frac{\rho}{\eta}\right) + (\mathbf{B}\cdot\nabla)\left(\frac{\chi}{C_A^2} - \frac{1}{\eta C_A^2}[\mathbf{B}\times\nabla\zeta]\cdot\nabla\Phi\right) = 0; \quad (22)$$

and the explicit equation relating the functions Φ and P_α,

$$P_\alpha = \mathrm{div}\left\{\frac{1}{C_A^2}\left(\nabla\Phi - \nabla\zeta\frac{(\mathbf{B}\cdot\nabla\Phi)}{\eta} - \mathbf{B}\frac{(\nabla\zeta\cdot\nabla\Phi)}{\eta} + \mathbf{B}\frac{(\nabla\zeta)^2(\mathbf{B}\cdot\nabla\Phi)}{\eta^2}\right)\right\}, \quad (23)$$

where $C_A^2 = B^2/\rho$ is the squared Alfvén speed. Equations (17)–(23) are similar to the corresponding reduced equations of the well-known models [4–11]. However, in contrast to the latter, equations (17)–(23) possess all of the symmetry properties of the basic set of equations; in particular, they admit solutions describing steady states with general plasma flows (9) and are applicable to configurations with arbitrarily shaped cross sections of the magnetic surfaces ψ = const in a steady state. On the other hand, the velocity field (17), strictly speaking, does not form a subclass of the exact solutions to the basic set of MHD equations. In this sense, the proposed MHD model should be regarded as a new, relatively independent set of equations. The question of the complete group of symmetries of the new model and the set of corresponding invariants requires further investigation and goes beyond the scope of our paper.

In solving particular problems, some of the higher-order terms in equations (17)–(23) can, in principle, be omitted. It should be noted, however, that special care is needed in doing this in order not to violate the self-consistent character of the resulting set of equations and their symmetry properties. As the simplest example, we derive the equations needed to analyze the stability and nonlinear dynamics of the kink modes in the absence of steady-state plasma flows ($\mathbf{V}_0 = 0$).

First, we neglect the term with $\mathbf{B}\cdot\nabla$ in equation (19), which thus becomes the local conservation law for the cross-helicity:

$$\partial_t\chi + \mathrm{div}(\mathbf{v}\chi) = 0. \quad (24)$$

This equation is a nonlinear generalization of the condition for minimizing the term $\gamma p_0 \mathrm{div}^2\boldsymbol{\xi}$ in the traditional energy principle for MHD stability [17]. In this case, the condition $\chi|_{t=0} = 0$ and equation (24) imply that $\chi = 0$ throughout the evolution. Then, note that, with allowance for (21), the derivative $\dot\zeta$ is small and contributes only to the terms that are as small as ϵ^2 in comparison with the leading-order terms in equation (20) (or to the terms that are on the order of ϵ^4 in the hierarchy of the full MHD equations). Consequently, we can set $\dot\zeta = \dot\eta = 0$; i.e., $\zeta = \varphi$ and $\eta = \mathbf{B}_0\cdot\nabla\varphi = B_T/R$, in which case equation (18) for the magnetic field can

be partially integrated and can be reduced to the equation for one scalar function $\hat{\psi}$:

$$\begin{aligned} \mathbf{B} &= \mathbf{B}_0 + [\nabla\zeta \times \nabla\hat{\psi}], \\ \partial_t\hat{\psi} + \mathbf{v}\cdot\nabla\hat{\psi} &= \frac{1}{\eta}\mathbf{B}_0\cdot\nabla\phi, \end{aligned} \tag{25}$$

where $\mathbf{v} = [\nabla\zeta \times \nabla\phi]/\eta$. Note that the function $\hat{\psi}$ differs from the perturbed poloidal flux satisfying the corresponding equation in (22).

Neglecting terms on the order of ϵ^2 in the remaining equations, we can assume that $B^2 = B_0^2 \approx B_T^2$ and $C_A^2 = B_T^2/\rho$. We set $p = p_0 + \tilde{p}$ and $\rho = \rho_0 + \tilde{\rho}$ (where the subscript 0 stands for the equilibrium parameter values) and eliminate the equilibrium parameters from the equilibrium condition to reduce equation (20) to

$$\begin{aligned} &\partial_t \mathrm{div}\left(\frac{\nabla_p\phi}{C_A^2}\right) + \mathrm{div}\left(\mathbf{v}\,\mathrm{div}\left(\frac{\nabla_p\phi}{C_A^2}\right)\right) \\ &= (\mathbf{B}_0\cdot\nabla)\left(\frac{R}{B_T}\mathrm{div}\left(\frac{\nabla_p\hat{\psi}}{R^2}\right)\right) \\ &+ [\nabla\zeta\times\nabla\hat{\psi}]\cdot\nabla\left(\frac{R}{B_T}\mathrm{div}\left(\frac{\nabla\psi_0}{R^2}\right)\right) \\ &+ [\nabla\zeta\times\nabla\hat{\psi}]\cdot\nabla\left(\frac{R}{B_T}\mathrm{div}\left(\frac{\nabla_p\hat{\psi}}{R^2}\right)\right) \\ &+ [\nabla\zeta\times\nabla\tilde{p}]\cdot\nabla\left(\frac{R}{B_T}\right) - \left[\nabla\zeta\times\nabla\left(\frac{(\nabla_p\phi)^2}{B_T^2}\right)\right]\cdot\nabla\left(\frac{\rho R}{B_T}\right), \end{aligned} \tag{26}$$

where $\nabla_p = \nabla - \nabla\varphi(\partial/\partial\varphi)$ is the poloidal gradient. Under the above assumptions, it is convenient to write equation (22) in the form

$$\begin{aligned} \partial_t(\tilde{\rho}R/B_T) + \mathbf{v}\cdot\nabla(\tilde{\rho}R/B_T) &= -\mathbf{v}\cdot\nabla(\rho_0 R/B_T), \\ \partial_t(\tilde{p}R^\gamma/B_T^\gamma) + \mathbf{v}\cdot\nabla(\tilde{p}R^\gamma/B_T^\gamma) &= -\mathbf{v}\cdot\nabla(p_0 R^\gamma/B_T^\gamma). \end{aligned} \tag{27}$$

Equations (25)–(27) constitute a closed self-consistent set, which accounts for the toroidal effects through the first order in a/R and the effects of the finite plasma pressure and nonuniform plasma density through the first order in $(k_\perp a)^{-1}$. When the nonlinear effects are most pronounced in a thin layer near a rational magnetic surface, the above effects can be neglected, in which case we can assume that $\rho = \rho_0$ and omit equation (27) and the last two terms on the right-hand side of equation (26).

4. ADIABATIC EQUATIONS FOR MHD CONVECTION NEAR THE THRESHOLD FOR FLUTE INSTABILITY

Along with relatively universal small parameters, such as the ratio B_p/B_T in tokamaks and β, many plasma-related problems may contain additional small parameters associated, e.g., with the closeness to the instability threshold for MHD modes. The additional parameters also provide the possibility of separating the motions adiabatically, in which case the role of slow motions is played by the most dangerous modes, specifically, those for which the stability condition can be violated. Of course, we must keep in mind that the adiabatic equations are valid as long as the system evolving in a nonlinear fashion remains near the instability threshold. Even with allowance for this circumstance, simpler adiabatic equations make it possible to reveal the main characteristic features of the nonlinear evolution of unstable modes and, in some cases, to describe the evolution of the instability fairly completely. Consequently, to illustrate the adiabatic separation of fast and slow motions, we will consider, as a second example, the systems near the instability threshold.

In order to exhibit the properties of this situation more clearly, we consider a simplified model problem that has a deep physical meaning and is, at the same time, nontrivial. Specifically, we consider a straight unbounded equilibrium plasma cylinder with a purely longitudinal initial current having an arbitrary radial profile. In other words, we are dealing with configurations similar to Z-pinches, in which the plasma is initially in equilibrium with the azimuthal magnetic field produced by the longitudinal plasma current. Generally, this equilibrium state is unstable against both kink perturbations, which give rise to the kink instability of the plasma column, and sausage modes, which cause the plasma to become inhomogeneous in the z direction but do not violate the axial symmetry of the column. However, instead of Z-pinches, we are modeling systems like compact tori [18, 19] and levitated dipole configurations, which are topologically equivalent to compact tori [20, 21]. In such systems, kink perturbations can be stabilized by a surrounding conducting wall or by a rigid internal ring. Consequently, assuming that, in the system under consideration, the kink modes are suppressed, we consider exclusively two-dimensional motions that do not violate the axial symmetry of the plasma cylinder.

As in the previous section, we describe MHD plasma dynamics in terms of the three Lagrangian flux coordinates $\{\psi, \theta, \zeta\}$, corresponding to the magnetic flux per unit length, the azimuthal angle, and the longitudinal coordinate, which coincides with the conventional z-coordinate ($\zeta_e = z$) in the equilibrium state. In the absence of kink perturbations, we have $\dot{\theta} = 0$. In terms of the flux coordinates, the frozen-in magnetic field can be written as $\mathbf{B} = [\nabla\zeta \times \nabla\psi]$. On the other hand, in the case of an arbitrary evolution of a two-

dimensional system, the magnetic field has the only nonzero component, which is conveniently described by one independent function, namely, the nondegenerate Jacobian $J = [\nabla\zeta \times \nabla\psi] \cdot \nabla\theta$. As in the previous section, the Jacobian J satisfies the continuity equation $\partial_t J + \mathrm{div}\,\mathbf{V}J = 0$, which plays the role of the frozen-in equation (4) in the example under discussion, so that we have $B^2 = r^2J^2$, where r is the conventional radial coordinate. It is also convenient to represent the plasma pressure as $p = s_m J^\gamma$, where the Lagrangian invariant s_m, satisfying equation (6), can be referred to as a "magnetic" entropy function or simply "magnetic entropy." The plasma density can be expressed in a similar manner, $\rho = fJ$, where f is a Lagrangian invariant. The magnetic entropy function is related to the ordinary entropy function, introduced in Section 3, by the simple relationship $s_m = sf^\gamma$.

With the notation adopted, the Lagrangian of the system has the form

$$\mathscr{L} = \int d\mathbf{r}^3\left(\rho\frac{V^2}{2} - \frac{s_m}{\gamma-1}J^\gamma - \frac{r^2J^2}{2}\right), \qquad (28)$$

and the ordinary static equilibrium condition can be written as

$$-\frac{J^\gamma}{\gamma-1}\nabla s_m + J\nabla\left(\frac{\gamma J^{\gamma-1}}{\gamma-1}s_m + r^2J\right) = 0. \qquad (29)$$

We can easily show that the solvability condition for equation (29) is that the equilibrium quantities be homogeneous in the z direction, in which case we can set $J_e = J_e(r)$ and $s_{me} = s_{me}(r)$ (here and below, the subscript e denotes equilibrium quantities). In equilibrium, r is a single-valued function of ψ,

$$\psi_e = \int_0^r rJ_e(r)dr;$$

consequently, at any instant, the Lagrangian invariant s_m depends only on ψ.

Then, following [13], we can readily show that the variational symmetry properties of the system admit not only static equilibria described by (29) but also axisymmetric steady states with neutral flows that have the velocity

$$\mathbf{V}_0 = \kappa(\psi,\zeta)\frac{\mathbf{B}}{\rho} + \frac{1}{J}[\nabla\theta \times \nabla\Phi_0(s_m(\psi,\zeta))] \qquad (30)$$

and are analogous to (9). Note also that, in such states, the plasma is not necessarily homogeneous in the z direction. In the evolution of the two-dimensional system under discussion, the momentum conservation implies that neutral flows along the magnetic field $\mathbf{B}$ give rise only to the additional centrifugal potential. To simplify the problem and to make the analysis more illustrative, we assume that there are no plasma flows along the field $\mathbf{B}$ ($\kappa = 0$), in which case the steady states of the system are homogeneous in the z direction (i.e., we have $\Phi_0(\psi)$, $s_m(\psi)$, and $f(\psi)$) and are described by equation (29), because the steady-state plasma flows along the z-axis have no impact on the force balance in equilibrium.

Kadomtsev [17] has shown that the equilibrium states described by (29) are stable against arbitrary two-dimensional perturbations under the condition $ds_{me}/dr > 0$, which implies that the plasma pressure should decrease sufficiently gradually with radius. This stability condition can be easily derived if we write the traditional energy principle of stability (see [17]) using the notation already adopted:

$$\int d\mathbf{r}^3\{(\gamma s_m J^{\gamma-2} + r^2)\mathrm{div}^2(\boldsymbol{\xi}J) + 2J^{\gamma-1}(\boldsymbol{\xi}\cdot\nabla s_m)\mathrm{div}(\boldsymbol{\xi}J) - J^{\gamma-1}(\boldsymbol{\xi}\cdot\nabla s_m)(\boldsymbol{\xi}\cdot\nabla J)\} > 0. \qquad (31)$$

According to (31), the most dangerous perturbations governing the stability boundary are convective modes such that $\mathrm{div}(\boldsymbol{\xi}J) = 0$.

Marginally stable states are those with $s_{me} = \mathrm{const}$. According to (29), the marginally stable profiles of the magnetic field and plasma pressure can be evaluated from the condition

$$\frac{\gamma J_e^{\gamma-1}}{\gamma-1}s_{me} + r^2J_e = \mathrm{const} = \frac{\gamma p_0}{(\gamma-1)J_0}, \qquad (32)$$

where p_0 and J_0 are constant values of p and J at the axis of the plasma cylinder. The marginally stable pressure profile is seen to decrease with r according to a power law on a characteristic radial scale such that $a^2 = p_0/J_0^2$. For Z-pinches, such pressure profiles are not of much interest, because they decrease too gradually at infinity. However, Vabishchevich *et al.* [22] showed that, in systems like a compact torus in which the toroidal plasma is bounded by a separatrix, the marginally stable pressure profile is such that the pressure vanishes at the separatrix. For such configurations, the nonlinear plasma dynamics near the states of marginal stability, $s_{me} = \mathrm{const}$, is extremely interesting from a physical standpoint.

To simplify the analysis of the nonlinear plasma dynamics near the state of marginal stability, we adiabatically separate the motions according to the proposed scheme. We start by varying the Lagrangian (28),

$$\delta\mathscr{L} = \int d\mathbf{r}^3\left\{\rho\mathbf{V}\cdot\delta\mathbf{V} - \frac{V^2}{2}\mathrm{div}(\boldsymbol{\xi}\rho) + \frac{J^\gamma}{\gamma-1}(\boldsymbol{\xi}\cdot\nabla s_m) + \left(\frac{\gamma s_m}{\gamma-1}J^{\gamma-1} + r^2J\right)\mathrm{div}(\boldsymbol{\xi}J)\right\}. \qquad (33)$$

In an arbitrary state, the variation of the Lagrangian (33) does not contain any small parameters, because, in contrast to the previous section, here we have $c_s \sim C_A$ (or $\beta \sim 1$). However, near the state of marginal stability,

we can represent the magnetic entropy as $s_m = \bar{s}_m + \tilde{s}_m(\psi)$, where $\bar{s}_m$ = const and $\tilde{s}_m \sim \epsilon^2 \bar{s}_m$. Since the small deviation of the magnetic entropy $\tilde{s}_m$ from that in the marginally stable state drives the plasma into unstable motion, we assume that $V \sim \epsilon c_s$, in which case the last term in the integrand in (33) is a quantity of order unity. The first term (with $\delta\mathbf{V}$) is *a priori* proportional to ϵ (as in the previous section), while the remaining terms are as small as ϵ^2.

The transformation consistent with the condition $\mathrm{div}(\boldsymbol{\xi}_a J) = 0$ forces the leading-order term in (33) to zero. From the standpoint of the energy principle (31), this transformation, which, in the two-dimensional case, can be represented as $\boldsymbol{\xi}_a = [\nabla\theta \times \nabla\delta\alpha]/J$, corresponds to the most dangerous perturbations. The first term in (33) can be made as small as ϵ^2 if the function $\delta\alpha$ is chosen to satisfy the condition $\partial_t\delta\alpha + \mathbf{V}\cdot\nabla\delta\alpha \sim \epsilon c_s|\nabla\delta\alpha|$ [cf. expression (15) in the previous section], i.e., to correspond to the relabeling transformation for fast magnetosonic oscillations. In this case, the two-dimensional adiabatic velocity field, which can be represented in the form

$$\mathbf{V}_a = \frac{1}{J}[\nabla\theta \times \nabla\Phi], \tag{34}$$

where $\Phi(r, z, t)$ has the meaning of the electric potential, corresponds to convective plasma motions in a quasi-potential electric field and contains neutral flows (30) with $\kappa = 0$ and $\Phi_0(\psi)$. Substituting the velocity field (34) into the continuity equation for J yields $\partial_t J = 0$. Then, to within terms on the order of ϵ^2, we can set $J = J_e(r)$, where $J_e(r)$ is determined from equation (32) with $s_{me} = \bar{s}_m$ and the quantity $\bar{s}_m$ is defined as

$$\begin{aligned}\bar{s}_m &= \lim\left(\frac{1}{\psi_e}\int_0^{\psi_e}\frac{p_e}{J_e^\gamma}d\psi_e\right)_{r\to\infty} \\ &= \lim\left(\frac{1}{\psi_e}\int_0^{r}\frac{p_e}{J_e^{\gamma-1}}r dr\right)_{r\to\infty}.\end{aligned} \tag{35}$$

Applying the above procedure to derive the equation of adiabatic motion, we obtain

$$\begin{aligned}\partial_t P_\alpha + \mathrm{div}\Bigg\{&\mathbf{V}P_\alpha + \frac{\rho}{J}\left[\nabla\theta \times \nabla\frac{V^2}{2}\right] \\ &+ \frac{J^{\gamma-1}}{\gamma-1}[\nabla\theta\times\nabla\tilde{s}_m]\Bigg\} = 0,\end{aligned} \tag{36}$$

$$P_\alpha = \mathrm{div}\left(\frac{\rho}{J}[\mathbf{V}\times\nabla\theta]\right) = \mathrm{div}\left(\frac{\rho\nabla\Phi}{r^2J^2}\right) = \mathrm{div}\left(\frac{\nabla\Phi}{C_A^2}\right).$$

Using the above representation $\rho = J_e f(\psi)$, where $f(\psi_e(r)) = \rho_e(r)/J_e(r)$, we can reduce the full set of adiabatic equations to the following two equations for two functions $\Phi(r, z, t)$ and $\psi(r, z, t)$:

$$\begin{aligned}&\partial_t\left(\frac{P_\alpha}{J_e}\right) + \frac{1}{rJ_e}\left[\nabla\Phi\times\nabla\left(\frac{P_\alpha}{J_e}\right)\right]_\theta \\ &+ \frac{f'(\psi)}{2rJ_e}\left[\nabla\left(\frac{(\nabla\Phi)^2}{2r^2J_e^2}\right)\times\nabla\psi\right]_\theta \\ &+ \frac{J_e^{\gamma-3}}{r}\tilde{s}_m'(\psi)\frac{\partial\psi}{\partial z}\frac{dJ_e}{dr} = 0,\end{aligned} \tag{37}$$

$$\partial_t\psi + \frac{1}{rJ_e}[\nabla\Phi\times\nabla\psi]_\theta = 0, \quad P_\alpha = \mathrm{div}\left(\frac{f(\psi)\nabla\Phi}{r^2J_e}\right).$$

Equations (37) are analogous (both in structure and in character) to two-dimensional hydrodynamic equations for an incompressible magnetized fluid. We can substantially simplify equations (37) by choosing the initial plasma density profile in a special way: f = const, in which case the analogy becomes especially clear. With this choice, the nonlinear structure of equations (37) allows us to draw an analogy with the Charney–Obukhov equation for planetary atmospheres [23] or the Hasegawa–Mima equation for drift waves [24]; however, unlike the latter, equations (37) account for the driving force for the convective instability. A detailed analysis of equations (37), in particular, with allowance for dissipative processes, goes beyond the scope of our paper. We can only note that, during the evolution described by these equations, the energy is expected to be transferred from large-scale to small-scale motions, while simultaneously the large-scale (of about a) perturbations of the function $\tilde{s}_m(\psi)$ (i.e., perturbations that give rise to convective instability) progressively decrease. In this case, throughout the evolution, the system should not run out of the applicability range of equations (37), which is governed by our basic assumptions.

5. CONCLUSION

To conclude, note that the proposed variational method for separating fast and slow motions is an efficient tool for deriving far simpler but fairly informative adiabatic equations for a large class of problems associated with nonlinear dynamic (in particular, MHD) processes in continuous media. The principle advantage of the method is that the adiabatic equations possess all of the variational symmetries (and the related conservation laws) inherent in the complete set of basic equations, which provides the basis for an adequate description of nonlinear dynamic processes with the help of reduced equations.

Using the method developed to separate the motions, we have derived adiabatic MHD equations for the two classes of problems that are of interest from the standpoint of confinement and stability of high-temper-

ature plasmas in toroidal magnetic devices. First, we have derived an improved version of the familiar reduced KPS equations. The refined equations, which possess all of the symmetry properties of the basic MHD equations, make it possible to investigate the nonlinear dynamics of tokamak plasmas with steady-state sheared flows. Second, we have derived a set of equations needed for two-dimensional modeling of MHD plasma convection near the threshold for flute instability in quasisteady magnetic confinement systems similar to compact tori with $\beta \sim 1$. This set of equations can also be used to study the nonlinear dynamics of plasmas with steady-state flows.

ACKNOWLEDGMENTS

This work was supported in part by the Russian Foundation for Basic Research, project nos. 97-02-17238 and 96-15-96815.

REFERENCES

1. V. E. Zakharov, Izv. Vyssh. Uchebn. Zaved., Radiofiz. **17**, 431 (1974).
2. P. J. Morrison, AIP Conf. Proc. **88**, 13 (1982).
3. B. V. Chirikov, in *Reviews of Plasma Physics*, Ed. by B. B. Kadomtsev (Énergoatomizdat, Moscow, 1984; Consultants Bureau, New York, 1987), Vol. 13.
4. B. B. Kadomtsev and O. P. Pogutse, Zh. Éksp. Teor. Fiz. **65**, 575 (1973) [Sov. Phys. JETP **38**, 283 (1974)].
5. B. B. Kadomtsev and O. P. Pogutse, Zh. Éksp. Teor. Fiz. **66**, 2067 (1974) [Sov. Phys. JETP **39**, 1017 (1974)].
6. R. White, D. Monticello, *et al.*, in *Proceedings of 5th International Conference on Plasma Physics and Controlled Nuclear Fusion Research, Tokyo, 1974* (IAEA, Vienna, 1975), Vol. 1, p. 495.
7. H. Strauss, Phys. Fluids **19**, 134 (1976).
8. H. Strauss, Phys. Fluids **20**, 1354 (1977).
9. H. Strauss, Nucl. Fusion **23**, 649 (1983).
10. R. D. Hazeltine, M. Kotschenreuther, and P. J. Morrison, Phys. Fluids **28**, 2466 (1985).
11. H. Strauss, J. Plasma Phys. **57**, 83 (1997).
12. R. Courant and D. Hilbert, *Methods of Mathematical Physics*, Vols. I and II (Gostekhizdat, Moscow, 1951; Interscience, New York, 1953, 1962).
13. V. I. Il'gisonis and V. P. Pastukhov, Fiz. Plazmy **22**, 228 (1996) [Plasma Phys. Rep. **22**, 208 (1996)].
14. V. P. Pastukhov, Pis'ma Zh. Éksp. Teor. Fiz. **67**, 892 (1998) [JETP Lett. **67**, 940 (1998)].
15. W. Newcomb, Nucl. Fusion Suppl. **2**, 451 (1962).
16. L. S. Solov'ev and V. D. Shafranov, in *Reviews of Plasma Physics*, Ed. by M. A. Leontovich (Atomizdat, Moscow, 1967; Consultants Bureau, New York, 1970), Vol. 5.
17. B. B. Kadomtsev, in *Reviews of Plasma Physics*, Ed. by M. A. Leontovich (Gosatomizdat, Moscow, 1963; Consultants Bureau, New York, 1966), Vol. 2.
18. A. G. Es'kov, R. Kh. Kurtmullaev, A. P. Kreshchuk, *et al.*, in *Proceedings of 7th International Conference on Plasma Physics and Controlled Nuclear Fusion Research, Innsbruck, 1978* [Nucl. Fusion Suppl. **2**, 187 (1979)].
19. W. T. Armstrong, R. K. Linford, J. Lipson, *et al.*, Phys. Fluids **24**, 2068 (1981).
20. A. Hasegawa, L. Chen, and M. E. Mauel, Nucl. Fusion **30**, 2405 (1990).
21. A. I. Morozov, V. P. Pastukhov, and A. Yu. Sokolov, in *Proceedings of the Workshop on D–3He Based Reactor Studies, Moscow, 1991*, p. 1C1.
22. P. N. Vabishchevich, L. M. Degtyarev, V. V. Drozdov, *et al.*, Fiz. Plazmy **7**, 981 (1981) [Sov. J. Plasma Phys. **7**, 536 (1981)].
23. V. I. Petviashvili and O. A. Pokhotelov, *Solitary Waves in Plasma and the Atmosphere* (Énergoatomizdat, Moscow, 1989).
24. A. Hasegawa and K. Mima, Phys. Fluids **21**, 87 (1978).

Translated by O. E. Khadin